COMMERCIAL IN CONFIDENCE

BGS Technical Report WK/99/12/C

ARK

Prepared for :

Petroleum Infrastructure Programme *Rockall Studies Group Project 98/1*

Rockall Trough : Irish Sector

REPORT ON THE COMPILATION, PRESENTATION AND INTERPRETATION OF GRAVITY AND MAGNETIC DATA

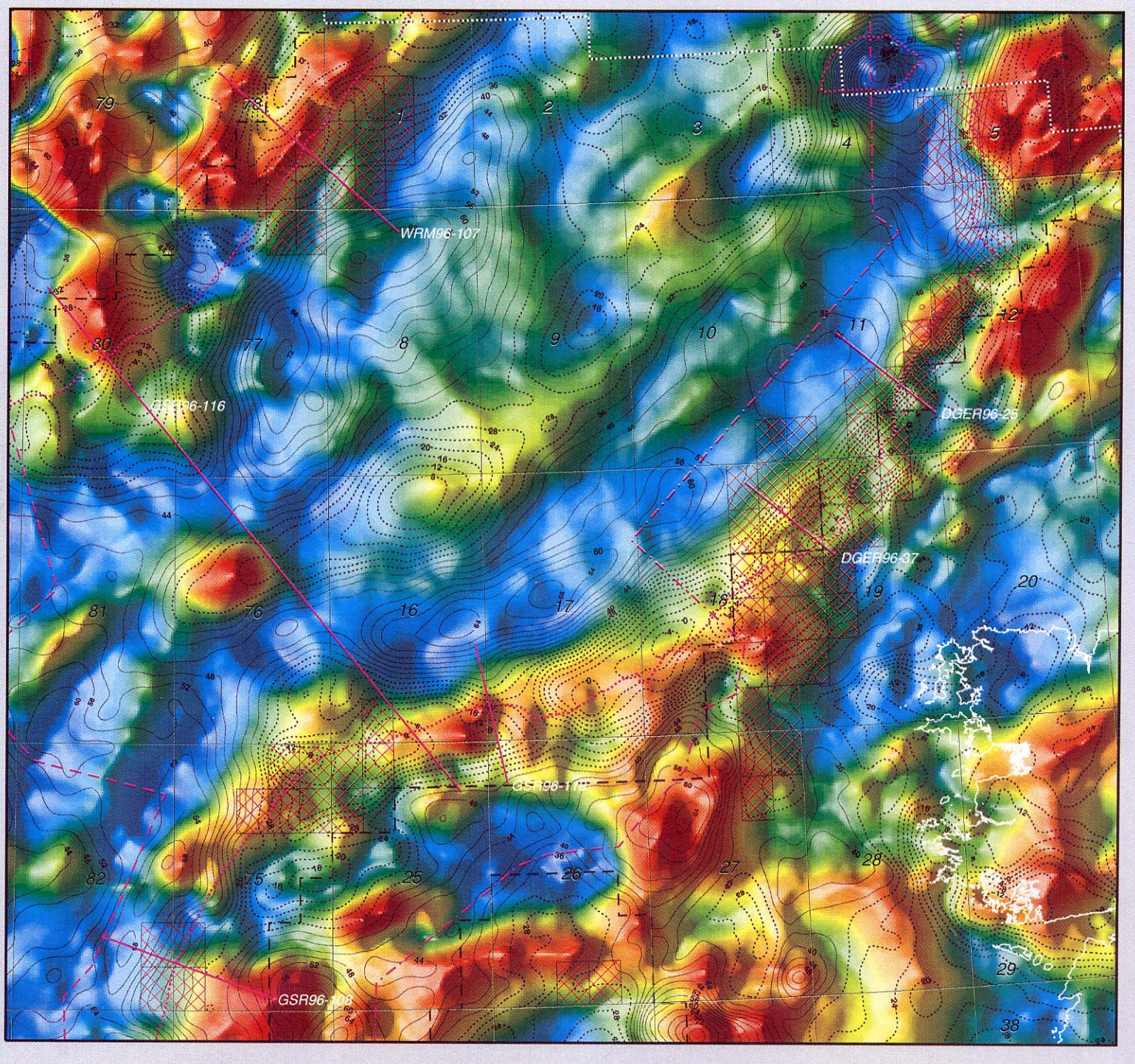

BRITISH GEOLOGICAL SURVEY **ARK Geophysics Ltd**

Petroleum Infrastructure Programme ***Rockall Studies Group Project 98/1***

Rockall Trough : Irish Sector

Report on the compilation, presentation and interpretation of gravity and magnetic data

compiled by R M Carruthers

Bibliographic reference:
CARRUTHERS, R M. 1999. Rockall Trough: Irish Sector. Report on the compilation, presentation and interpretation of gravity and magnetic data *(British Geological Survey Technical Report WK/99/12/C)*

For further information:

The Group Manager
Regional Geophysics Group
British Geological Survey
Keyworth
Nottingham NG12 5GG
Tel: +44 (0)115 936 3356
Fax: +44 (0)115 936 3145

or

ARK Geophysics Ltd
Mill Court
Featherstone Road
Wolverton Mill
Milton Keynes MK12 5EU
Tel: +44 (0)1908 222566
Fax: +44 (0)1908 222577

Direct contacts:

Mick Lee / Richard Carruthers
E-mail: m.lee@bgs.ac.uk
r.carruthers@bgs.ac.uk

Web site: www.bgs.ac.uk
(Regional Geophysics Pages)

Andy McGrandle / Paul Versnel
andy.mcgrandle@arkgeo.demon.co.uk
paul.versnel@arkgeo.demon.co.uk

www.arkgeo.com

CONTRACTUAL INFORMATION

This report and associated products were produced under the terms of contract number 98.16.21 between Enterprise Oil plc and the Natural Environment Research Council for "The provision of consultancy services in connection with the Petroleum Infrastructure Programme Group 2."

As part of the terms of the contract, ARK Geophysics Ltd was sub-contracted by the Natural Environment Research Council to undertake specific aspects of the work. This is covered by contract GA/98F/61/S1 between the Natural Environment Research Council and ARK Geophysics Ltd.

***ARK Geophysics Ltd**: "has provided expertise in potential field geophysics to the oil, gas and mineral exploration industry since 1986. ARK works principally for international oil exploration companies - acquiring, processing and interpreting gravity and magnetic data - and has built an excellent reputation for high quality work and for achieving deadlines. We achieved registration for the international quality management standard ISO9002 in 1994 and remain the only ISO9000 accredited, potential field service company. Our emphasis on quality and rapid turn-around is made possible by a strong team of geophysical staff who are all specialists in potential field methods, and by continuous investment in innovative software."*

EXECUTIVE SUMMARY

This study of potential field (ie. gravity and magnetic) data from the Rockall area west of Ireland was undertaken jointly by the British Geological Survey (BGS) and ARK Geophysics Ltd for the Rockall Studies Group. The project, number 98/1, forms part of the Petroleum Infrastructure Programme established by the Petroleum Affairs Division of the Department of the Marine and Natural Resources on 4th June 1997.

Project activities were divided into three parts:

A: ***Data compilation and grid generation*** - to assemble all the available data, including airborne, satellite, marine and land sources, and to generate grids from the network-adjusted compilations.

B: ***Data presentation*** - to produce a representative suite of images from grids of the basic gravity and magnetic anomaly data and from grids derived by further processing.

C: ***2D/3D modelling*** - to generate a representative set of 2D models comprising six lines over the margins of the Rockall Trough and two longer, regional lines extending across its full width; also, to create a generalized 3D model in order to estimate the apparent basin thickness and apparent magnetization over the project area.

Project deliverables were a set of anomaly grid files and CGM plot files of the images derived from them, together with the 2D and 3D model outputs, supplied in digital form (on CD-ROM or Exabyte tape). One set of encapsulated paper plots of the images was supplied to PAD.

The images provide a valuable insight into the structural pattern of the region with evidence of significant, extensive features cutting across the north-easterly trend of the Rockall Trough itself. There is also an inverse correlation between a number of major anomalies ie. gravity anomaly highs coinciding with magnetic anomaly lows and *vice versa*.

Two-dimensional (2D) gravity modelling of basin structure near the shelfbreaks is difficult because the response is dominated by the combined effects of marked changes in ground level (bathymetry) and of crustal thinning. There is general agreement with the available seismic interpretations; the remaining disparities need to be addressed using higher resolution datasets and a more detailed analysis than was possible in this project. Regional profiles set the context for looking at broader issues of crustal structure. There was little seismic information from beneath the Tertiary within the Rockall Trough on the profiles used and significant uncertainty remains in accounting satisfactorily for the potential field response.

A three-dimensional (3D), full-crustal model was constructed for the whole area. The thickness of the cover sequence was then optimized to minimize the residual anomalies between calculated and observed free-air gravity responses. This approach reproduces many of the known features in outline form and provides a framework for developing more sophisticated models where there is better data/control. The latest RAPIDS seismic experiments should be especially helpful in refining the deeper parts of the model. Sections extracted from the 3D model are in qualitative agreement with the 2D interpretations. The amount of variation allowed in fitting the 3D model was restricted. to avoid undue amplification of 'noise' overall with the result that short wavelength features are not reproduced accurately. Differences in magnetization within the upper crust (taken from the base of the cover sequence derived from the 3D gravity optimization) were calculated separately.

CONTENTS

ANNEXES

[coloured divider]

[coloured divider]

[coloured divider]

[coloured divider]

LIST OF FIGURES

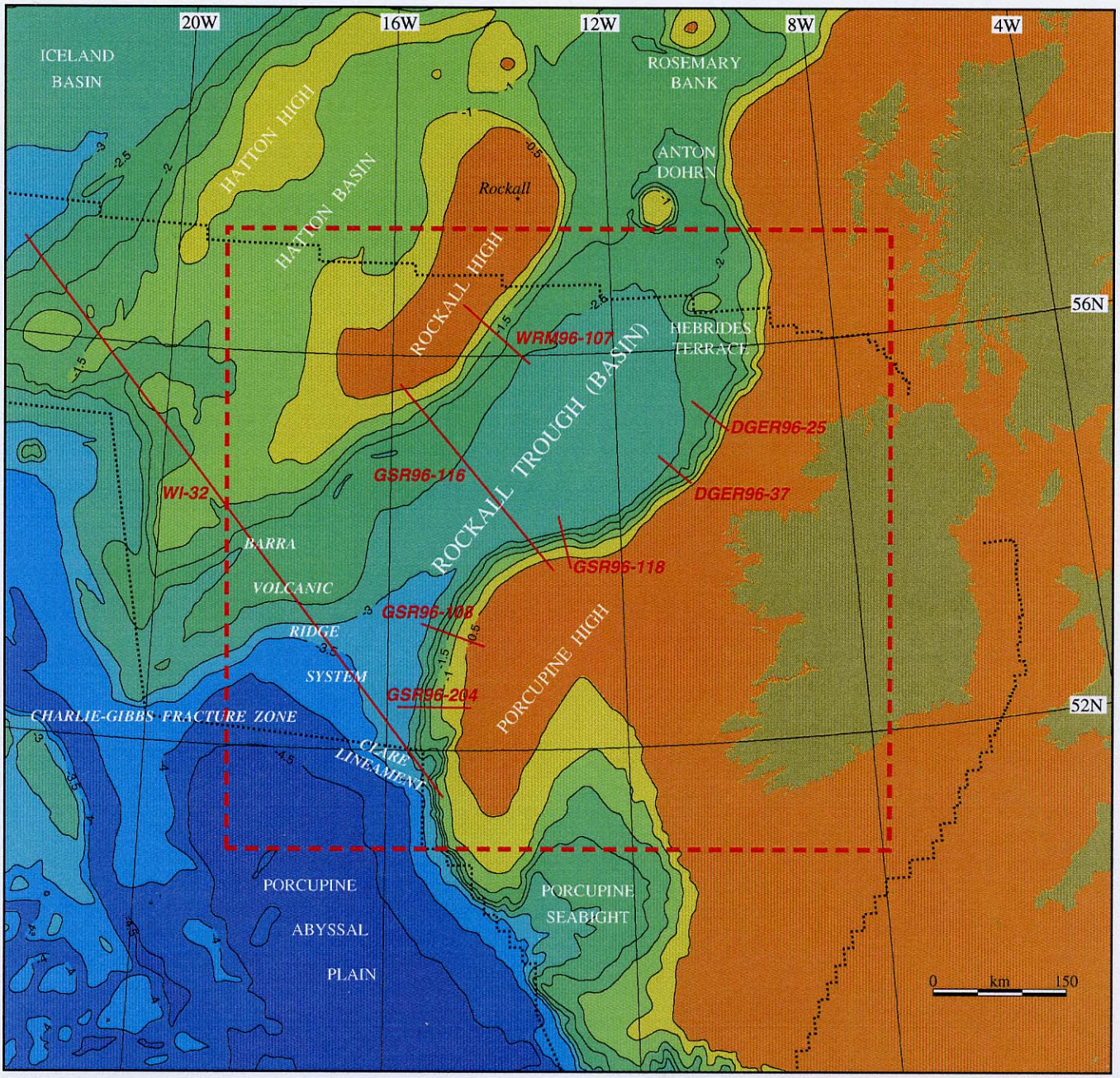

Figure 1 Location map with project area and modelled seismic sections shown in red (bathymetric contours at 500 m intervals)

1. INTRODUCTION

1.1 Background

The Petroleum Infrastructure Programme (PIP), established by the Petroleum Affairs Division (PAD) of the Department of the Marine and Natural Resources on 4th June 1997, was conceived as a means of promoting hydrocarbon exploration in Ireland and its designated continental shelf. This report refers to work undertaken for the Rockall Studies Group (RSG), a component of PIP with funding initially from sixteen oil companies. The RSG, as represented by its Sub-surface Technical Committee, is interested in the deeper geological aspects of the Irish Rockall area and it was recognized at an early stage that potential field (ie. gravity and magnetic) data could contribute to these investigations.

Following an invitation to tender from RSG, a contract (number 98.16.21 with Enterprise Oil plc) was awarded jointly to the British Geological Survey (BGS) and ARK Geophysics Ltd, bringing together proposals submitted independently by ARK and BGS. For administrative convenience BGS was named as the main contractor, with ARK acting under sub-contract (ARK project number: PIP98045) to BGS. The study is referred to as RSG Project 98/1: "Compilation, presentation and interpretation of gravity and magnetic data in the Irish Rockall Trough".

The study was extended well beyond the area of immediate interest so as to provide a better sense of the regional context and the relation between the southern Rockall Trough and adjoining features such as Porcupine Basin, the Irish mainland and the Rockall Plateau. Maps/images were produced using a UTM projection with the central meridian at 15°W (ie. zone 28) in the area 250-1000 km easting and 5650-6350 km northing (approximately 19°W to 7°W and 51°N to 57.2°N). A general location map is provided as figure 1.

A separate project, RSG 97/3, was concerned with establishing a structural nomenclature for the Irish Atlantic margin (Naylor and Shannon, 1999). The agreed terminology is followed in this report expect for the use of Rockall 'Trough' instead of Rockall 'Basin' (as the former had already been used in the production of the final maps). The structural element map produced as part of this work should be used as the reference for the geological setting of the geophysical maps also. A number of key seismic sections interpreted as part of Project 97/3 to investigate the nature and extent of the known basins provided the starting point for the 2D modelling of gravity and magnetic anomaly profiles.

1.2 Project organisation and outputs

There were three distinct, but related aspects to the work programme:

Data compilation

- assemble, merge and network-adjust the land, marine and airborne data available in 'x,y,z' format for the ground surface relief (mainly bathymetry) and the gravity and magnetic fields;
- generate digital grids from these adjusted data, including information from the public domain (such as free-air gravity values derived from satellite altimetry) as necessary to complete the coverage, including a margin of about 100 km for the working grids (to reduce edge effects when applying subsequent filtering operators).

Data processing and visualisation

- transform the basic grids as necessary to derive additional parameters which further enhance particular aspects of the data eg. isostatically-compensated Bouguer gravity anomalies, horizontal gradients, residual anomalies, pseudo-gravity anomalies etc.
- generate a representative suite of images for reproduction at a scale of 1:1M using colour and shading effects to display the data to best effect and to maximize the structural information conveyed.

Integrated modelling of gravity and magnetic anomalies

- 2D modelling along six selected profiles with seismic interpretations over the margins of the Rockall Trough;
- 2D modelling of two regional profiles with seismic interpretations crossing the Rockall Trough;
- 3D modelling of the full area to provide an estimate of 'apparent basin' thicknesses and of upper crustal magnetization.

Data compilation and the 2D modelling of the six shorter profiles were undertaken by ARK, with the remainder of the products being the responsibility of BGS.

The specified outputs of the project as supplied to all members were:

1. grids of the bathymetry, free-air gravity and total field magnetic anomaly data together with any derived grids used in producing the images - distributed in ASCII x,y,z format;
2. plot files of the representative suite of images and 2D and 3D models in CGM, JPG and Postscript formats;
3. 2D model profiles and 3D model outputs as CGM and Postscript plot files
4. hard copy of the final report.

Digital data were supplied on Exabyte 8mm cartridge tape or CD-ROM as requested. The distributed digital products are itemized in annexes as follows:

- maps/images (Annex A1)
- grids (annexes A2and A3)
- digital plot/data files (Annex A3)

In addition, a set of encapsulated printed maps was produced for PAD.

This report describes the processing techniques applied, the images produced and the modelling results. A selection of customized images is provided at reduced scale to illustrate the main features in the study area (Annex A4); Map 19 is a direct, scaled-down copy of the 1:1M map to show the style of layout/presentation adopted in the digital CGM files. Profiles resulting from both 2D and 3D modelling are provided in Annex A5.

1.3 Geological setting

Apart from some specific areas such as the Slyne, Erris and Porcupine basins in which more extensive exploration, including drilling, has taken place, most of the region remains poorly understood. In particular, the nature of the Mesozoic history of the Rockall Trough (and Rockall Plateau) is the subject of conjecture and inference from a very limited amount of hard information. This position is improving slowly with the acquisition of more deep seismic data of better quality

(cf. the results from RSG Project 97/11 should be especially interesting in adding to these) but conventional seismic surveys tend to suffer from the adverse effects of lavas and sills within the Palaeogene and Cretaceous successions. The potential field data provide further insights into the structural framework but, as noted by Musgrove and Mitchener (1996), it can be misleading to attribute gravity/magnetic anomalies directly to basement geometry unless other constraints are available.

The Rockall Trough enters the project area from the north at a point just to the south of the Anton Dohrn Seamount (Fig.1). It continues on a south-westerly trend between Rockall Bank, which lies on the eastern margin of the Rockall Plateau (comprising the Hatton Basin and the Rockall and Hatton highs), and the UK/Irish continental shelf to the east. The Hebrides Terrace Seamount Centre lies on the eastern margin of the trough, distinguishing it from the more centrally located Rosemary Bank and Anton Dohrn seamounts; it may also be younger in origin - Palaeocene rather than Cretaceous in age. All three seamounts rise more than 1000 m above the local seabed.

The floor of the Rockall Trough slopes steadily down from about 2000 m to 4000 m to the south-west and generally steepens more rapidly at its eastern margin. The margins of the trough are of particular interest for hydrocarbons exploration as they comprise a series of rotated fault blocks in which Mesozoic sedimentary rocks have been preserved.

The southern limit of the Rockall Trough is taken to be marked by the Charlie-Gibbs Fracture Zone, with the linear magnetic anomalies characteristic of oceanic crust being seen over the Porcupine Abyssal Plain beyond this. It is assumed here that the Rockall Trough itself is underlain by highly attenuated and intruded continental crust. On the northern side of the Charlie-Gibbs Fracture Zone, the Barra Volcanic Ridge System has been identified from seismic data, showing a direct correlation between strongly reflective seismic basement highs and positive magnetic anomalies. Megson (1986) and Bentley and Scrutton (1986) attribute these features to Cretaceous igneous activity during the early stages of development of the Charlie-Gibbs Fracture Zone.

The structural elements map from project RSG 97/3 summarizes the main features known within the area, and published results from the seismic experiments describe the current state of knowledge on deep crustal structure and overall basin geometry. It is assumed that the reader is familiar with the general geological context: descriptions of the Rockall Trough given in the BGS Interpreters' Supplements, volumes 10S and 11S are not repeated here though an extended bibliography has been retained (Annex A6). Specific points relating to the information contained in the gravity and magnetic images and the results of the modelling are discussed in the relevant sections below.

2. DATA SOURCES, COMPILATION AND GRIDDING

The aim for this phase of the project was to collate all available datasets of gravity and magnetic data from the PAD database, BGS database, Hydrographic Office, DMA, DIAS, GSI and proprietary surveys that members of the study group had supplied for the sole use of the project.

Data for Ireland as provided by DIAS (gravity) and GSI (magnetic) were made available on the basis that they could be used only in compiling the working grids and for the production of images. That is, they were not to be included in any of the output grids supplied to the group members, nor were they to be used in the 3D modelling (see also Annex A3). Any members wishing to access the onshore data should contact DIAS and GSI directly.

The data are derived from a wide variety of sources with significant differences in acquisition parameters and quality and there is a general tendency for the coverage to become more sparse in an east to west direction. It is important to bear these factors in mind when assessing the final grids and the changes in anomaly characteristics across any image derived from them. Changes in either the density of survey coverage or in bathymetry can have a marked influence on the frequency content of the images which needs to be recognized as such.

2.1 Data sources

The following data were made available to the project (quantities refer to the those falling within the area of the final grids ie. excluding the working margin)

Gravity data:	
Existing line data from the PAD database held by ARK	61045 km
Supplied line data from the BGS, Hydrographic Office and DMA	165588 km
Extra line data obtained from Aran, HGS, Mobil, Enterprise and LCT surveys	22653 km
Line data supplied by the BGS in the area north-east of Ireland	5443 km
Land gravity stations covering Northern Ireland	11257
Land gravity stations covering Eire (DIAS)	23257
Sandwell satellite gravity data (version 7.2)	(gridded dataset)
Marine magnetic data:	
Aran marine data	211 km
HGS marine data	3913 km
LCT marine data	3918 km
Existing data from the PAD database held by ARK	16342 km
Data supplied from the BGS	13485 km
Data as supplied from Mobil	6460 km
Aeromagnetic data:	
Huntings aeromagnetic data	9922 km
Faireys aeromagnetic data	13949 km
Northern Ireland aeromagetic data	11264 km
Combined dataset of aeromagnetic data	47337 km
SSL aeromagnetic data (Irish waters only)	14193 km
GSC aeromagnetic compilation	(gridded dataset)
GSI aeromagnetic compilation	(gridded dataset)

2.2 Locations

All point location information was transformed into the UTM co-ordinate system adopted for the project, that is, with the central meridian at 15°W and referred to the Hayford 1909 (also known as the International 1924) spheroid. The navigation data were checked and edited as required. Note that the distance between points varied widely between surveys.

2.3 Bathymetry

Bathymetry data were converted into ARKive format and were visually inspected utilising the ARK proprietary interactive graphics package. Data spikes, dropouts, positive marine values and other spurious values were either set to null individually or the lines including them were removed from the dataset.

Mis-ties in the corrected bathymetry data as calculated at line intersections gave an initial root-mean square (RMS) error of 108.9 m. These were minimized by a procedure consisting of optimal DC shifts, followed by constrained linear ramps and piecewise datum adjustments. The final RMS error was 25.3 m, with 97% of mis-ties less than 10 m. Adjusted values at line intersection points were then used to create the levelled bathymetry by fitting an Akima spline under tension through the differences to form a new surface.

Adjusted marine bathymetry data were merged with the coastline (set to a value of zero) and elevation data from the land gravity stations. Data were then gridded at a node interval of 2 km using continuous curvature splines under tension.

Nodes from a second grid derived from the digitised contours of the GEBCO97 compilation were spliced in to complete the coverage over the full project area where the available marine survey data were thin or non-existent.

The final grid was sub-sampled to a node spacing of 1 km.

2.4 Gravity data

Marine gravity data were edited, adjusted and levelled using similar procedures as for the bathymetry. Their distribution is illustrated in Map 2 (Annex A4) Mis-ties for the corrected free-air gravity data at line intersections were reduced from an initial RMS error of 7.03 mGal to a final value of 1.22 mGal with 96% of mis-ties better than 1 mGal. Levelled marine free-air gravity data were then combined with land station data (as Bouguer anomaly values at 2.67 Mg/m^3) and gridded at a node interval of 2 km. A grid computed from the free-air gravity data as derived from satellite altimetry (Sandwell, 1992, Carlowicz, 1995) was used to complete the coverage to the west.

Densities of 2.2 Mg/m^3 and 2.75 Mg/m^3 were adopted for calculating offshore Bouguer correction values using a 3D method (ie. including terrain effects). These densities are considered appropriate for resolving features over the shelf and deeper water areas respectively (see discussion in reports accompanying BGS Image Atlas volumes 9, 10 or 11). The corrections were then added to the free-air gravity anomaly data to give Bouguer gravity anomaly values at the respective densities. Bouguer anomaly values on land, calculated for a density 2.67 Mg/m^3, were then merged with the offshore data for gridding at a node spacing of 2 km.

The satellite data were corrected and gridded independently and the two grids spliced together, using the satellite gravity where the marine survey coverage was poor.

The final grids were sub-sampled to a node spacing of 1 km.

2.5 Magnetic data

Magnetic point data (see Map 3, Annex A4, for their distribution) were edited to remove spikes, dropouts, and other spurious values. The marine dataset was then upwardly continued to 450 m to match the height adopted for the aeromagnetic data.

Mis-ties in the combined marine and airborne magnetic anomaly dataset were reduced from initial RMS errors of 23.01 nT to 12.57 nT (with 96% of mis-ties better than 10 nT) prior to generating a grid at a node spacing of 2.4 km from the levelled dataset.

Separate grids were assembled from *The Arctic and North Atlantic Oceans Magnetic Compilation (GAMMAA5: Geological Survey of Canada):* and a magnetic compilation for the Irish mainland from PAD/Geology Survey of Ireland. These were spliced together with the levelled marine + airborne magnetic anomaly in such a way as to retain the maximum anomaly resolution.

The final grid was sub-sampled to a node spacing of 1.2 km.

2.6 Data quality

The process of gridding inevitably tends to smooth out the higher frequency signals present in the along-track data as these are much more closely spaced than the distance between lines. Even in a high resolution survey, with line separations of only a few hundred metres, some high frequency signal will be lost by gridding although grid nodes close to valid data points will be reliable.

For this project the individual datasets had quite different specifications and for the area as a whole it was appropriate to adopt a grid node interval of 2 km, making allowance for the more sparsely covered areas. The result of this is that any anomaly with a wavelength of less than approximately 4 km will suffer from under-sampling, with the consequent possibility of aliasing. For the purposes of further processing, all the final grids were sub-sampled to a node interval of 1 km and, for presentation, interpolated again to 0.5 km. This reduction in grid node interval clearly adds nothing to the information content as such.

In the case of the satellite gravity data there is a further loss of resolution, first because the altimetry data themselves are effectively averaged over an area of about 7x4 km and, second, as a result of the processing needed to extract the free-air anomaly values as such. Comparison of satellite and marine gravity data indicates that the former tend to distort the shape of anomalies somewhat and are limited to resolving wavelengths of no less than about 15 km.

The externally sourced magnetic grids have another level of uncertainty attached in terms of understanding the processing procedures followed. In particular, the Geological Survey of Canada's data are part of a much larger compilation and the processing will not necessarily have been best suited to this area, bearing in mind the additional data available for this project.

3. GRID PROCESSING

The basic working grids were subject to a variety of additional smoothing and filtering operations using in-house BGS software, both to improve the appearance of the images produced from them and to generate additional parameters for display. Most of these operations involve Fourier transformations (ie. working in the frequency domain) with the exception of simple functions such as horizontal gradients. Grid augmentation of ≥20% was applied to the working grids to minimize any distortion as a result of edge effects when using Fourier operators.

The problems associated with gridding gravity and magnetic datasets are well documented. Along-track information is closely sampled whereas line separations are often large in relation to the required anomaly resolution. Thus, the effects of data sampling are sometimes seen in the images as linear trends (including 'bull's eyes' and 'string-of pearls' anomaly characteristics) which coincide directly with ships' tracks or flight lines. A balance has to be reached between over-smoothing features of interest as against leaving too much 'noise' in the output or mis-representing anomalies as a result of under-sampling (ie. aliasing). The approach adopted here has been to retain as much 'signal' as possible, accepting that some noise effects will remain but without degrading the overall appearance unduly. Increasing water depths are equivalent to raising the observation surface and they similarly lead to an attenuation of high frequency content in the anomaly pattern - this should be distinguished from the loss of character resulting from wider line separations.

A particular problem encountered with the original gravity anomaly grids arose from the systematic change in data quality and anomaly resolution from the more detailed land data in the east to the satellite data in the west. The latter show a dimpling effect with a wavelength of 10-20 km which is considered to be an artefact of the procedure by which they are derived from the satellite altimetry. Also, where the marine survey coverage becomes sparser, the anomaly resolution decreases overall and individual, line specific effects are more apparent. Land survey data tend to exhibit higher frequency noise characteristics which can reflect variations in superficial geology as well as survey quality.

In order to accommodate the different smoothing requirements across the gravity anomaly grids as a whole, whilst avoiding any abrupt changes in filter characteristics at survey boundaries, a variable upward continuation procedure was adopted. This technique involved generating an equivalent source distribution to reproduce the grid values as compiled initially followed by calculation of the gravity values at a new observation surface above this. The output observation surface was varied from a height of 300 m over Ireland, increasing steadily from 500 m to 1 km westwards across the continental shelf and then to 2 km in the area covered by satellite data (ie. from near the shelfbreak). These 'continued' grids were taken as the starting point for all further processing.

The original total field magnetic anomaly grid was re-sampled from 1.2 km to 1 km node spacing for consistency with the other datasets. Residual high frequency noise in the working grid was removed by applying a light smoothing filter within the EarthVision package (Dynamic Graphics). The reduced-to-pole magnetic field (calculated for a contemporary field inclination of 68.7° and declination 13°W), as used for most of the magnetic anomaly images has, in effect, been subject to further smoothing by application of the transformation filter.

A list of the grids used in creating the images and supplied to Group members, together with a brief description of what they represent is provided in Annex A2. The rationale behind the use of these grids is also discussed below in relation to the images themselves.

4. IMAGE PROCESSING

4.1 Data display

All images and maps were generated by the BGS proprietary *COLMAP97* colour image production system. However, the composition facility 'zcmp' within the ZEH plotting software was utilized in order to add the location map and the ARK and RSG logos to the legends for the final outputs in-house. As noted in Annex A3, this caused some difficulties subsequently when distributing the CGM plot files to group members because the 'zcmp' utility was less widely used than expected.

The processed data grids have been displayed mainly in the form of coloured, shaded-relief images. Colour is assigned initially on the basis of anomaly amplitude, with these basic colours then being modulated to simulate shading effects proportional to the local field gradients. The effect is equivalent to treating the anomalies as a topographic surface, illuminated for a specific sun angle. Shading is particularly useful for enhancing the subtle trends contained within the anomaly gradients and allows different trends to be emphasized by changing the direction of 'illumination'.

In most cases, colours have been assigned in a non-linear way, approximating an equal-area distribution over the image as a whole. This helps to discriminate the small variations in regions of slacker gradients which would otherwise be lost with a linear colour scale. Some adjustments to the actual equal-area values were made to avoid the tendency to generate relatively large, concentrated blocks of colour at the extremes of the scale.

Line contours are invaluable for quantifying the colour range and for conveying the 'true' anomaly gradients in so far as they are based on a linear scale where practical. Note, however, that to minimize problems caused by the large dynamic range and variable frequency distribution of the magnetic anomalies, a stepped linear scaling (rather than automatic contour thinning) has been used on some maps ie. the line contour interval is fixed over specific sections of the range, but increases at higher anomaly values. This helps in resolving the line contour information and in maintaining visibility of the underlying colours, accepting that the representation of gradients varies between the different sections.

Of necessity, a selective approach has been adopted to limit the number of maps designed for 'hard-copy' output but the grid files themselves can be used as input to commercial imaging software (eg. ER Mapper) which allows interactive on-screen viewing of changes in the display parameters. The illumination direction varies between images, recognizing that no one direction is ideal for highlighting all the trends which can be seen. Similarly, different colour scales are included to illustrate the advantages of varying these parameters.

The maps have been designed for plotting at a scale of 1:1M. There is some advantage in standing back from the hardcopy output to get a better perspective; it can also be useful to compare hardcopy with the more compressed images as viewed on screen which sometimes show 'lineaments' more clearly.

The descriptions that follow are intended as a guide to the type of information that can be extracted from the images but they do not cover all the features of potential interest. It is assumed that reference will be made to the relevant images in order to appreciate specific points made in the comments on the different maps. ***Those images included as part of the selection in Annex A4 are indicated by an asterisk in the headings.***

4.2 Description of images

Map 1: (*) Bathymetry/topography image with 2D modelled profile locations

This image has been produced as a colour-filled contour image. Figure 1 illustrates the form of the data but in a somewhat different style from Map 1 itself. Shaded relief is not very helpful where there are large areas with long slopes and/or little variation compared to the overall range in value and in this case it serves only to emphasize 'noisy' aspects of the grid.

Apart from relation to aspects of the underlying geological structure, bathymetry data are used explicitly in both 2D and 3D modelling and they are also needed for calculating the Bouguer anomalies and isostatic corrections. Thus, any errors in the bathymetry will be propagated into the processed data and their interpretation.

Bathymetry is especially important in respect to the gravity data as the low density of sea water means that it can generate large anomalies: as a guide, a change of 100 m in the water column is equivalent to about 5 mGal (for a density contrast of 1.2 Mg/m^3 with the adjacent sediments). These anomalies are seen directly in the free-air anomaly maps as no topographic corrections are included at this stage. In fact, the influence of a large body of water, such as that within the Rockall Trough, is much less than might be expected because the reduced mass near the surface is offset to a first approximation by thinning of the crust at depth. This relates to Airy's hypothesis of isostasy whereby the crust is considered to 'float' on the underlying mantle so that the loading at a level beneath the deepest part of the crust is constant laterally. Nevertheless, significant effects can be seen, more especially over localized features such as seamounts and where rapid changes in water depth occur eg. crossing the shelfbreak.

Bouguer gravity anomaly values are corrected for bathymetry by allowing for the difference in density between the water and the underlying sediments: on land, this becomes the difference between the rock forming the topography and the surrounding air - a mass excess rather the deficit off shore. Note also that off shore the observation surface remains constant (ie. at sea level) whereas on land it usually follows the ground relief. The bathymetry is also used in estimating crustal thicknesses by assuming an Airy isostatic model in which sea water is the only significant loading factor. This, in turn, forms the basis for calculating the isostatically-compensated Bouguer gravity anomaly values.

The control on bathymetry is generally good over the continental shelf where the relatively low relief means that few artefacts would be expected at the mapping scale of 1:1M. However, there is some doubt about the reliability of the data over the Porcupine High where the available marine survey lines were more widely separated. The final grid here was based on the marine data although the GEBCO97 contouring is somewhat different. Some errors are also to be expected over the shelfbreak where the gradients are especially steep along parts of the eastern margin of the Rockall Trough and where major canyons, both transverse and longitudinal to the slope are known to occur. The reliability of the GEBCO97 data in the more remote western half of the project area is thought to be relatively good, given the more limited coverage.

Care is needed when processing the bathymetry data to avoid artefacts in the form of 'overshoots' generated by the gridding algorithm. Ground relief is inherently a less smoothly varying function than a potential field and problems occur, for example, where flat-bottomed valleys have steep sides. Some interactive grid editing was done to remove the more obvious examples of this near the shelfbreak north of Porcupine Bank.

It can be seen that the shorter profiles selected for 2D modelling lie over the margins of the Rockall Trough where the changes in bathymetry are most severe.

Map 2: (*) Location map of digital data points taken from marine gravity survey tracks

The individual points from gravity survey data subject to network adjustment are indicated as crosses: in many cases these merge to appear as lines when plotted at 1:1M scale but in some cases the sampling is more sparse.

The land data from Ireland are not shown for reasons of confidentiality. Satellite data points have also been excluded because the close network of tracks along which values have been calculated gives a misleading impression of the information content. The tracks themselves form closely intersecting sets which trend approximately NNW-SSE and SSW-NNE.

It can be seen that the available marine survey coverage becomes rather sparse in the western half of the project area and the line selected for splicing in the satellite grid lies close to or inside the shelfbreak along the Irish margin of the Rockall Trough. Additional detailed surveys, not available for this compilation, do exist but these would probably not greatly improve the appearance of images over the Rockall Trough/Plateau at the regional scale used for this project. In principle, better results are achievable by controlling the satellite grid with the existing marine lines but there were no means for doing this efficiently.

Map 3: (*) Location map of digital data points taken from magnetic survey tracks

As in Map 2, only the point data, adjusted as part of this compilation, are displayed. Values imported from existing grid compilations (eg. over Ireland and the western third of the project area) are excluded because they give no indication of the distribution of the data from which they were derived. The Canadian grid is supplied at node interval 5 km and the original data have been subject to a variety of adjustment and filtering processes in achieving the final product. In some areas, including the Rockall Plateau, directional filtering was applied. When looked at in greater detail this is seen to have exaggerated the degree of correlation along SW-NE trends within the Rockall region.

The magnetic survey coverage is better than that for the gravity data allowing the line along which the Canadian compilation grid was spliced in to be placed west of 15°W. Thus, much of the Rockall Trough lies within the area of the survey data set.

Map 4: (*) Free-air gravity anomaly image (Bouguer anomaly values on land)
[in full colour; shaded-relief illumination from the west]

Illumination from the west brings out most of the anomaly trends to be seen in this dataset, including those cross-cutting the Rockall Trough. With the vertical exaggeration used, the long 'shadows' cast by some of the larger anomalies results in loss of detail but this is offset by the ability to see the smaller features elsewhere.

As noted above, the free-air anomaly grid has been smoothed by a variable continuation process. This retains more of the high frequency signal to the east, although the Bouguer gravity anomalies over land have also been attenuated somewhat to emphasize regional features such as the SW-NE Caledonoid trend. The published 1:1.5M gravity anomaly map covering Britain, Ireland and adjacent areas (BGS, 1997) shows a little more of the detail. Distinctive gravity anomaly lows

occur along the west coast over the Donegal and Galway granites whereas the anomaly low further south is associated with the thick Devonian sequence of the Munster Basin.

The amplitude range of the gravity anomalies increases markedly beyond the Irish inner shelf region with a combination of shallow, dense basement rocks and igneous centres being responsible for the anomaly highs. Most of the known basins are associated with gravity anomaly lows as would be expected, although their impact is often relatively subdued in the images at this scale of presentation. Thus, the North Celtic Sea Basin, North Porcupine Basin, Slyne Basin and Malin Basin can be identified to some extent. The Main Porcupine Basin has a more dramatic appearance with a central gravity anomaly high separating deep flanking anomaly lows. This geometry bears little relation to the sedimentary structure to a depth of about 8 km and is only superficially linked to the Porcupine Median Volcanic Ridge or bathymetry: without the seismic evidence it would be difficult to reach the correct model from the gravity data alone. Gravity anomaly values in the Seabight Basin also remain relatively high despite the continuation of a thick sedimentary sequence, indicating the presence of highly attenuated or dense underlying crust.

Further west, the influence of changes in bathymetry on the free-air gravity anomalies is clearly seen in the strong gradients over the shelfbreak. Shelf margins often show a characteristic free-air gravity anomaly signature. This is an expression of the interaction between changes in bathymetry, sediment and crustal thicknesses which, in turn, reflect changes in the nature of the crust and the sedimentation processes as the margin developed. Temperature is an important influence on crustal rigidity and the degree of isostatic balance maintained: thus, in the initial phases of rifting an Airy model with zero elastic thickness is often appropriate whereas with subsequent cooling, and the displacement of sea water by sediment, the additional loading may not result in a proportionate change in local crustal thickness. The influence of magmatism and associated underplating represents a further level of complication in the case of the north-east Atlantic margin.

The simplest signature for a passive margin has a free-air gravity anomaly high on its shelf side and an anomaly low on the oceanic side, with an overall amplitude of perhaps 200 mGal. (Note that, for present purposes, the highly-attenuated continental crust under the Rockall Trough is equated with oceanic-type crust.) However, in this part of the Rockall Trough, both margins show free-air gravity anomalies with somewhat lower amplitudes (closer to 100 mGal) together with evidence of secondary gravity anomaly ridges within the trough itself. This pattern is similar to that predicted with a weak crustal rheology on both sides of the margin (Watts, 1995). Another possible influence on the longer wavelength gravity anomaly pattern is suggested from the interpretation of data from the RAPIDS seismic experiment. O'Reilly *et al.* (1996) describe evidence for serpentinization of the upper mantle beneath the Rockall Trough where sea water has penetrated along fractures though the attenuated crust. The inference is that, as with the Porcupine Seabight Basin, the gravity anomaly pattern within the trough is not simply an expression of sedimentary basins and basement highs.

A distinctive free-air gravity anomaly high near the south-western end of the Rockall Trough (in Quadrant 100) is associated with somewhat shallower waters. This is an area of igneous activity with intrusions and the Barra Volcanic Ridge System nearby. The latter are linked with magnetic anomaly highs whereas they tend to correlate with local troughs rather than ridges in the gravity anomaly field. As noted below, there appears to be a more widespread inverse correlation between gravity and magnetic anomalies within the Rockall Trough.

The Charlie-Gibbs Fracture Zone does not show as a prominent feature at this scale. The change from continental to oceanic crust does not inevitably mean a large contrast in physical properties such as bulk density and the discontinuity in anomaly pattern is best seen when viewing a larger

area. Similarly, there is more evidence of the putative Clare Lineament in the additional coverage provided by the full working grids.

The Rockall High is thought to comprise continental crust of near normal thickness, consistent with the shallow water depths. High gravity anomaly values are linked to basic intrusions and shallow basement with only a thin sedimentary cover sequence. Further north-west, anomaly values reduce again into the Hatton Basin where thicker sediments can be identified in seismic data.

Map 5a: Horizontal gradient of free-air gravity anomaly (Bouguer anomaly on land) [in full colour; shaded-relief illumination from the north-west]

Horizontal gradients reach a local maximum over linear discontinuities such as faults and the upper margins of more localized anomalous bodies such as dense basic igneous centres or sedimentary basins of relatively low density. The value used here is the magnitude of the horizontal gradient so there is no sense of direction into or away from an anomaly high/low. Note that a feature such as a gravity anomaly ridge will now be represented by maxima over both flanks in the horizontal gradient image, with a minimum (of zero) along the ridge line itself (cf. Map 4). Note also the difference from a vertical derivative map which retains more of the character of the original field (ref. Map 6).

The horizontal gradient image brings out more detail of the anomaly structure, enhancing the subtle features partly revealed by applying shaded relief to the original image. This also emphasizes the additional resolution available with the better data coverage in the east, for example in comparing the response over the Rockall High with that from the inner Irish shelf.

Map 5b: Horizontal gradient of free-air gravity anomaly (Bouguer anomaly on land) [in blue-red colour; shaded-relief illumination from the north-east]

This image is based on the same grid as Map 5a but uses a different colour scale and the illumination direction is changed to bring out other trends. Detail in the amplitude variations in the gradient is not usually especially informative and reducing the amount of colour variation focuses attention more on the structural details, even if at first sight the image appears to have less visual impact.

Map 6: Residual free-air gravity anomaly from 10 km upwardly continued field [in full colour; shaded-relief illumination from the west]

There is a variety of techniques for generating residual anomaly maps, the aim being to remove the longer wavelength, background variations assumed to originate from deeper sources and so to highlight the nearer-surface features. Vertical derivatives serve this purpose. They are often very effective where the data are of high quality though, otherwise, they can appear noisy. High-pass or band-pass filters, based perhaps on an analysis of power spectra, can be used for focussing on specific features. The removal of a low-order trend surface, generated either as orthogonal polynomials or by any standard grid smoothing package, is another alternative.

The approach adopted here is to smooth the field by upward continuation and to subtract the result from the original field: the output is similar to a smoothed first vertical derivative, taken over a finite distance. The subtracted field becomes smoother as the continuation distance is increased and so the residual retains more of the original anomaly. Conversely, taking a small continuation distance leaves only the higher frequency (ie. shorter wavelength) anomalies in the residual. A

value of 10 km was adopted here, to give an intermediate degree of filtering and avoid over-emphasis on the higher frequencies which are not well specified with this dataset.

Map 7a: (*) Isostatically-compensated Bouguer gravity anomaly (at 2.75 Mg/m^3) [in full colour; shaded-relief illumination from the north-west]

The Bouguer correction is almost invariably applied to land-based gravity data in order to reduce to strong correlation with local topography seen in the free-air anomaly data. In marine gravity surveys the problem is less acute in that the observation surface now remains fixed, at sea level, and the seabed relief is more distant. The Bouguer correction works well in shelf areas where relief on the sea floor is usually of relatively small amplitude, cut into the more recent sediments.

Where deeper water occurs, more particularly beyond the shelfbreak, Bouguer anomaly maps usually show a strong inverse correlation with bathymetry. This follows from the fact that the sea water effect (as allowed for in the Bouguer correction) is partially compensated at depth by crustal thinning. In oceanic areas this means that the free-air anomaly itself (ie. not the Bouguer corrected value) is close to zero where isostatic balance is achieved. Thus, a further correction has been applied, removing the gravity effect attributable to changes in the depth to the Mohorovičić Discontinuity (Moho) based on a modified Airy-root model of isostatic compensation for relief on the ground surface (ie. at seabed in off-shore areas). Note that this compensation only takes account of the effect of a ground surface varying relative to sea level: *it does not make any allowance for the change in loading between areas with deep basins as against basement highs.*

In assigning a density to the Bouguer correction the value appropriate to the formation into which the relief is cut is usually applied. This is, typically, 2.2 Mg/m^3 for the UK continental shelf. However, in areas such as the Rockall Trough, the main body of water is effectively replacing basement with a density of perhaps 2.75 Mg/m^3 rather than Cenozoic sediments. This difference in density has a noticeable affect on the ability to resolve specific features in the anomaly pattern such as basins near the shelfbreak, more especially when a further correction has been applied to compensate for the predicted changes in crustal thickness across the margins.

The contribution from the base of the crust has been calculated assuming an elastic thickness of 5 km whereas for true Airy isostatic compensation this thickness is 0 km. By assigning some rigidity to the crust the loading effects are distributed more widely and the resulting model for the Moho has a smoother form. This was used in part in recognition of known departures from the Airy isostatic response as deduced from deep seismic experiments over the UK and Irish shelves. A standard crustal thickness of 30 km (ie. for ground level at 0 km) was assumed, with a density contrast of 0.4 Mg/m^3 across the base of the crust. The sea-water replacement density for calculating the change in load was set at 2.5 Mg/m^3 rather than the Bouguer reduction density. Again, this was done to make some allowance for the fact that the crustal thickness is not simply a reflection of the ground surface relief, the implication here being that some of the load is offset at deeper levels within the aesthenosphere. (Note that grids with the same reduction and compensation densities are included as part of the digital data set.)

This image at the higher reduction density should be compared with the free-air anomaly (Map 4) and the compensated Bouguer anomaly at the lower density (Map 8) to appreciate the effects of changing the reduction parameters. As the Moho contribution originates at depth its gravity effect is relatively smooth and the result is to modulate the datum to which the Bouguer anomalies are referred. The adjustment in levels is obvious as a change in colour balance between the three maps. In this case the higher Bouguer reduction density is under-compensated, leaving a positive bias to

the anomaly values over the deeper waters in the western half of the map. In effect, we are defining a regional background field which is then used to generate a specific type of residual anomaly map.

Map 7b: Isostatically-compensated Bouguer gravity anomaly (at 2.75 Mg/m^3) [in full colour; shaded-relief illumination from the north-east]

The change in anomaly datum over the trough allows the shading to bring out more continuity in some of the lineament trends and the difference with illumination direction is more marked in comparison with the free-air anomaly images. This image emphasizes a number of distinctive features cutting across the trough along (north-)north-west trends. It also gives a more obvious sense of the Charlie-Gibbs Fracture Zone and Clare Lineament.

The occurrence of large isostatic gravity anomalies within the Rockall Trough itself is perhaps surprising and there is no evidence at this time that they relate directly to the upper, sedimentary part of the sequence: their possible origin is discussed further in the context of the 3D modelling results (Section 6).

Map 8: Isostatically-compensated Bouguer gravity anomaly (at 2.20 Mg/m^3) [in full colour; shaded-relief illumination from the north by east]

As discussed in relation to Map 7a, the reduction density of 2.2 Mg/m^3 is expected to give the best representation of anomalies over the shelf areas. The same crustal root model was applied as in maps 7a and 7b: thus, with the load correction density now being higher than the Bouguer reduction density there is over-compensation for the deeper waters, leaving the adjusted anomaly values with a negative bias here. This allows the Bouguer correction to account for local variations in water depth relative to the sedimentary cover whilst accepting that this probably under-represents the effective mass deficit within the Rockall Trough.

The main interest of these images lies in the qualitative differences in anomaly pattern over the margins of the Rockall Trough rather than in the anomaly values as such. As an example, compare the response off the western flank of the Porcupine High in quadrants 74, 75, 82 and 83, where a more prominent ridge/trough anomaly pattern is seen with the higher Bouguer reduction density. If this geometry is not reflected in the geological structure there may be problems with the bathymetry data, or the crustal thinning could be displaced relative to the shelfbreak.

It is also noticeable that there is a more distinct change in compensated anomaly value across the Charlie-Gibbs Fracture Zone when the same reduction and load densities (at both 2.2 Mg/m^3 and 2.75 Mg/m^3) are used. The change in value over the Porcupine Abyssal Plain is less obvious with the intermediate load density adopted for maps 7 and 8

Map 9a: (*) Horizontal gradient of isostatically-compensated Bouguer gravity anomaly [in full colour; shaded-relief illumination from the north-west]

The overall appearance of the image of horizontal gradients is less obviously affected by the isostatic compensation procedure (cf. Map 5a) but, in detail, it can be seen that significant differences are present, more especially near the shelfbreak (compare, for example, the data in quadrants 5, 11,12,18,19). This becomes important in assessing specific features such as the Erris High/Basin system. Apart from resolving more detail, the compensated data also provide a check on data quality as they will tend to exaggerate any inconsistencies between the gravity and bathymetric datasets.

Map 9b: Horizontal gradient of isostatically-compensated Bouguer gravity anomaly [in blue-red colour; shaded-relief illumination from the north-east]

The amplitude information has been limited by reducing the number of colours. This is designed to give more focus to the structural content. Use of the orthogonal illumination direction relative to Map 9a has the effect of suppressing north-easterly trending features. Note, also, that some of the more diffuse lineaments with longer wavelengths which may be recognized in the basic anomaly images are less obvious in the gradient maps.

Map 9c: (*) Horizontal gradient of isostatically-compensated gravity potential [in full colour; shaded-relief illumination from the west by north]

The gravity potential is not widely used in this type of study but it can provide additional insight in the longer wavelength aspects of the data. The acceleration due to gravity, the parameter measured in gravity surveys (and from which the free-air and Bouguer anomalies etc. are derived) is the vertical derivative of the gravity potential. Thus, by integrating the anomaly field, an estimate of the variation in the originating potential can be obtained. This is also closely linked with the geoid. There are also similarities with the approach used in Map 18 for looking at deeper structure in the magnetic anomaly data.

The image shows the horizontal gradient of the potential, as calculated by integrating the compensated Bouguer gravity anomaly (at 2.75 Mg/m^3). As before, the gradient highs (ie. red colours) will tend to demarcate discontinuities and the margins of anomalous masses, but looking more at the deeper-seated trends; gradients close to zero (ie. blue colours) occur near anomaly turning points such as ridge/trough axes and where the field varies only slowly. As with maps 9a and 9b, it is helpful to compare this image with Map 7a in order to appreciate the shift in anomaly location relative to the source.

Map 10: 10 km continuation residual of Bouguer anomaly (isostatically-compensated) [in full colour; shaded-relief illumination from the north by east]

The procedure for generating this residual is the same as that used for Map 6 and the overall appearance of the maps is similar - as would be expected given that the Bouguer and isostatic correction terms are dominated by the longer wavelengths components. Differences are seen in detail, more especially near the shelfbreaks.

Map 11: Euler deconvolution solutions from isostatically-compensated gravity data

Deconvolution techniques provide one approach to determining the location of the source of any particular anomaly, including its depth. They depend upon a specific mathematical formulation which approximates the true nature of the sources as found in reality: the extent to which the approximation is valid determines the reliability of the outcome. Some further details regarding the Euler deconvolution as used here are given in Annex A7.

The parameters adopted in calculating the solutions for this map were designed to look at the larger-scale features, using a 20 km window to help suppress the effects of noise. No attempt was made to focus the solutions more specifically by, for example, only accepting points close to a local maximum in the anomaly gradient: the less well constrained solutions can help in maintaining the continuity of trends in plan view, even if the depths are poorly constrained. Each solution is represented by a line, colour-coded according to depth. The line is oriented to be orthogonal to the local horizontal gradient with a length proportional to the magnitude of the total anomaly gradient at that point.

Solution depths are not considered to be reliable in absolute terms although the relative values (ie. shallower/deeper) are indicative. Thus, the Porcupine Basin and the Rockall Trough do contain most of the deeper solutions. The somewhat disjointed nature of the overall pattern is probably a reflection of the interference between cross-cutting north-east and north-north-west trends as much as any problem with the field data themselves. Nevertheless, solutions do appear to be in sharper focus in the east where the gravity anomaly field is better defined.

The Charlie-Gibbs Fracture Zone appears to be associated with a band of more diffuse solutions, whereas some more specific sets can be linked to features such as the Erris High, the western margin of the Slyne Basin and other basins near the margin of the Porcupine High. Shallower solutions occur over the Rockall High with an increase in depth towards the Hatton Basin. Shallower solutions observed within the Rockall Trough can be attributed to structure affecting the Tertiary sediments.

Map 12: Total magnetic field anomaly (as compiled at 450 m)
[in full colour; shaded-relief illumination from the north-west]

The magnetic anomaly pattern often shows more character than the gravity field because of the larger range in magnetization as compared to density, and because the magnetic sources are intrinsically dipolar rather than monopolar. These factors are important in understanding the magnetic anomaly pattern in that a single source gives rise to an anomaly with both positive and negative components. Whereas the gravitational force can be considered as always directed towards the centre of the earth, the inclination of the external magnetic field varies systematically between -90° and +90° and the total field direction may deviate locally in the vicinity of strongly magnetic rocks. In relatively high, northern latitudes the positive component of the anomaly is usually the more concentrated and of higher amplitude, with a more diffuse negative response around it, especially to the north (NB: the response also depends on the dip of the source body). This assumes that the magnetization is predominantly *induced* by the earth's present-day magnetic field according the magnetic susceptibility of the rocks present.

Some rocks such as Tertiary intrusives and volcanics, can retain a strong *remanent* magnetization locked into the crystal structure at a time when the earth's magnetic field was oriented in a different direction. The observed anomaly represents the vector addition of any induced and remanent components of magnetization. Tertiary igneous centres provide a good example of the differences between the gravity and magnetic responses. Almost invariably the bigger, basic bodies give rise to large gravity anomaly highs which are approximately circular in form.

Typically, late Cretaceous - Palaeogene centres were formed when the earth's magnetic field was reversed relative to the present day but at a similar palaeo-latitude: in such cases, and where their remanent magnetization is significantly larger than the induced effect, the result is a predominantly negative observed anomaly. The situation is often complicated by separate phases of activity occurring over a period when the earth's field changed between normal and reversed directions. Also, basaltic lavas associated with the centres can provide an additional, strong response. Where these occur in shelf areas at relatively shallow depths, Tertiary lavas are often characterized by a noisy magnetic anomaly pattern with a negative bias (eg. around the Faeroe Islands) from short wavelength, high amplitude variations. In deeper waters, or where buried beneath thick sedimentary cover, the basalt signature is smoothed and becomes difficult to distinguish from sources in the basement. The effects of induced magnetization usually predominate in the latter.

The total magnetic field anomaly data for the Irish Rockall area have been compiled at an effective observation surface of 450 m above sea level. Taken together with data distribution factors and the

gridding and processing procedure, this has had the effect of smoothing out some of the higher frequencies, as seen in Map 12, more especially over land and shelf areas to the east.

South-west - north-east Caledonoid trends are clearly visible but, as with the gravity anomaly images, there is also evidence of significant cross-cutting structure. A number of examples of an inverse correlation between gravity and magnetic anomaly responses occur. Thus, over the Porcupine Basin, there is a deep, extensive magnetic low coincident with the large gravity anomaly high: a similar relation holds for anomalies in the centre of Quadrant 100 (cf. maps 20 and 21). Features such as the Charlie-Gibbs Fracture Zone are expressed more by changes in anomaly trend across them rather than by direct association.

The distinctive magnetic anomaly high within the Rockall Trough near the centre of Quadrant 76, linked to a compressional structure seen to affect the Tertiary sequence in the seismic data, has no associated gravity expression. It marks the north-east limit of a number of stronger magnetic anomalies seen within the trough whereas further north-east, excepting the Hebrides Terrace Seamount, the anomalies tend to be more subdued. There is evidence that the magnetic anomaly in Quadrant 76 lies close to the line of a major discontinuity extending north-west through the deep magnetic anomaly low in Quadrant 93 and south-eastwards through the North Porcupine Basin. Other lineaments of this type appear to be present but it is useful to view a larger area than that covered by the current project when assessing their reality.

Map 13: (*) Reduced-to-pole magnetic anomaly (as compiled at 450 m)
[in full colour; shaded-relief illumination from the north-east]

Reduced-to-the-pole values were calculated assuming induced magnetization only and so the response over some Tertiary sources (igneous centres, lavas etc) may be distorted unless their magnetization direction is simply reversed relative to the present-day field. Superficially, the resulting image is similar to the total field response (Map 12), bearing in mind that some of the change reflects the difference in illumination direction. With a polar (ie. inclination 90°) inducing field, the maxima tend to increase in amplitude and migrate northwards, with some modification of the flanking gradients. In general, the anomalies now appear in slightly sharper focus. For example, the magnetic anomaly high in the Quadrant 44 has a clearer along-axis trend linking it directly to the southern section of the Porcupine Median Volcanic Ridge. The response along the eastern margin of the Rockall Trough also shows a more continuous zone of steepened gradients.

It is not always easy to recognize igneous centres on the basis of their magnetic character alone as sources within the basement can also give rise to large anomalies. The reversed polarity over the Hebrides Terrace Seamount and the Blackstones Bank igneous centre is a good indicator but with the localized positive anomalies elsewhere the source is more ambiguous. The 'Brendan Centre' does not stand out especially and it seems to comprise a number of discrete components. Other anomalies can be associated with known structure. For example, there is an extended magnetic anomaly high over a section of the Erris High on the boundary of quadrants 11 and 12, with larger anomalies on the south-east margin of the Erris Trough.

Map 14a: Horizontal gradient derived from reduced-to-pole magnetic anomaly
[in full colour; shaded-relief illumination from the north-west]

The horizontal gradients highlight shallower structure and the variety of trends present within the data. Gradients are noticeably slacker in the more northerly section of the Rockall Trough and over south-west Ireland and the Celtic Sea areas. South of the central magnetic anomaly high in Quadrant 76, a broad, arcuate belt of shorter wavelength, higher amplitude gradient anomalies

sweeps west-east across the trough, taking a more north-easterly heading over the Irish shelf and mainland. The relatively few north-south trends seen are mainly restricted to the south of this zone.

A distinct change in anomaly character over the Rockall Plateau in the north-west of the image is linked to data quality. The marked loss of high frequency character and complexity across Quadrant 93 and west of Quadrant 94 is expected from the coarser nature of the original grid spliced in from the Canadian compilation to the west. There is an inherent filtering effect further south where the water is deeper (ie. the magnetic sources are further from the observation surface) which partly masks the change in data distribution.

Map 14b:(*) Horizontal gradient derived from reduced-to-pole magnetic anomaly [in blue-red colour; shaded-relief illumination from the north-east]

As used in earlier images, the more limited blue-red colour scale gives a different emphasis to the data and the perception of anomaly patterns. The strongest gradients are clearly concentrated along the western margin and north-east corner of the image, with some isolated examples elsewhere.

Map 15: Reduced-to-pole magnetic anomaly upwardly continued by 2.5 km [in full colour; shaded-relief illumination from the north-west by west]

Upward continuation of the data by 2.5 km has the effect of smoothing the magnetic anomalies, acting as a form of low-pass filter. This emphasizes the deeper, underlying trends including the persistence of Caledonoid trends over the length of the Rockall Trough. The easterly offset in the eastern margin of the Rockall Trough around the around the northern end of the Porcupine High is paralleled by a magnetic anomaly ridge separating the North and Main Porcupine basins. The extension of this latter ridge to the west leads to a prominent magnetic high of unknown origin. There is no associated gravity anomaly high to suggest it represents an igneous centre and the absence of any obvious negative magnetic component is consistent with an older source within the basement. The north-easterly trends also seen in this area may, in fact, be more significant in terms of structural relationships.

Map 16a: (*) Residual RTP magnetic anomaly from 2.5 km upwardly-continued field [in full colour; shaded-relief illumination from the north-north-west]

Upward continuation of the data by 2.5 km rather than 10 km (as when calculating the gravity anomaly residuals) raises the threshold of the high-pass filtering effect, recognizing the higher frequency content of the magnetic data.

The extra resolution of the anomaly pattern helps in isolating specific features such as the southern end of the Porcupine Median Volcanic Ridge and detail associated with the Hebrides Terrace Seamount and the Erris High. It also emphasizes those areas with little magnetic variation in contrast to others of more intense activity such as the east-west trending belt passing through the northern end of the Porcupine High.

Map 16b: Residual RTP magnetic anomaly from 2.5 km upwardly-continued field [in grey scale; shaded-relief illumination from the west by south]

While colour overlays are useful in conveying amplitude information they can distract from the finer structural detail within the shaded-relief presentation itself. The limited blue-red colour adopted for some of the images of horizontal gradients partly addresses this issue, but grey-scaled images go one step further. This type of display also provides a useful check on data quality and the change in frequency content over the image as a whole.

Map 17: Magnitude of analytic signal from 1 km upwardly continued magnetic field [in full colour; shaded-relief illumination from the west-north-west]

The analytic signal (as referred to in the literature in recent years in techniques for estimating source depths) is a vector quantity defining the full anomaly gradient including both horizontal and vertical components. The value displayed here is its magnitude. Vertical derivatives are more susceptible to noise in the source data and the ability to define gradients reliably depends on factors such as the gridding interval, degree of smoothing applied and on the original data distribution.

For shallower sources the analytic signal is at a maximum over the edges of the causative bodies but with increasing depth (relative to width) or loss of high frequency signal content, the form of the original anomaly is retained. The shape of the analytic signal anomaly itself is a measure of the source depth.

As with the horizontal gradient images, it should be remembered that by using anomaly magnitudes any sense of the relative highs and lows in the original magnetic anomaly pattern has been lost: all gradients are plotted as positive values.

Map 18: (*) Horizontal gradient of magnetic pseudo-gravity transformation [in full colour; shaded-relief illumination from the north-north-east]

The pseudo-gravity transformation simulates the response that would be expected if the sources of the magnetic anomaly variation were replaced by an equivalent density distribution. This results in a simpler form of calculated field which, of itself, is not usually of great interest. However, the horizontal gradients of this field can provide a good indication of the edges of sources, more particularly, those of deeper origin (ie. with longer wavelength characteristics).

A good example of the effectiveness of this procedure is provided by the gradient anomaly ridge offset by about 30 km north-west of the 1000 m bathymetry contour on the eastern margin of the Rockall Trough between quadrants 75 and 11. This ridge is now a more clearly defined feature which shows a strong correlation with the flank of the gravity anomaly high (cf. maps 4 or 7a and 9c). The horizontal gradients of the standard gravity/magnetic anomaly are less continuous because of their higher frequency content (eg. maps 9a and 14a).

Map 19: (*) Euler deconvolution solutions from magnetic RTP anomaly data

The procedure for calculating and displaying Euler solutions from the magnetic data was the same as that followed for Map 11 (see, also, Annex A7 for further details). Some adjustments were made to the parameters used, in particular to the structural index and the solution rejection criteria.

The resulting pattern of solutions is less coherent than might be hoped but the information is still considered to be useful as a guide to relative source depths and in suggesting some correlations which are less obvious in the images themselves.

Map 20: (*) Reduced-to-pole magnetic image with gravity anomaly line contours [in full colour; shaded-relief illumination from the west]

There are several ways of combining the gravity and magnetic datasets in order to show the degree of correlation between the anomaly patterns directly. Composite parameters such as the normalized sum or product of the two grids give a clear indication of where the anomaly maxima/minima coincide but low-intermediate values can arise from a variety of combinations. Another approach

is to overlay the amplitude information as colour from one grid draped over the relief derived from the other. This is effective providing the anomaly patterns are not too complex.

The technique preferred here is to overlay the line contours from one grid onto the coloured, shaded-relief image of the other. The line contours are annotated but as a further aid to distinguishing relative anomaly values a change from solid to dotted lines is made near the mean value of the dataset (ie. with lower values as dotted lines). With this style of presentation it is possible to match specific features unambiguously between the two datasets, which is not always the case when using other methods.

The degree to which an inverse correlation holds between a significant number of gravity and magnetic anomaly responses within the deeper water areas is now seen to be high. Similarly, the distinctive magnetic anomaly high on the boundary between quadrants 74 and 75 coincides with a reduction in gravity anomaly value. Other magnetic anomaly highs along the eastern margin of the Rockall High are effectively lost within the free-air gravity anomaly gradient over the shelfbreak and emerge only weakly in the isostatically-compensated images.

Map 21: Isostatically-compensated gravity image with RTP anomaly line contours [in full colour; shaded-relief illumination from the west]

Line contours give a different impression of the anomaly pattern compared to the image display: as they are based on an equal interval rather than equal area distribution they tend to preserve the gradient information better than the image itself. Thus, it is worth comparing maps 20 and 21, in which the assignments of the anomaly fields to image and line contours are reversed, to check on the representation of specific features as well as on the overall sense of how the fields relate.

5. RESULTS OF 2D MODELLING

5.1 Background

A total of eight lines was selected for modelling. Six of these were restricted to the shelf margins whereas the other two regional lines provide continuous sections across the Rockall Trough. The starting point for the models was the seismic interpretations produced as part of the Structural Nomenclature Project 97/3 (see Naylor and Shannon, 1999, for further details of the seismic data and their sources). These extended, typically, into Lower Palaeozoic or basement rocks on the shelf but picks were restricted to higher levels (Tertiary or Cretaceous) within the Rockall Trough itself.

The modelling was split between BGS (regional lines) and ARK Geophysics Ltd (shelf margin lines). As each organization used its own software, the procedures adopted and the style of presentation of the results differs somewhat. While agreement was reached on the general approach it was thought useful to retain the alternative styles as an indication of their influence on the models produced.

5.1 Methodology

Modelling of potential field data in two dimensions (2D) assumes that the structures are oriented at right-angles to the line of section and that they extend for a large distance (relative to their depth) along strike. The effect of strike-limited bodies can also be calculated reliably if they are centred on the profile. The geology is represented by polygons which define units of specified density and magnetization and a complex model can be constructed in this way. Both gravity and magnetic effects can be calculated simultaneously, within a few seconds, and adjustments to the model are usually made on an interactive basis. Optimization procedures are available for automatically adjusting the model to minimize differences between the calculated and observed fields but forward modelling is usually preferred to maintain more control over the changes made.

Free-air gravity and total field magnetic anomaly values were used as the observed data against which the models were tested. This meant that the ground surface and sea water had to be included as part of the model for calculating the gravity response. Bouguer anomalies have the advantage of reducing the influence of off-line sources near the profile but they give a rather false view of the anomalies in deep water areas and it is useful to have the option to check for and adjust possible errors in the bathymetry.

All the interpreted seismic time sections were depth converted for potential field modelling by ARK Geophysics Lrd using simple 'mean' velocities. The resulting models were then extended in depth to beyond the Moho so as to include the effects of crustal thinning directly. No regional fields as such have been removed from the gravity data on the assumption that all the observed lateral variations are attributable to sources which can be represented directly in the model: any contributions from within the aesthenosphere and below are accommodated in setting the base level.

It should be noted that potential field methods are best applied to identifying and delimiting steeply dipping bodies, that is, where strong lateral variations occur: the contributions of sub-horizontal units can only be resolved near their margins and feather-edges will rarely be detected. Thus, it is not usually possible to infer the thickness of extensive, horizontally-bedded sediments with any

certainty nor to indicate how properties vary with depth within them. The ambiguities are greatly reduced near basin margins and over basement structures.

5.2 Data limitations

It is generally considered best practice to model potential field data along profiles coincident with survey lines rather than relying on values derived from grids. This ensures that the higher frequencies are retained in the profile and that problems associated with interpolating across poorly controlled areas are avoided. However, individual lines may be subject to noise, navigation error, instrumental drift, datum shifts etc. whereas gridded data can give a more representative view providing the data coverage is reasonable. In order to utilize the seismic interpretations made available for this project it was necessary to rely on potential field values derived from the grids, except in the case of one line for which gravity data were taken from an adjacent track.

The magnetic data inevitably suffer from the limitations of gridding and in the area covered by these models the available data were relatively sparse, with line spacings typically greater than 10km. The loss of high frequency components is similar to that seen in the satellite gravity data with the result that the effect of smaller bodies, such as sills within the sedimentary section, will not be recorded in the extracted profile data. Thus, only large scale, basement features have been modelled magnetically.

Apart from limiting the resolution of the anomalies in plan view, the loss of high frequencies leads to a tendency to overestimate source depths. This follows from the fact that it is the anomaly gradients which constrain the depth interpretation: only shallow sources can generate the steeper gradients. In principle, slacker gradients may arise from a more gradual variation near surface rather than from a deep body. If the true anomaly gradients are not reproduced in the 'observed' dataset this ambiguity is extended.

5.3 Physical properties

There is little direct evidence on which to assign physical property values, that is density and magnetization, within the project area. Over much of the ground it is not clear what units are actually present at depth and most ideas rely on an interpretation of the available seismic data. Various attempts have been made to establish a relation between seismic velocity and formation density and the Nafe-Drake curve and Gardner's formula were used here as a guide for sedimentary rocks. The latter is defined as:

$$\text{density (Mg/m}^3\text{)} = \text{velocity}^{0.25}\ \text{(m/s)} \times 0.3095$$

Estimates of interval velocities generalized from the seismic sections suggested the following values (pers. comm. D. Naylor):

UNIT	*VELOCITY m/s*
Tertiary	1800 - 2500
Upper Cretaceous	2000 - 2500
Lower Cretaceous	2500 - 3500
Jurassic	3500 - 4500
Permo-Triassic	4300 - 5000
pre-Permian	>5500

The velocities adopted for depth-converting the digitized interpretations of the seismic sections and the equivalent densities for these units are given in the table below. The colour coding approximates that adopted for the plots of the models for the six shorter profiles. Somewhat different colour schemes were used for the regional models and 3D sections.

Unit	*Colour*	*Velocity*	*Density (Mg/m^3)*	*Mag. susc (SI)*
Water		1490	1.03	0
Tertiary – Neogene		1800	2.10 - 2.14	0
Tertiary–Palaeogene		2100	2.15 - 2.22	0
Cretaceous		3000	2.13 - 2.29	0
Jurassic		4000	2.32 - 2.50	0
Permo-Triassic		4750	2.44 - 2.55	0
Upper Palaeozoic		5000	2.59 - 2.68	0
Basement/upper crust		5500	2.67 - 2.78	0.002 – 0.057
Lower crust		n/a	2.83 - 2.87	0.005– 0.039
Mantle		n/a	3.03 - 3.20	0

Physical properties used for modelling profiles along margin of Rockall Trough

The magnetic response is assumed to arise mainly from the underlying basement and to be predominantly induced in origin. Remanent magnetization can be significant within the Tertiary lavas and is often reversed, giving characteristic, negative magnetic anomalies. These are more easily recognized as such by a noisy pattern of short wavelength, high amplitude anomalies when the lavas are at shallow depth. Sills tend to show a more muted response, either because of their more isolated mode of occurrence or because they are less strongly magnetic. They can sometimes be identified in high resolution data, more especially when they are faulted or steeply dipping and lie at shallower depths. A number of the igneous centres within and bordering the Rockall Trough also appear to have reversely-magnetized components, as for example the Hebrides Terrace Seamount and Blackstones Bank igneous centres in the north. However, there is no clear evidence in the magnetic anomaly data of a contribution from Palaeogene lavas elsewhere along the margins of the Irish Rockall Trough and they have not been included within the models.

5.4 Shelf margin models

Gravity and magnetic modelling was undertaken by ARK Geophysics Ltd along the six profiles crossing the margins of the Rockall Trough: five lines are located to the east, with one line on the western flank of the trough. The relevant seismic lines are:

WRM96-107
DGER96-25
DGER96-37
GSR96-108
GSR96-118
GSR96-204

The models retain the seismic line numbers.

Modelling was undertaken using ARK's proprietary software, ARKFIELD, which allows the user to observe the model simultaneously in depth in relation to the potential field profiles and in time as superimposed on the seismic data. The time-depth conversion was based on the generalized velocity information referred to above.

ARKFIELD applies an automatic adjustment, usually as a constant or in some cases as a linear slope, to provide a best fit between the observed and calculated fields. This is reported as the model offset and is apparent in the difference between scales on the left and right side vertical axes. Ideally, all the final models for the area would have the same offset but the datum was allowed to float given that the profiles are quite widely separated and that control on the physical properties and depths to the Moho in the models is relatively poor. The offset between magnetic values is more diagnostic in that the background susceptibility is zero with no contribution expected from below the Moho. The shortness of the profiles also makes it more difficult to establish a consistent reference level although all models have been extended well beyond the limits of the seismic lines to take some account of the adjoining geology. Generally, it is possible to consider any body with a strike of greater than 10 km to be 2D in nature within the accuracy in the observed data. Note that it is particularly difficult to set the level of the magnetic anomaly datum reliably, allowing for the effects of sources in the surrounding area, when dealing with short profiles.

Residual anomalies between the observed and calculated fields were minimized mainly by adjusting those areas with the least seismic control, that is, especially in the properties and structure of the basement. However, it was almost invariably necessary to make some alteration to the seismically derived part of the models. This is not surprising given the approximations involved in the depth conversion and uncertainties in some of the picks. A fit to within 3 mGal or 50 nT has been considered reasonable in the circumstances. Due to the more complex nature of the magnetic field and the greater number of unknowns, it is not uncommon for the magnetic response to diverge more than the gravity model. Some additional bodies have been introduced at depth to help account for residual magnetic anomalies but for the most part the calculated anomalies reflect the response that would be given from sources directly associated with the mapped basement surface.

The figures included in Annex A5 of this report show the upper 10 km of the models at a variable scale and vertical exaggeration factor as necessary to fit them onto an A4 page. The results from 3D gravity modelling are also illustrated for direct comparison (though not at the scale). Larger-scale plots at 1:100k are included as CGM files as part of the digital data set (cf. Annex A3). These show the density and magnetic susceptibility contributions to the response separately (and combined at 1:200k) over the complete depth range.

LINE WRM96-107

This is the only section on the western margin of the Rockall Trough. It shows a near complete sequence of sediments within the Rónán Basin, bounded by shallow basement underpinning the Rockall High to the west; a relatively narrow ridge to the east separates this basin from the thicker Tertiary sequence in the Rockall Trough itself.

Whereas the seismic interpretation showed only Neogene sediments over the Rockall High, the modelling suggests that a slightly thicker sedimentary section is present. A layer of Cretaceous sediments has been added to the model to allow for this although the gravity modelling of itself cannot discriminate between Tertiary and Cretaceous (or older) sediments in this type of situation.

In the eastern section of the line, the seismic interpretation did not identify the basement surface as such beneath the Rockall Trough. The final model suggests that basement underlies Cretaceous and Jurassic sediments although the presence of block faulted Permo-Triassic rocks is not precluded here. Similarly, the overall thickness of the sedimentary sequence is poorly constrained and might be expected to be somewhat greater than depicted within the Rockall Trough (see, for example, the RAPIDS sections): this could be accommodated in the gravity model by using a higher density for the lower crust and mantle or by thinning the crust.

Tertiary lavas are known to occur around Rockall Island and a large basic intrusion probably accounts for the large gravity anomaly high seen here, with the granite of Rockall Island itself representing a minor, differentiated component. Metamorphic rocks have also been found on the Rockall High and the magnetic anomaly pattern suggests that lavas may be less widespread to the south. The magnetic anomaly high that correlates with the Ladra High flanking the Mesozoic basin seen in this section has an elongate form. The absence of a corresponding gravity anomaly high suggests the presence of a basement structure capped by a sedimentary sequence - a view supported by the relatively low densities required in the model at the ridge. Residual magnetic anomalies in the final model imply some offset in source geometry relative to the ridge, consistent with the sedimentary cover being thicker. The basement may be displaced or change in magnetic character across an eastward-dipping fault, related to the Ladra High and bounding the Rockall Trough. Alternatively, the discrepancy may reflect aliasing of the magnetic anomaly itself as the survey line spacing is about 15 km in this area.

A significant feature has been included at depth within the basement below the Rockall High to help account for the observed magnetic anomaly. It can be seen that this does not reproduce the steeper gradients flanking the anomaly, indicating that the some contribution must also arise from shallower levels. The smaller magnetic anomaly high near 75000 m along the profile is also not fully reproduced by the relief shown on the magnetic basement surface. Adding relief to fit the magnetic response would tend to increase the gravity anomaly residuals suggesting that the basement does in fact show more lateral variation in its properties, possibly related to faulting.

LINE DGER96-25

This line is complementary to line WRM96-107 in that it lies on the opposite, south-eastern margin of the Rockall Trough. It is dominated by the influence of a basement ridge - the Erris High - surrounded by a relatively continuous sedimentary sequence. Other than under the Erris High no basement had been interpreted in the original section.

Both gravity and magnetic profiles show strong similarities with line WRM96-107 suggesting that the overall structural framework is similar. Note that for this line the observed gravity data are taken directly from an adjacent line, projected onto the correct location, rather than from the grid: in practice, there is little difference between the two.

The final model has a relatively low density for the basement rocks under the Erris High and, again, the observed magnetic anomaly is not reproduced in detail by setting the magnetic basement at this level. A broader, somewhat deeper magnetic source would provide a better fit, allowing the possibility of more sedimentary cover (or a different style of basement) over the ridge itself.

The thick sedimentary section of the Erris Basin to the east accounts for the gravity anomaly quite well at this scale although there is a difference in the calculated gradient which would need to be explained, together with the need to add to the magnetic anomaly, in a more detailed appraisal.

The model shows Cretaceous directly overlying basement within the Rockall Trough, indicating what is close to the minimum thickness of sedimentary section that would be expected.

LINE DGER96-37

This section is located about 80 km south from line DGER96-25 where the Erris High structure is more deeply buried, beneath perhaps 4 km of sedimentary rocks, accounting for the absence of any associated gravity anomaly high. However, the magnetic signature remains similar, albeit broader and with reduced amplitude, supporting the view that the magnetic anomaly reflects a more fundamental change in the nature of the basement across the margin of the Rockall Trough. The model shows magnetic basement extending westwards to what might be a shallow-angled extension of faulting associated with the Erris High. Alternatively, it may be stepped down across a series of more steeply-dipping faults west of the ridge.

In terms of variations from the original seismic interpretation, it was necessary to 'transfer' the upper Palaeozoic sequence from the area of the Erris High eastwards into the Erris Basin. Retaining the Palaeozoic layer within the central zone results in a large mis-fit in the gravity anomaly response which is difficult to offset at other levels. It was also necessary to increase the depth to basement to the west by including Permo-Triassic strata explicitly within the Rockall Trough (with the current levels for the lower crustal interfaces). There is no obvious reason geologically for the apparent deepening of the basement relative to line DGER96-25. It seems more likely that Jurassic, and perhaps Permo-Triassic, strata are present beneath the latter also (and line WRM96-107), implying the need for some adjustment to the representation of the lower crust beneath the Rockall Trough on these lines.

The basement is shown as being sub-divided into a number of blocks apart from those used to account for the variations seen in the magnetic data. These are indicative of possible lateral changes in depth or properties but with little clear evidence to justify them. The need to increase calculated magnetic anomaly values at the eastern end of the line suggests that further variations are needed within the basement here and that the Palaeozoic units may wedge out, allowing the basement surface to be set at a higher level.

LINE GSR96-118

This line lies on the northern margin of the Porcupine High and shows the familiar stepped form of free-air anomaly profile, exaggerated somewhat here by the steeper continental slope near 20000 m distance. A discrepancy between the observed and calculated gravity anomaly gradients in this area is probably linked to the bathymetry in the sense that the satellite gravity data do not resolve the detail fully at this wavelength whereas the model does show the correct water depths. (There is a case for matching the frequency content more closely by extracting the seabed profile from the bathymetry grid rather than taking the seismic picks.) The large density contrast at the seabed, combined with its relatively shallow depth, makes the model particularly sensitive at these levels.

The main change from the seismic interpretation has been the addition of Palaeozoic formations in the central and eastern sections of the line. This is, in fact, an indication of the difficulty in defining this type of layered geometry from the potential field data: much of the gravity anomaly can be taken up by increasing the thickness of the crust instead. The divergence in the gravity profiles at the northern end of the line may also arise from variation within the lower crust.

The observed magnetic anomaly is not properly explained by the form of the basement in the current model as based on the seismic interpretation. Adding magnetic rocks at depth helps to improve the fit in terms of the long wavelength aspects but clearly fails to reproduce the detail. Some magnetic material is needed at higher levels to explain the steeper anomaly gradients. The magnetic anomaly maps (eg. Map 12) shows that the anomaly near 30000 m distance is a local feature lying along the north-western flank of the Fursa Basin and its source probably extends into the zone modelled as being Palaeozoic. This suggests that the modelled crust needs to be thickened, thus reducing the calculated gravity anomaly and allowing the basement, including a more magnetic component, to be restored to higher levels beneath the margin of the Fursa Basin.

LINE GSR96-108

Few adjustments were made to the input model for this line on the western margin of the Porcupine High in order to produce a reasonable fit between the observed and the calculated anomalies, other than at the eastern end of the profile. The strong gradient in the magnetic anomaly data lies on the flank of a large local anomaly as can be seen in the images (eg. Map 12). This anomaly has been attributed to the Donn Igneous Centre although the associated gravity anomaly is less pronounced than might be expected (ie. in comparison with the known centres further north along the shelf, such as Geikie). It lies at the northern end of a gravity anomaly ridge whereas a similar (but not necessarily related) magnetic anomaly occurs 50-60 km along the magnetic anomaly strike to the north-east, in a regional of lower, nondescript gravity anomaly. This variation suggests that the magnetic anomaly may originate within the basement rocks themselves rather than from a more recent intrusion.

The final model includes a strongly magnetised body extending to a shallow level within the sedimentary pile beyond the eastern end of the seismic line. It appears as if its flank needs to extend further west in order to increase the anomaly levels. However, this causes an unwanted increase in the calculated gravity anomaly values. In fact, some distortion will occur in the magnetic response by not allowing for the limited strike length of this body, the calculated values for an extended source being too low.

As with line GSR96-118, the calculated gravity anomaly gradient is steeper than the observed response over the continental slope. Again, while this is provisionally attributed to smoothing of the bathymetric signature in the observed gravity anomaly data, mis-representation of the basin margin in the model may be a contributory factor.

Density variations have been included between the fault blocks within the Pádraig Basin to improve the fit of the gravity anomalies, although their effect is relatively minor. There is no evidence of significant lateral variation within the basement. In particular, the magnetic anomaly data do not show the basin margin response seen in the previous lines.

The depth to basement over the Porcupine High is significantly greater than might be expected, given its geological setting as a platform area and the high background level of the gravity anomaly (cf. Bouguer gravity anomaly values calculated at a reduction density of 2.2 Mg/m^3 as shown in Map 8). The effects of crustal thinning related to Porcupine Basin and the Rockall Trough account for much of the gravity anomaly but these cannot be quantified with sufficient reliability to determine how much of the anomaly remains to be assigned to sedimentary cover. The indications from published sources relating to this area are that there is only a veneer of Upper Palaeozoic / Mesozoic rocks overlying a meta-sedimentary basement, possibly intruded by granites as well as more basic bodies.

LINE GSR96-204

The original seismic interpretation required little alteration in fitting the general form of the observed anomalies for this most southerly of the profiles, 85 km beyond line GSR96-108. It is difficult to know how far to go with the model in terms of matching the detail of anomaly gradients more closely. As noted previously, the steep gradient near the bottom of the continental slope appears not to be resolved fully by the satellite gravity data. However, there is evidence of a more localized feature within the basement near 200000 m distance in that the response from the basement swell is broader than that observed in the magnetic anomaly. Similarly, the observed magnetic anomalies east of the North Brona Basin show a higher frequency content than those calculated, suggesting that the Upper Palaeozoic units in the model should thin more rapidly onto the Porcupine High, thus raising the level of the basement surface. The magnetic anomalies probably relate mainly to changes in depth to the basement across faults but there may also be changes in magnetic properties between the blocks.

The North Brona Basin itself is associated with the lowest magnetic anomaly values along the profile whereas the gravity anomaly is more subdued and not easily isolated from shelf edge effect. Note that a large automatic offset has been applied in order to match the magnetic anomaly levels indicating that the broader context of the setting here has not been addressed.

5.5 Regional models

The BGS interpretations of the two regional lines crossing the full width of the Rockall Trough are intended to give a better indication of the overall geological context and also to illustrate the nature of the potential field response at a broader scale. They are not reliable in any detailed, quantitative sense of defining formation depths and should be used as a qualitative guide to structural relationships. Full-scale plots are supplied at 1:500k and at 1:750k as digital CGM files (cf. Annex A3) and the results are reproduced at A3 size in this report (cf. Annex A5).

As before, the upper layers within the models were taken directly from the interpreted seismic sections after depth conversion. The underlying layers rely mainly on published ideas of crustal structure deduced from deep seismic experiments, together with the basic principle of maintaining a degree of isostatic balance. There is no representation of a mid-crustal layer as would be expected beneath the shelf areas and a single interface is used to separate upper and lower units. The vertical distribution of density through the crust is poorly constrained at best and in this case the main concern was to represent the changes in magnetization as simply as possible. A mid-crustal layer of intermediate density (~2.85 Mg/m^3) can be considered to lie between a depth of about 10 km and the lower crust.

Physical property values are similar to those used in the shorter profiles except that densities in the Tertiary and Cretaceous were set somewhat higher when this appeared to help in balancing the models overall. The models were taken to a depth of 40 km and the background density set to 2.97 Mg/m^3, representing an 'average' density through the model to this level. This background density is arbitrary in the sense that it follows from the form of the model as it is set up initially. A starting model including a mid-crustal layer or different mean densities for the sedimentary cover would use a slightly different background density.

Magnetic properties are represented by susceptibility and, independently, by remanent magnetization (ie. with the direction of the vector also specified); background values of magnetization, both induced and remanent, are zero.

LINE GSR96-0116

This line lies near the initial, transverse profile of the RAPIDS wide-angle seismic experiments, being closest at its north-western end and diverging to the south. The depth to the Moho beneath the Rockall Trough was interpreted from the RAPIDS line to be about 16 km from sea level with 5-6 km of sedimentary cover. Crustal thicknesses beneath the Rockall High and the Irish shelf were 30-35 km. As noted above, the mid-crustal structure has been simplified in the models with the density in the shelf areas kept at 2.78 Mg/m^3. To compensate for the relatively low densities at depth, the base of the crust is set somewhat shallower than would be expected. The layer of intermediate density, 2.72 Mg/m^3, used as a transitional zone above higher values for the attenuated crust beneath the Rockall Trough, has been extended across the length of the model.

The free-air gravity anomaly profile shows the characteristic signature often seen crossing a continental margin: a low near the foot of the continental slope and a high developed on the shelf side. This follows from the different depths at which the sea water and crustal thinning contributions to the gravity anomaly originate. Free-air anomaly values rise again to near zero towards the centre of the Rockall Trough, suggesting that the area as a whole is close to isostatic equilibrium. Any effects arising from lateral variations within the cover sequence are superimposed on these large amplitude, long wavelength anomalies. *It is important to appreciate that the gravity anomaly lows along the margins of the Rockall Trough are, for the most part, reflecting broader crustal structure and not the presence of sedimentary basins, although the latter do make a contribution.* In order to identify the response attributable to the basins it is necessary to have good control on both bathymetry and gravity anomaly values. Structure within the cover sequence will be distinguished to some extent by its higher frequency content in the anomaly pattern but crustal thinning aspects will determine background levels and thus the amplitude of the residual anomalies on which estimates of overall basin thickness depend.

The form of the Moho as modelled is noticeably asymmetric, with the steeper slope on the south-eastern margin of the Rockall Trough only partly reflecting the seabed profile. Lessening this gradient would allow for a thicker sedimentary sequence in basins beneath the continental slope itself but the satellite gravity data are not sufficiently reliable in defining the anomaly here. It was difficult to fit the observed gravity anomaly in detail without some adjustment to the initial model over this margin. A wedge of Mesozoic rocks included in the seismic interpretation of the southern flank of the Macdara Basin near 250 km (profile distance) has in fact been assigned a higher, 'Upper Palaeozoic' density in order to avoid producing a local residual anomaly low whilst increasing the depth to basement over a wider area.

Juassic / Permo-Triassic rocks are shown schematically as extending across the width of the Rockall Trough although there is no basis for distinguishing between them, or the Cretaceous. The Tertiary compressional feature noted in the centre of the trough causes some difficulty in that this structural high, with its distinctive magnetic anomaly high, corresponds with lower gravity anomaly values. As this feature is offset slightly from the profile its magnetic anomaly is under-stated by more than 200 nT and the source must reach shallower depths than shown in the model. Thinning of the Tertiary here has been compensated by relative thickening of the underlying Mesozoic layers, but larger-scale structures are needed to account for the high-low-high gravity anomaly pattern between 100 km and 200 km. The attenuated crust has generally been assigned a

higher density but the source of the magnetic anomaly high over the compressional feature is associated with lower densities. This inverse correlation was referred to in discussing the images and occurs elsewhere to the south-west. Volcanic rocks are a possible explanation, with the analogy of the Porcupine Median Volcanic Ridge. The amplitude of the gravity anomaly low is only satisfied by introducing low density material (or a sag) within the upper mantle. This could be related to current ideas of widespread serpentinization caused by sea water penetrating along through-crust fractures (eg. O'Reilly, 1996), although the modelled geometry here looks artifical. The magnetic anomaly low (and gravity anomaly high) to the north-west required a body with reversed magnetization which, if genuine, implies a Tertiary volcanic origin. Whereas the compressional structure and its related magnetic anomaly high are local features, the two gravity anomaly ridges flanking a central low are seen in the images to be of regional significance.

The north-western flank of the Rockall Trough requires more low density material than was implied by the seismic interpretation. In particular, the Conall Basin has effectively been extended to the north-west between 45 km and 55 km. An alternative explanation is that granites have been intruded into the basement in this zone. The thickness of the Conall Basin itself was also modified to improve the fit of the gravity anomalies. The continuation of Upper Palaeozoic rocks to the north-west is intended only as indication that there may be some local cover, of whatever age, on the basement here.

High magnetic anomaly values over the Rockall High are attributed to a combination of basic intrusions and magnetic units within the basement itself. It is necessary to extend these magnetic rocks across this margin of the Rockall Trough to account for the observed anomalies. Significant volumes of magnetic rock are also included in the model on the Irish shelf, though the evidence that they continue beneath the trough is less clear here.

LINE WI-32

The southern end of the Rockall Trough shows some marked differences in terms of the potential field anomalies and is notable for the occurrence of the Barra Volcanic Ridge System.

The line crosses the Porcupine High at an oblique angle and so Moho depths appear to increase less rapidly beneath it. There is also a need to increase the density of the crust to the south-east from the margin of the Rockall Trough to help account for the rise in gravity anomaly values. The high magnetization of these rocks is consistent with the source being shallow metamorphic basement and/or basic intrusions. It is not clear if the combined gravity and magnetic anomaly high at 745 km represents similar basement or a discrete intrusion but it underlies the Jurassic basin interpreted from the seismic line. Additional Mesozoic basins are suggested to the south-east of this in order to explain the variations in gravity anomaly here. It is more difficult to reconcile the seismic and gravity evidence at 715 km where a structural high lies within a zone of lower gravity anomaly. The images show no evidence of a local anomaly which might suggest a granite source and it may be that inversion has preserved a thick Mesozoic sequence locally (the representation in the model is only diagrammatic, indicating that a unit of lower density is needed to satisfy the observed gravity anomaly).

The Barra Volcanic Ridge System as picked out from the seismic data is apparently related to reduced gravity and higher magnetic anomaly values. Lavas can have a density as low as about 2.55 Mg/m^3, as used in the model, but some additional low density material is needed to the south-east. Magnetic data along this line control the gridding and it is surprising that the magnetic anomaly low expected from the geometry of the lavas at 600 km has not been picked up. Other

'ripples' in the observed gravity anomaly data to the south-east may be genuine indications of structure affecting the base of the Tertiary sediments although the feature interpreted from the seismic section at 660 km is not well represented.

The large gravity anomaly high centred near 500 km is part of a prominent, extensive feature seen clearly in the images and associated with lower magnetic anomaly values. There is no simple 'source' for this anomaly in the model and it appears to emerge from a combination of factors including a reduction in water depth from the south-east and crustal thinning from the north-west. It appears to be a case where the thicker Neogene sediments have effectively replaced the water, with the extra load being supported by a more rigid crust.

6. RESULTS FROM 3D MODELLING

The use of fast Fourier transform techniques, combined with the availability of increased computing power, enables 3D modelling of gravity and magnetic data to be undertaken on a 'real-time' basis. When combined with effective graphics this provides a powerful facility for testing geological models against the potential field data. Results presented here have been calculated using software developed within BGS (GMOD and BMOD) whereby a complex, multi-layered earth is represented by a set of grids defining both the interfaces between layers and the variations in density/ magnetization within each layer. Specified grids can be optimized automatically to minimize the residuals between the observed and calculated fields.

The primary objective of the modelling was to provide a first-pass interpretation of the gravity data in terms of the sedimentary cover sequence, and of the magnetic anomaly pattern as attributed to variation within the upper crust. Some constraints on the models were provided by published information on crustal structure and basin geometry but the results remain highly speculative overall.

6.1 Gravity modelling procedure

The gravity model was taken to a depth of 45 km and includes the ground surface, overlain by sea water as appropriate, a sedimentary cover sequence, upper and lower crustal layers and the upper mantle. A further sub-division has been introduced within the lower crust to allow for discrepancies between depths to the base of the crust (as defined by the 'Moho') mapped on the basis of the available deep seismic surveys and the geometry predicted assuming Airy isostasy. Note that the former show some significant variations unrelated to the present-day ground surface. The seismic coverage is very limited and to some extent inconsistent where lines intersect. Thus, control on Moho depths from both Airy and seismic sources is unreliable and values have been assigned mainly by informed guesswork. By including both surfaces in the model it is hoped that a better overall approximation to reality is achieved.

The Airy root depths are calculated for a very simple model which assumes that the Moho responds only to the change in load represented by the present-day ground surface (ie. bathymetry in this area). No account is taken of other lateral variations within the crust arising from sedimentary basins, basic intrusions etc. Nevertheless, the effects of the water are widespread and would be a significant factor during the development of the Rockall Trough when the crust was more ductile. Some of the subsequent, local changes will be supported internally by the cooler, stronger crust.

The depths calculated for the root are not calibrated in absolute terms. As noted above, the objective was to constrain the overall geometry rather to define a real boundary as such. The root model was similar to that adopted for compensating the Bouguer anomaly data for imaging purposes. The load replacement density was set to 2.5 Mg/m^3, the contrast across the Moho to 0.4 Mg/m^3 and the compensation depth to 30 km and the calculation assumed an elastic thickness for the crust of 1 km. Varying these parameters alters the amplitude of the inferred crustal thinning across the Rockall Trough and, effectively, the background field to which the contribution attributable to the cover sequence in the model is referred. The values adopted were thought to give a reasonable approximation to the expected depth range and they were set so that the calculated depths were generally deeper than the seismic estimates. Where the original surfaces did

cross they were, in effect, re-allocated so that the shallower / deeper values were always assigned to the seismic / Airy grid sets respectively.

The interface separating the upper and lower crust is even less well defined as a specific interface although a similar division of seismic velocity is not uncommon in the literature. It is included here more as a means of partitioning the density contrast between the cover sequence and the mantle, rather than as a representation of a 'real' boundary such as the Conrad discontinuity: its level was set as a fixed proportion of the thickness of the crust as measured between seabed and the clipped seismic Moho.

In order to reduce problems in matching the frequency content of the bathymetric and free-air anomaly grids the observation surface was taken to be at 1 km above sea-level. This has the effect of suppressing the influence of the shorter wavelength variations in water depth which are not expressed in the gravity data, in particular where the latter rely on satellite observations. Otherwise, these differences will be assigned to changes in the optimized basin thicknesses. The observed anomaly dataset was taken as the original grid smoothed by upward continuation to 2 km. It was found that the higher frequency content retained to the east by the variably continued grid (as adopted for the imaging) resulted in an unduly noisy output from the optimization process. Modelling was undertaken using grids with the original node interval of 2 km.

Initially, the sedimentary layer was assigned a constant thickness of 2 km and a density of 2.45 Mg/m^3. The latter is representative of predominantly clastic Permo-Triassic deposits as found both on the shelf and on-shore UK; it also lies near the middle of the range 2.15-2.75 Mg/m^3 which might be expected from a sequence with poorly-consolidated Tertiary sediments near surface and Cretaceous shales buried at depths of 6 km or more within the major rift zones.

Densities for the lower crust and upper mantle were set at 2.97 Mg/m^3 and 3.31 Mg/m^3 respectively, giving a relatively low contrast (cf. values of as much as 0.5 Mg/m^3 quoted in some of the literature). The transitional layer resulting from the inclusion of both estimates of Moho depth was assigned a density of 3.09 Mg/m^3 initially. In geological terms, this zone may relate in some areas to current ideas of underplating as linked with Tertiary igneous activity. The effects of crustal rigidity in relation to isostasy and crustal loading may also be a factor. No specific allowance was made in the model for the transition to oceanic crust south-west of the Charlie-Gibbs Fracture Zone.

The adopted background density (2.982 Mg/m^3 in this case) can be considered as the mean density of a notionally representative lithosphere, defined to a depth of 45 km, and is chosen to give the required datum level as calculated for the starting model relative to the observed anomaly values. This starting model effectively sets the 'regional' gravity field and the thickness or density of specified layers are then adjusted to minimize the residuals between the calculated and observed anomalies. The degree of fit achieved is controlled both by the number of iterations and the low-pass filter setting on the frequency content of the allowed variations. Thus, although only one parameter can be optimized at a time, it is possible to partition the residual anomaly between different layers by suitable choice of these settings - essentially, by restricting the optimization to the lower frequency components in the early stages. In principle, it is always possible to achieve a close fit to the observed data but this has to be balanced against the known limitations of the model and the need to retain a plausible basin geometry, consistent with the available geological control.

The outputs from the modelling inevitably reflect the prejudices of the interpreter to the extent that these influence the setting of unknown or poorly constrained parameters. In the present case, one assumption was that the thickness of sediment within the Rockall Trough should be of the order of

5 km. It was also thought reasonable to distribute some of the residual anomaly throughout the deeper parts of the model. Thus, modifications were made to the seismic Moho depths, more especially near the shelf margins, to maintain optimized thicknesses of the cover sequence greater than the Tertiary sequence interpreted on the 2D seismic profile lines. The density of the transitional layer was also manipulated by grid editing to help account for some of the larger gravity anomalies within the Rockall Trough. These changes applied to the starting model. Within the optimization routine itself, a somewhat arcane processing sequence was followed which included adjustments to the density of the upper crust from its initial value of 2.78 Mg/m^3 and successive opening of the low-pass filter settings in moving the base of the cover sequence.

Results from be 3D modelling are displayed in both map and profile form. The latter is particularly useful for checking the optimized outputs directly against both the seismic interpretations and the 2D modelling (cf. Annex A5).

Map 22a: (*) Apparent basin thicknesses as derived from a regional 3D full-crustal model

The results of the modelling, displayed as thicknesses in this map, represent an attempt to isolate the contribution of the cover sequence from the observed gravity anomaly. They are, perhaps, better thought of as a re-calibrated residual anomaly distribution. There is clearly a gross over-simplification of the geology in the approach adopted but it provides a regional context in which to set an appraisal of areas of specific interest. More detailed models can then be developed where there are data of higher resolution and with better seismic controls.

Previous models of this type for area further north along the Atlantic margin have allowed less high frequency content into the final maps. In the present case, specific comparisons were made with the independently-derived 2D models. These indicated that at least a part of the information emerging from the 3D models was consistent with known geological structure but that features of interest such as the Erris High remained quite heavily suppressed, with some residual anomaly unaccounted for. This type of feature, with an anomaly width of about 10 km, is close to the limits of resolution with the available dataset and a model grid node spacing of 2 km but a significant improvement in both the match and the geological representation is possible. However, achieving a good fit here has undesirable consequences elsewhere, in amplifying what is essentially noise, such that the appearance of the map becomes chaotic.

The present map is a compromise in that it includes some of the higher frequency information without fully accounting for the residual anomalies; the shaded-relief presentation helps in revealing these structures but it does emphasize the noisier aspects also. Comparison of the 2D and 3D model sections indicates that this is partly a function of presentation scale. The 3D model does reasonably well in revealing the basic form of basin/ridge structure seen in the seismic data without fully recovering the amplitudes - as would be expected.

As noted above, the map is more correctly described as a form of residual gravity anomaly. However, in comparing the results with maps 6 and 10 it can be seen that some major readjustments occur as the background crustal model is progressively refined. The Porcupine Seabight Basin provides a good indication of this in that the axial gravity anomaly high has been offset to allow 5-6 km of 'apparent basin thickness' to emerge. Gravity anomaly highs within the Rockall Trough have also been suppressed to some extent whereas areas of thin cover over the Rockall and Porcupine highs are expanded. The cover sequence is generally thinner near the south-west end of the Rockall Trough, with a distinct change in character south of a north-west - south-east trending zone 40-50 km north-east of profile line WI-32. This appears to have some relation to

the occurrence of the Barra Volcanic Ridge System. There is also evidence of a trough/ridge geometry on the southern side of the Charlie-Gibbs Fracture Zone.

The shelf margins remain particularly difficult because of sensitivity to errors in gradients in the bathymetry, the Moho(s) and the observed gravity data themselves. Any short wavelength features in these areas needs to be viewed critically. A good example of this occurs along the western margin of the Porcupine High (cf. comments on Map 8 above) where a particularly complex pattern emerges from the model. Although this representation of the geological structure is not reliable in itself there are indications of buried Mesozoic fault blocks in the seismic data. Perhaps the main value of this type of preliminary modelling is that it can bring attention to such areas. By refining the model subsequently, as better control becomes available in difficult areas, it can then be used to interpolate/extropolate more effectively elsewhere. The resolution can also be improved significantly within smaller areas by the use of finer grids and by accounting for the known part of the sedimentary sequence more rigorously.

There is scope for 're-calibrating' the thicknesses in areas of the map where the model layer density of 2.45 Mg/m^3 is thought to be unrepresentative as a mean value. This might apply to the Clare Basin, for example, where the expected Carboniferous sequence is likely to have a higher density. Where a thicker sequence of Tertiary sediments occurs the overall thickness is likely to be overestimated (ie. the mean density is actually lower). To a first approximation, it is only necessary to maintain the implied mass (2.45 x thickness) within the layer for the results to be valid. Where the thicknesses are known then the mean density can be revised accordingly. The Slyne Basin is less conspicuous than might be expected, possibly for this reason.

Map 22b: (*)Apparent basement surface relief from a regional 3D full-crustal model

This map shows the base of the cover sequence as defined by the optimized model, using a different illumination direction compared to Map 22a. The most obvious change in balance between the two maps is beneath the deeper waters near the south-western end of the Rockall Trough. The Celtic Sea Basin shows the reverse characteristics, with a thick sedimentary sequence beneath relatively shallow water.

Another area to note is that lying by the western flank of the Porcupine High. The depth map offsets some of the more extreme variation in thickness (cf.Map 22a), confirming the close relation between the bathymetry and the model response here

6.2 Magnetic modelling

Magnetic modelling was undertaken using the same basic approach but with some different constraints and a simpler crustal model. The immediate objective here was to suggest the distribution of magnetization within the crystalline basement/upper crust.

Previous 2D and 3D model studies had shown the inherent ambiguity in distinguishing magnetic sources within the basement from igneous rocks (lavas and/or sills) at higher levels within the Tertiary and Cretaceous sequences in deep-water areas. As the latter were widespread, magnetizations in the 3D models had been optimized within an upper layer of constant thickness extending up to the ground surface. Some of the longer wavelength components were assigned to the underlying crust but the resulting images closely resembled the form of the observed anomaly.

For this study it was assumed that the influence of the Tertiary lavas was less significant so that the upper surface of the magnetic layer could reasonably be set at the base of the cover sequence derived from the gravity inversion. Various alternative forms were tested for the base of this layer. As before, a layer of constant thickness yielded results similar to the anomaly maps themselves, albeit calibrated in terms of magnetization. Fixing the base at a constant depth, produces a marked change in balance across the area as magnetizations have to rise significantly where the layer thins out (eg. beneath the Rockall Trough) compared to the much greater thicknesses beneath the shelf areas. Taking the base to the seismic Moho exaggerated the latter effects even more. In producing the final output the upper magnetized layer was assumed to have a minimum thickness of about 1.5 km. Half of the remaining difference in thickness between the seismic Moho and the base of the cover sequence was then added to the depths to give a surface varying in depth between 8 km and 18 km below sea level.

The starting model comprised simply the ground surface, the base of the cover sequence obtained from the gravity model, the surface as defined in the previous paragraph, and the seismic Moho. The observation surface was set at 1.5 km above sea level to allow for the loss of some high frequency components in the compiled grid. Initially, the deepest layer was assigned a magnetization of 1 A/m and this was optimized to take out a low-order background field. Optimization was then transferred to the layer representing the upper crust. No other adjustments were made in producing the final output.

Map 23 (*) Apparent magnetization in the upper crust from a regional 3D model

The modelling process acts a low-pass or smoothing filter which focusses attention on the broader-scale features and, as expected, the optimized magnetizations do show some change of emphasis from the reduced-to-pole anomaly image (Map 13). In particular, there now appears to be a region of higher magnetization within the Rockall Trough in the northern part of the area, beyond a north-west - south-east line passing about 30 km north-east of profile GSR96-116. This takes in the Hebrides Terrace Seamount with its distinctive reversed polarity response (cf. also seen further east over the Blackstones Bank igneous centre). Areas of strongly negative magnetization generally imply the presence of Tertiary igneous centres and/or thick sequences of basalt of Palaeocene (/Cretaceous) age whereas the more positive values (as, for example on the Rockall and Porcupine highs) are as likely to originate from within the basement itself.

As it is, absolute levels of magnetization cannot be fixed reliably from the magnetic anomaly alone. Thus, the fact that positive values are shown does not, of itself, mean that the source is normally magnetized (basement or intrusions), more especially where the anomaly is of relatively short wavelength: a reduction in magnetization or thickness of reversely polarized basalts is an equally valid interpretation of some anomalies.

Broad areas of negative magnetization are also characteristic of thick, non-magnetic sedimentary sequences. Such areas can be regarded as 'windows' revealing information on the background variation arising from changes at mid-crustal levels (down to the Curie point where rising temperatures result in the loss of ability to retain magnetization) although they will include some effects from adjoining magnetic sources.

As noted above, the magnetic response does not of itself distinguish older sources within the basement from subsequent intrusions. The nature of any associated gravity anomalies, combined with the form of the anomalies themselves (eg. circular or elongate), can be a guide to the source but some ambiguity usually remains. No attempt is made here to classify the different anomalies overall but a few points of general interest are raised.

It is tempting to assume that the prominent areas of negative magnetization to the south-west of the Rockall high arise from sources contemporaneous with the major rifting episodes and that they represent reversely magnetized basic intrusions together with normally magnetized bodies. Thick lavas could also be present here but there is no evidence of the higher frequency magnetic anomalies that might be expected over these relatively shallow water depths. However, data coverage in this area is relatively poor and the anomalies may be heavily aliased and filtered.

The isolated body of high magnetization related to a Tertiary compressional feature in Quadrant 76 is clearly defined and the Porcupine Median Volcanic Ridge also has an expresssion. A set of three strongly magnetic blocks/bodies which may have a similar origin extends northwards along the Porcupine High, diminishing in both areal extent and magnitude. The last lies at the end of profile GSR96-108 and, as noted previously, is probably more closely linked to an anomaly to the north-east. The anomaly ridge to the east separates the Porcupine and North Porcupine basins and is associated with faulting.

A more obvious expression of the Charlie-Gibbs Fracture Zone might have been expected although there is a change in trend to a distinctive negative feature with a south-south-east strike to the south of it. The Barra Volcanic Ridge System does not stand out especially either, apart from the positive zones near the centre of profile WI-32.

7. CONCLUSIONS AND RECOMMENDATIONS

The compiled datasets provide a good basis for an assessment of the regional structures influencing the Irish Rockall Trough. However, data coverage is not uniform and deteriorates significantly towards the west, resulting in a loss of information content distinct from the effects of increasing water depths and the geology itself.

The suite of maps derived from the grids was designed to bring out as much information as possible using a variety of processing and display techniques although, inevitably, this selection will not meet all of the users' requirements. The grids themselves are also supplied so that alternative images can be generated by RSG members' using their own software to meet more specific objectives and to increase the range of products, for example in terms of illumination directions. The data were gridded at a node spacing of 2 km and map production at scales of larger than about 1:1M is not recommended in terms of gaining extra resolution.

A variety of structural elements and trends is apparent in the maps but it is important to recognize that there is no simple correlation between the anomalies as such and the geology. Modelling helps in understanding the nature of these relationships. As illustrated by the 2D models, the level of detail that can be resolved from these datasets is rather coarse in comparison with that of interest in evaluating hydrocarbon prospects. Nevertheless, they are particularly useful for understanding the regional context in which to set more local studies where higher resolution survey data are available. In particular, this study is important in helping to establish the contribution to the gravity response attributable to crustal thinning in areas near the shelfbreak.

A regional 3D model has been constructed which reproduces many of the known geological features, in a qualitative sense at least, from the gravity data. This should provide a useful starting point for constructing more detailed models over more specific targets and could be refined as additional information becomes available, for example, from deep seismic experiments. In principle, it is preferable to work in a 3D rather than a 2D environment in developing reliable models.

This project has illustrated the value of the potential field data and any likely requirements for imaging on a regional scale can be met with the suite of grids produced. There is further scope for refining the 2D and 3D models by a more detailed appraisal of the results in the context of the available seismic data. The results from the latest RAPIDS deep seismic experiments would provide an obvious opportunity for developing ideas on the deeper crustal structure.

The resolution of the imaging and modelling techniques could be improved significantly by focussing the study on areas with better data coverage. A more detailed attempt to address the problems of modelling potential data along the margin of the Rockall Trough should be of benefit to all group members.

ANNEX A1: *LIST OF IMAGES*

Map 1: Bathymetry/topography image with 2D modelled profile locations

Map 2: Location map of digital data points taken from marine gravity survey tracks
Map 3: Location map of digital data points taken from magnetic survey tracks

Map 4: Free-air gravity anomaly image (Bouguer anomaly values on land); illuminated from W
Map 5a: Horizontal gradient of free-air gravity anomaly (Bouguer anomaly on land); illuminated from NW
Map 5b: Horizontal gradient of free-air gravity anomaly (Bouguer anomaly on land); illuminated from NE
Map 6: Residual free-air gravity anomaly from 10 km upwardly continued field; illuminated from W
Map 7a: Isostatically-compensated Bouguer gravity anomaly (at 2.75 Mg/m^3); illuminated from NW
Map 7b: Isostatically-compensated Bouguer gravity anomaly (at 2.75 Mg/m^3); illuminated from NE
Map 8: Isostatically-compensated Bouguer gravity anomaly (at 2.20 Mg/m^3); illuminated from N by E
Map 9a: Horizontal gradient of isostatically-compensated Bouguer gravity anomaly; illuminated from NW
Map 9b: Horizontal gradient of isostatically-compensated Bouguer gravity anomaly; illuminated from NE
Map 9c: Horizontal gradient of isostatically-compensated gravity potential; illuminated from W by N
Map 10: 10 km continuation residual of Bouguer anomaly (isostatically-compensated); illuminated from N by E
Map 11: Euler deconvolution solutions from isostatically-compensated gravity data

Map 12: Total magnetic field anomaly (as compiled at 450 m); illuminated from NW
Map 13: Reduced-to-pole magnetic anomaly (as compiled at 450 m); illuminated from NE
Map 14a: Horizontal gradient derived from reduced-to-pole magnetic anomaly; illuminated from NW
Map 14b: Horizontal gradient derived from reduced-to-pole magnetic anomaly; illuminated from NE
Map 15: Reduced-to-pole magnetic anomaly upwardly continued by 2 km; illuminated from NW by W
Map 16a: Residual RTP magnetic anomaly from 2.5 km upwardly-continued field; illuminated from NNW
Map 16b: Residual RTP magnetic anomaly from 2.5 km upwardly-continued field; illuminated from W by S
Map 17: Magnitude of analytic signal from 1 km upwardly continued magnetic field; illuminated from WNW
Map 18: Horizontal gradient of magnetic pseudo-gravity transformation; illuminated from NNE
Map 19: Euler deconvolution solutions from magnetic RTP anomaly data
Map 20: Reduced-to-pole magnetic image with gravity anomaly line contours; illuminated from W
Map 21: Isostatically-compensated gravity image with RTP anomaly line contours; illuminated from W

Map 22a: Apparent basin thicknesses as derived from a regional 3D full-crustal model; illuminated from W
Map 22b: Apparent basement surface relief from a regional 3D full-crustal model; illuminated from NNE
Map 23: Apparent magnetization in the upper crust as derived from a regional 3D model; illuminated from W

ANNEX A2: *DESCRIPTION OF DIGITAL GRID/DATA FILES*

Binary/ASCII files used in image production

The binary filenames used for map production (and as quoted in the information box in the lower right-hand corner of the map legends) are given first in italics. Equivalent names for the ASCII files as written to Exabyte 8mm cartridge tape and CD-ROM for data transfer purposes follow in square brackets (see also Annex A3). The maps in which the files were used are given in bold italics.

1. *bathy+isles+npbmod.sg [bathy.mod]* ***(Map 1)****:* elavation/bathymetry -
   the basic grid was modified slightly using the EarthVision graphics editor to remove a gridding overshoot in quadrants 16/17 and to keep a couple of small islands in quadrants 134/135 above water.

2. *fag_smp01_upp3to2.sg [fa_grav.mod]* ***(Map4)****:* free-air gravity anomaly -
   light smoothing with EarthVision filter and variable upward continuation of from 300 m in the east to 2 km over the western half of the map to allow for the change in data quality.

3. *fag_upp3to2.1hd [fa_grav.1hd]* ***(Maps 5a and 5b)****:* horizontal gradient of the free-air gravity anomaly -
   magnitude of the horizontal gradient derived from grid 2.

4. *fag_res10km.sg [faa_10km.res]* ***(Map 6)****:* residual free-air gravity anomaly -
   grid 2 was upwardly continued by 10 km and the result subtracted from grid 2.

5. *iso_bag275_up_et5.sg [isog_275.mod]* ***(Maps 7a/7b, 20 and 21)****:* isostatically-compensated Bouguer gravity anomaly -
   the basic Bouguer gravity anomaly grid at a reduction density of 2.75 Mg/m^3 was variably continued (as for grid 2) and from this was subtracted the gravity anomaly attributable to the present-day topographic load as reflected at the base of a crust with an elastic thickness of 5 km in isostatic equilibrium. The reference crust was assigned a thickness of 30 km with a load replacement density offshore of 2.5 Mg/m^3 (sea water 1.03 Mg/m^3) and a density contrast of 0.4 Mg/m^3 at its base.

6. *iso_bag220_up_et5.sg [isog_220.mod]* ***(Map 8)****:* isostatically-compensated Bouguer gravity anomaly -
   as for grid 5 except that the starting point was the basic Bouguer gravity anomaly grid at a reduction density of 2.20 Mg/m^3.

7. *iso_bag275_up_et5_1hd.sg [isog_275.1hd]* ***(Maps 9a and 9b)****:* horizontal gradient of the isostatically-compensated Bouguer gravity anomaly -
   magnitude of the horizontal gradient derived from grid 5.

8. *iso_bag275_up_et5_gpot.1hd [isog_pot.1hd]* ***(Maps 9c)****:* horizontal gradient of the isostatically-compensated Bouguer gravity anomaly potential -
   grid 5 was integrated to give the equivalent potential (ie. of which the acceleration due to gravity is the vertical derivative) and the magnitude of the horizontal gradient of this potential then calculated.

9. isog_275_res10km.sg [isog_10k.res] ***(Map 10)****:* residual isostatically-compensated Bouguer gravity anomaly -

grid 5 was upwardly continued by 10 km and the result subtracted from grid 5.

10. mag_tf_smp01.sg [mag_p01.smo] ***(Map 12)****:* total magnetic field anomaly -

the basic anomaly grid, referred to IGRF 1980 and at an effective elevation of 450 m above mean sea level, was lightly smoothed using an EarthVision filter.

11. mag_rtp.sg [mag.rtp] ***(Maps 13, 20 and 21)****:* reduced-to-pole magnetic field anomaly -

grid 10 was reduced-to-pole assuming a contemporary field inclination of 68.7° and a declination of 13°W.

12. mag_rtp_1hd_smp01.sgi [mag_rtp.1hd] ***(Maps 14a and 14b)****:* horizontal gradient of the reduced-to-pole magnetic anomaly -

the magnitude of the horizontal gradient was derived from grid 11 and smoothed in EarthVision; the result was then interpolated and any resulting negative values clipped to zero.

13. mag_rtp_up2p5.sg [rtp_2p5.up] ***(Map 15)****:* upwardly-continued reduced-to-pole magnetic anomaly -

grid 11 was upwardly continued by 2.5 km.

14. mag_rtp_res2p5_smp05.sg [rtp_2p5.res] ***(Maps 16a and 16b)****:* residual reduced-to-pole magnetic anomaly -

grid 13 was subtracted from grid 11 and the result was then smoothed using the EarthVision filter.

15. mag_rtp_up1_AS_smp05.sg [rtp_up1.AS] ***(Map 17)****:* the analytic signal of the reduced-to-pole magnetic anomaly -

the magnitude of the reduced-to-pole magnetic anomaly gradient (directly related to the so-called analytic signal) was calculated from grid 11 after upward continuation by 1 km and smoothed using the EarthVision filter.

*16. mag_psg_1hd.sg [*mag_psg.1hd*]* ***(Map 18)****:* the horizontal gradient of the pseudo-gravity anomaly -

the pseudo-gravity values were calculated from grid 12 and the magnitudes of the horizontal gradients then calculated.

17. 3dg_t02.sgi [3dg_thk.sed] ***(Map 22a):*** the optimized thickness of the sedimentary cover sequence as defined by the 3D gravity model.

18. 3dg_e03.sgi [3dg_top.uc] ***(Map 22b):*** the optimized depth of the sedimentary cover sequence (and of the top of the basement) as defined by the 3D gravity model.

19. 3dm_p02.sg [3dm_uc.mag] ***(Map 23):*** the optimized magnetization within the basement/upper crust as defined by the 3D magnetic model.

Additional ASCII grid files

The grids as compiled by ARK Geophysics Ltd:

20. bathy.ark: bathymetry/topography

21. fa_grav.ark: free-air anomaly offshore, Bouguer anomaly at 2.67 Mg/m^3 on land

22. ba220.ark: Bouguer anomaly corrected at 2.20 Mg/m^3 offshore, at 2.67 Mg/m^3 on land

23. ba275.ark: Bouguer anomaly corrected at 2.75 Mg/m^3 offshore, at 2.67 Mg/m^3 on land

24. mag2.ark: total field magnetic anomaly (NB: grid node interval 1.2 km NOT 1 km)

Grids not used in generating images:

25. ba_220.iso: isostatically-compensated Bouguer anomaly calculated as in grid 6 above but with the bathymetric load density and Bouguer reduction density offshore both set to 2.20 Mg/m^3

26. ba_275.iso: isostatically-compensated Bouguer anomaly calculated as in grid 5 above but with the bathymetric load density and Bouguer reduction density offshore both set to 2.75 Mg/m^3

Point data files:

1. gravnav_xy.ann [grav_xy.dat] ***(Map 2)****:* x,y grid co-ordinate locations of digital point gravity survey data used in the compilation.

2. magnav_xy.ann [mag_xy.dat] ***(Map 3)****:):* x,y,grid co-ordinate locations of digital point magnetic survey data used in compilation.

3. eul_isog_0p5_60_7_9.ann [euler_g.dat] ***(Map 11)****:* gravity Euler solution locations as x,y grid co-ordinates and depths (negative below sea-level) -

Euler deconvolution results were obtained using grid 5 and its 1st vertical derivative as inputs and a structural index of 0.5. Other parameters (60/7/9) refer to the error constraints placed on z, x and y for acceptable solutions.

4. mag_eul_1p0_50z.ann [euler_m.dat] ***(Map 19)****:* magnetic Euler solution locations as x,y grid co-ordinates and depths (negative below sea-level) -

Euler deconvolution results were obtained using grid 11 and its 1st vertical derivative as inputs and a structural index of 1.0. The parameter 50z refers to the error constraint placed on depths for acceptable solutions.

5. landmask.pol: this is the outline of the mask used to exclude the onshore Ireland area from the grids. All grid nodes within it have been set to null (ie. 1e+20). The mask only applies to the exported grids and to the images of the 3D modelling results (maps 22a, 22b and 23) - in the latter case, a secondary zone of masking is included to avoid edge effects.

ANNEX A3: *DETAILS OF DIGITAL OUTPUT FILES*

It was agreed at the project proposal stage that the maps/images should be distributed in a digital format, allowing RSG members to produce hardcopy output in-house as required. Only one set of printed maps was supplied as part of the contract- to PAD.

The original specification was for a set of plot files to be provided, together with the grid files used in generating the images. CGM format was approved for the former, with ASCII (rather than binary) for the latter. Although straightforward in principle this did lead to a number of practical problems, more particularly in respect of the images. The end result is that a number of alternative plot file formats has been provided, as discussed below.

Grid/data files

As a requirement of the terms on which data were made available to the project the basic working grids had to be clipped to the map/image area defined by UTM grid eastings 250 km and 1000 km and grid northings 5650 km and6350 km. Also, the area covered by the Irish landmass had to be excluded by setting these grid values to 'null' (defined as 1e+20).

Clearly, for further processing (eg. using Fourier techniques) over the full area, it will generally be necessary to strip out the null values and re-grid. Some grid editing software (eg. EarthVision) allows the user to sketch in generalized contours over the masked area. Alternatively, additional data points can be defined explicitly to provide a more realistic representation of the field than a simple extrapolation procedure.

The grids have been written in full, with one point per line as:

x <tab>y<tab>node value

where: x and y are specified in kilometres.
units of the grid values are as labelled on the colour bar of the images (generally using mGal, nT, km etc. as appropriate).

See Annex A2 for further details of the grids and the filenames adopted.

The output is ordered by rows starting from the bottom, (ie.south-west) corner of each grid.

Some additional data are also supplied in ASCII format. These comprise the Euler solutions and the digital data point locations.

Plot files

Two basic problems emerged after generating the 'final' suite of maps, supplied as hardcopy to PAD.

- The Zeh compositing facility 'zcmp' had been used in order to include the inset location map and RSG and ARK logos on the map face. Hardcopy versions of the combined images can be plotted directly without difficulty from this software. However, going through the intermediate step of generating the composite CGM as a separate file resulted in some corruption of the original colour tables.

- The CGM files make use of the extended Zeh fonts set ZPS-PFNT. If this is not implemented on the local printer then some of the text will take default styles and may not scale as intended.
- Although widely available in the oil industry, the Zeh software is not used by all RSG members.

In order to resolve the main difficulty associated with a software specific product, a separate set of composited CGM plot files was created using a slightly simplified style of presentation (NB: this had no effect on the basic image).

It was also realized that CGM's are not very convenient for quick-look, screen viewing purposes. A set of JPEG images is provided to meet this requirement. The images were initially captured from the screen display and then converted.

When producing examples of the images at a reduced (A3) scale for inclusion in the final report it proved necessary to revert to Postscript output files to maintain reasonable quality. This incomplete set has also been supplied (the scale being approximately 1:2.9M).

Data structure as written to Exabyte / CD-ROM

The data were made available on Exabyte 8mm cartridge tape or CD-ROM as preferred by individual group members. In order to preserve the integrity of file names on CD-ROM (given the character length restrictions on this medium) the names of the grid files were modified from those shown in the information box of the images themselves (as described in Annex A2).

Exabyte tapes were written from a Silicon Graphics UNIX workstation using the command:

tar -cvbf 20 /dev/rmt/tps0d6v.8200 *

CD-ROMs were written to the ISO9660 (/Joliet) standard from a PC running under NT.

The files, amounting to about 1.2 Gbytes in total, are organized within a set of 5 subdirectories (2D_MODEL, CGM_CMP, CGM_FULL, GRID_DAT and JPEG_PS) according to data type: The limited capacity (650 Mbytes) of the CD-ROMs meant that the data had to be distributed between two disks with 2D_MODEL, CGM_CMP and GRID_DAT on disk 1 and CGM_FULL and JPEG_PS written to disk 2.

Listings of the contents of each of the subdirectories follow, giving the sizes of the files as written:

/2D_MODEL CGM plot files showing observed/calculated gravity and magnetic anomalies and the corresponding models. Each line is plotted at two scales:

the 6 shorter profiles are supplied as separate gravity and magnetic component models at 1:100k horizontal scale with a vertical exaggeration of 0.667, and as a single plots at 1:200k horizontal scale with a vertical exaggeration of 1:1

the two regional lines are plotted as combined gravity/magnetic models at 1:750k horizontal scale with a vertical exaggeration of 1:2.5 and at 1:500k with a vertical exaggeration of 1:1.

total size: 61907 blocks x512 bytes (approx. depending on device directory structure)

File name	*Date (last modified)*	*Size (bytes)*
2d_107.cgm	Oct 29 18:44	1764804
2d_107g.cgm	Oct 29 18:44	2044858
2d_107m.cgm	Oct 29 18:44	2133200
2d_108.cgm	Oct 29 18:45	1672964
2d_108g.cgm	Oct 29 18:44	1732560
2d_108m.cgm	Oct 29 18:44	1848672
2d_116.cgm	Oct 31 15:53	56552
2d_116x1.cgm	Oct 31 15:53	55292
2d_118.cgm	Oct 29 18:45	1929286
2d_118g.cgm	Oct 29 18:44	2070392
2d_118m.cgm	Oct 29 18:44	2168194
2d_204.cgm	Oct 29 18:45	1371106
2d_204g.cgm	Oct 29 18:45	1517728
2d_204m.cgm	Oct 29 18:45	1630580
2d_25.cgm	Oct 29 18:45	1604974
2d_25g.cgm	Oct 29 18:45	1659946
2d_25m.cgm	Oct 29 18:45	1742798
2d_32.cgm	Oct 31 15:54	63762
2d_32x1.cgm	Oct 31 15:59	62370
2d_37.cgm	Oct 29 18:45	1306502
2d_37g.cgm	Oct 29 18:45	1577704
2d_37m.cgm	Oct 29 18:45	1673876

/CGM_CMP these files are the component images used for compositing the 'final' maps which comprise the RSG and ARK logos and the inset location map (common to all compositions) together with the relevant main image with its legend. The Zeh composition (*.cmp) files are also supplied for direct use with 'zcmp' but the images could be combined using other software available to the user.

total size: 676763 blocks x512 bytes (approx. depending on device directory structure)

File name	*Date (last modified)*	*Size (bytes)*
ark_logo.cgm	Jul 13 19:13	841682
insetmap.cgm	Jul 13 19:13	856150
rsg_logo.cgm	Jul 13 19:13	3636652

File name	*Date (last modified)*	*Size (bytes)*
map1.cgm	Jul 20 08:28	10088154
map10.cgm	Oct 29 17:43	11036184
map11.cgm	Jul 19 10:30	4216510
map12.cgm	Jul 20 09:04	14331516
map13.cgm	Jul 20 09:15	15028738
map14a.cgm	Jul 20 09:15	4973926
map14b.cgm	Jul 20 09:16	4942650
map15.cgm	Jul 20 09:18	11996018
map16a.cgm	Jul 20 09:21	13860690
map16b.cgm	Jul 20 09:22	4910670
map17.cgm	Jul 20 09:28	11786546
map18.cgm	Jul 20 09:34	11215914
map19.cgm	Jul 19 11:17	4612170
map2.cgm	Jul 19 09:28	39045730
map20.cgm	Jul 20 09:47	9994518
map21.cgm	Oct 29 17:43	15047860
map22a.cgm	Oct 30 14:41	13263670
map22b.cgm	Oct 30 14:42	11684776
map23.cgm	Oct 30 14:42	10491412
map3.cgm	Jul 19 09:43	37718236
map4.cgm	Jul 20 08:29	10817678
map5a.cgm	Jul 20 08:29	4981366
map5b.cgm	Jul 20 08:30	4948702
map6.cgm	Jul 20 08:31	11595356
map7a.cgm	Jul 20 08:33	9983088
map7b.cgm	Jul 20 08:37	9983144
map8.cgm	Jul 20 08:38	10117342
map9a.cgm	Jul 20 08:39	4973554
map9b.cgm	Jul 20 08:40	4948950
map9c.cgm	Jul 20 08:42	8511182

/CGM_CMP (continued)

File name	*Date (last modified)*	*Size (bytes)*
map1.cmp	Nov 6 14:10	1473
map10.cmp	Nov 6 14:10	1475
map11.cmp	Nov 6 14:11	1475
map12.cmp	Nov 6 14:11	1475
map13.cmp	Nov 6 14:11	1475
map14a.cmp	Nov 6 14:12	1477
map14b.cmp	Nov 6 14:12	1477
map15.cmp	Nov 6 14:12	1475
map16a.cmp	Nov 6 14:12	1477
map16b.cmp	Nov 6 14:13	1477
map17.cmp	Nov 6 14:13	1475
map18.cmp	Nov 6 14:13	1475
map19.cmp	Nov 6 14:14	1475
map2.cmp	Nov 6 14:14	1473
map20.cmp	Nov 6 14:14	1475
map21.cmp	Nov 6 14:14	1475
map22a.cmp	Nov 6 14:15	1477
map22b.cmp	Nov 6 14:15	1477
map23.cmp	Nov 6 14:15	1474
map3.cmp	Nov 6 14:15	1473
map4.cmp	Nov 6 14:16	1473
map5a.cmp	Nov 6 14:16	1475
map5b.cmp	Nov 6 14:16	1475
map6.cmp	Nov 6 14:17	1473
map7a.cmp	Nov 6 14:17	1475
map7b.cmp	Nov 6 14:17	1475
map8.cmp	Nov 6 14:18	1473
map9a.cmp	Nov 6 14:18	1475
map9b.cmp	Nov 6 14:18	1475
map9c.cmp	Nov 6 14:19	1475

/CGM_FULL complete images (ie. including logos and inset map) with a slightly modified presentation from that derived using zcmp with the files in CGM_CMP.

total size: 1020448 blocks x512 bytes (approx. depending on device directory structure)

File name	*Date (last modified)*	*Size (bytes)*
zmap1.cgm	Jul 20 11:19	17454764
zmap10.cgm	Oct 29 17:46	18394602
zmap11.cgm	Jul 19 15:16	9027716
zmap12.cgm	Jul 20 11:45	21689942
zmap13.cgm	Jul 20 11:46	22387156
zmap14a.cgm	Jul 20 11:47	2332514
zmap14b.cgm	Jul 20 11:48	12305126
zmap15.cgm	Oct 29 17:47	19354464
zmap16a.cgm	Jul 20 12:17	21219108
zmap16b.cgm	Jul 20 12:18	12277034
zmap17.cgm	Jul 20 12:39	19145134
zmap18.cgm	Jul 20 12:40	18574332
zmap19.cgm	Jul 19 15:42	9371250
zmap2.cgm	Jul 19 17:40	31966772
zmap20.cgm	Jul 20 12:42	17352948
zmap21.cgm	Oct 29 17:45	22406290
zmap22a.cgm	Oct 31 15:35	20619222
zmap22b.cgm	Oct 31 15:35	19040004
zmap23.cgm	Oct 31 15:36	17846944
zmap3.cgm	Jul 19 18:18	25241298
zmap4.cgm	Jul 20 11:24	18176112
zmap5a.cgm	Jul 20 11:26	12338932
zmap5b.cgm	Jul 20 11:29	12310360
zmap6.cgm	Jul 20 11:31	18953774
zmap7a.cgm	Jul 20 11:33	17341506
zmap7b.cgm	Jul 20 11:38	17341562
zmap8.cgm	Jul 20 11:39	17475922
zmap9a.cgm	Jul 20 11:40	12332142
zmap9b.cgm	Jul 20 11:41	12310608
zmap9c.cgm	Jul 20 11:42	15869588

/GRID_DAT ASCII files of the grids used in creating the images, gravity and magnetic Euler solution information and gravity and magnetic data point locations.

total size: 510455 blocks x512 bytes (approx. depending on device directory structure)

File name	*Date (last modified)*	*Size (bytes)*
3dg_thk.sed	Nov 2 11:48	8782941
3dg_top.uc	Nov 2 11:55	9271566
3dm_uc.mag	Nov 2 11:58	9272722
ba220.ark	Nov 2 12:14	8008035
ba275.ark	Nov 2 12:15	8088799
ba_220.iso	Nov 2 13:21	8849241
ba_275.iso	Nov 2 13:22	8841669
bathy.ark	Nov 2 12:10	8308425
bathy.mod	Jul 16 12:23	9496595
euler_g.dat	Sep 17 14:58	2141130
euler_m.dat	Sep 17 14:58	2391120
fa_grav.1hd	Jul 16 12:27	9091797
fa_grav.ark	Nov 2 12:47	7868557
fa_grav.mod	Jul 16 12:27	8930835
faa_10km.res	Jul 16 12:26	9072750
grav_xy.dat	Jul 16 12:47	14563177
isog_10k.res	Jul 16 12:32	9099097
isog_220.mod	Jul 16 12:28	8980539
isog_275.1hd	Jul 16 12:30	9122293
isog_275.mod	Jul 16 12:29	8783063
isog_pot.1hd	Jul 16 12:31	8779544
landmask.pol	Jul 13 18:35	1283
mag.rtp	Jul 16 12:33	9032816
mag2.ark	Nov 2 12:48	6613313
mag_p01.smo	Jul 16 12:37	9091979
mag_psg.1hd	Jul 16 12:32	9128863
mag_rtp.1hd	Nov 2 14:46	8793820
mag_xy.dat	Jul 16 12:47	14058841
rtp_2p5.res	Jul 16 12:35	9061605
rtp_2p5.up	Jul 16 12:36	9031893
rtp_up1.AS	Jul 16 12:36	8782845

/JPEG_PS a full set of 'jpeg' format images derived by a screen-capture procedure together with selected Postscript file versions as reproduced in this report.

total size: 172071 blocks x512 bytes (approx. depending on device directory structure)

File name	*Date (last modified)*	*Size (bytes)*
map1.jpg	Jul 18 14:39	344714
map10.jpg	Jul 18 17:06	402878
map10.ps	Oct 29 18:32	5046369
map11.jpg	Jul 18 14:48	402406
map12.jpg	Jul 18 17:07	411848
map12.ps	Oct 29 18:32	5936398
map13.jpg	Jul 18 17:07	423733
map14a.jpg	Jul 18 17:08	390723
map14b.jpg	Jul 18 17:08	328185
map14b.ps	Oct 29 18:32	4129858
map15.jpg	Jul 18 17:09	390386
map16a.jpg	Jul 18 17:10	435075
map16a.ps	Oct 29 18:33	6180974
map16b.jpg	Jul 18 17:10	238382
map17.jpg	Jul 18 17:13	440090
map18.jpg	Jul 18 17:14	420724
map18.ps	Oct 29 18:33	6013983
map19.jpg	Jul 19 08:54	421530
map2.jpg	Jul 19 08:52	275026
map20.jpg	Jul 19 08:54	414635
map20.ps	Oct 29 18:33	6254065
map21.jpg	Jul 19 08:55	413432
map22a.jpg	Nov 2 11:38	372087
map22a.ps	Oct 29 20:07	5490569
map22b.jpg	Nov 2 11:38	369246
map22b.ps	Oct 29 20:08	5255829
map23.jpg	Nov 2 11:38	371938
map23.ps	Oct 31 15:48	5120401
map2_ps.gz	Oct 29 18:33	3524434
map3.jpg	Jul 19 08:53	335089
map3_ps.gz	Oct 29 18:33	3953785
map4.jpg	Jul 18 17:04	379105
map4.ps	Oct 29 18:33	5001824
map5a.jpg	Jul 18 14:41	357132
map5b.jpg	Jul 18 14:41	308303
map6.jpg	Jul 18 17:04	391974
map7a.jpg	Jul 18 17:05	365290
map7a.ps	Oct 29 18:33	5617947
map7b.jpg	Jul 18 17:05	371346
map8.jpg	Jul 18 17:06	361629
map9a.jpg	Jul 18 14:46	369223
map9a.ps	Oct 29 18:33	4156760
map9b.jpg	Jul 18 14:46	318111
map9c.jpg	Jul 18 14:47	390439
map9c.ps	Oct 29 18:33	5184352

ANNEX A4: *SELECTED MAPS REPRODUCED AT A3 SIZE*

A selection of maps/images reproduced at a nominal scale of 1:2.9M from the prepared suite of maps (cf. Annex A1) available as digital plot files:

Map 2 - gravity data point distribution
Map 3 - magnetic data point distribution
Map 4 - free-air gravity anomaly
Map 7a - isostatically-compensated Bouguer gravity anomaly
Map 9a - horizontal gradient of compensated Bouguer gravity anomaly
Map 9c - horizontal gradient of gravity potential
Map 10 - residual compensated Bouguer gravity anomaly
Map 12 - total magnetic field anomaly
Map 14b - horizontal gradient of reduced-to-pole magnetic anomaly
Map 16a - residual magnetic anomaly
Map 18 - horizontal gradient of pseudo-gravity anomaly
Map 19 *** - Euler deconvolution solutions from magnetic data
Map 20 - gravity anomaly line contours on shaded relief image of magnetic anomaly
Map 22a - apparent basin thickness from a 3D gravity model
Map 22b - apparent basement surface relief from a 3D gravity model
Map 23 - apparent magnetization of upper crust from a 3D magnetic model

Note that the layout of these maps has been simplified from that used for the CGM plot files in order to improve legibility and the view area of the images at the reduced scale (approx 1:2.9M).

Map 19 is an example of a direct reduction of the CGM plot file. This indicates the full legend style to be expected when plotting at true scale from the CGMs.

ROCKALL TROUGH - IRISH SECTOR PIP/RSG Project 98/1: Compilation/presentation/interpretation of gravity and magnetic data

MAP 2: Location map of digital data points taken from marine gravity survey tracks

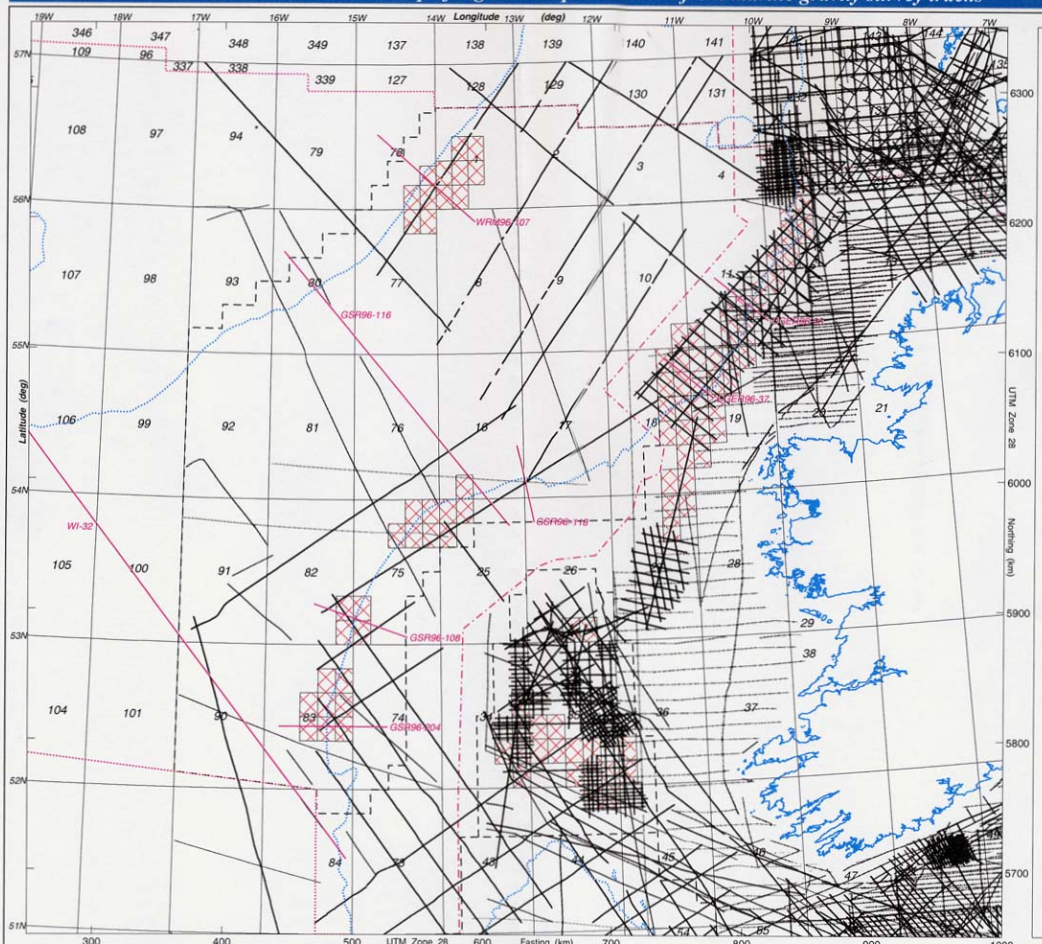

NOTE:

- satellite track data not shown;
- Irish land data points not shown.

ARK

ROCKALL TROUGH - IRISH SECTOR PIP/RSG Project 98/1: Compilation/presentation/interpretation of gravity and magnetic data

MAP 3: Location map of digital data points taken from magnetic survey tracks

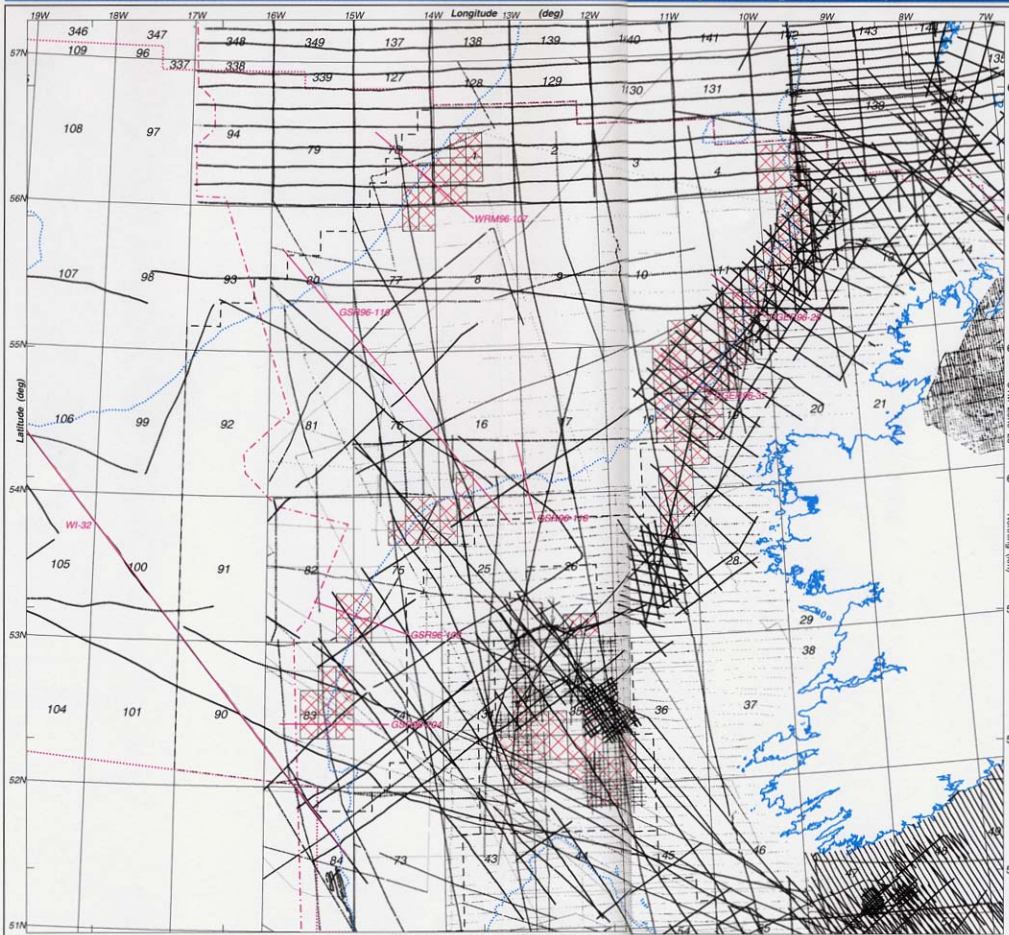

NOTE:

- data sourced from grids are not shown.

ARK

ROCKALL TROUGH - IRISH SECTOR PIP/RSG Project 98/1: Compilation/presentation/interpretation of gravity and magnetic data

MAP 4: Free-air gravity anomaly image (Bouguer anomaly values on land)

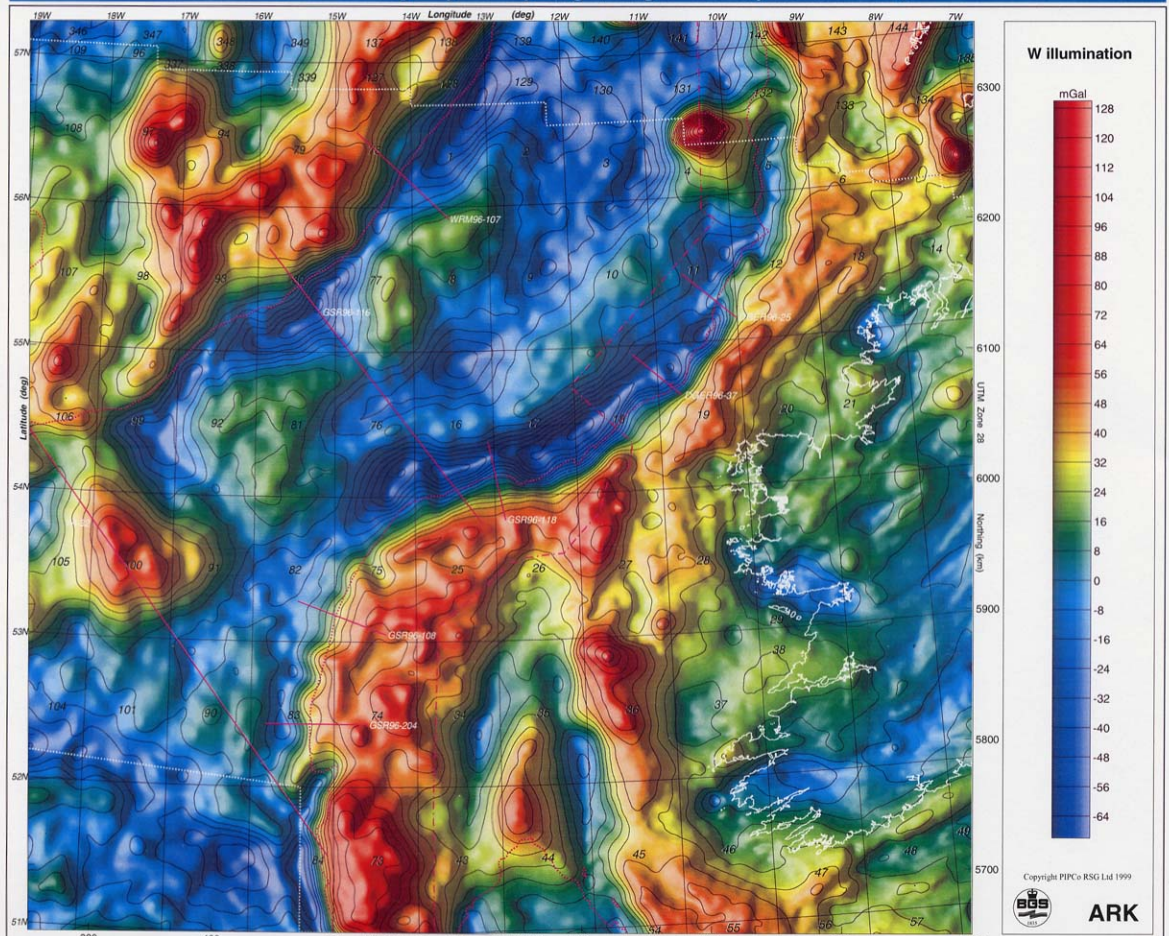

ARK

ROCKALL TROUGH - IRISH SECTOR PIP/RSG Project 98/1: Compilation/presentation/interpretation of gravity and magnetic data

*MAP 7a: Isostatically-compensated Bouguer gravity anomaly (at 2.75 Mg/m**3)*

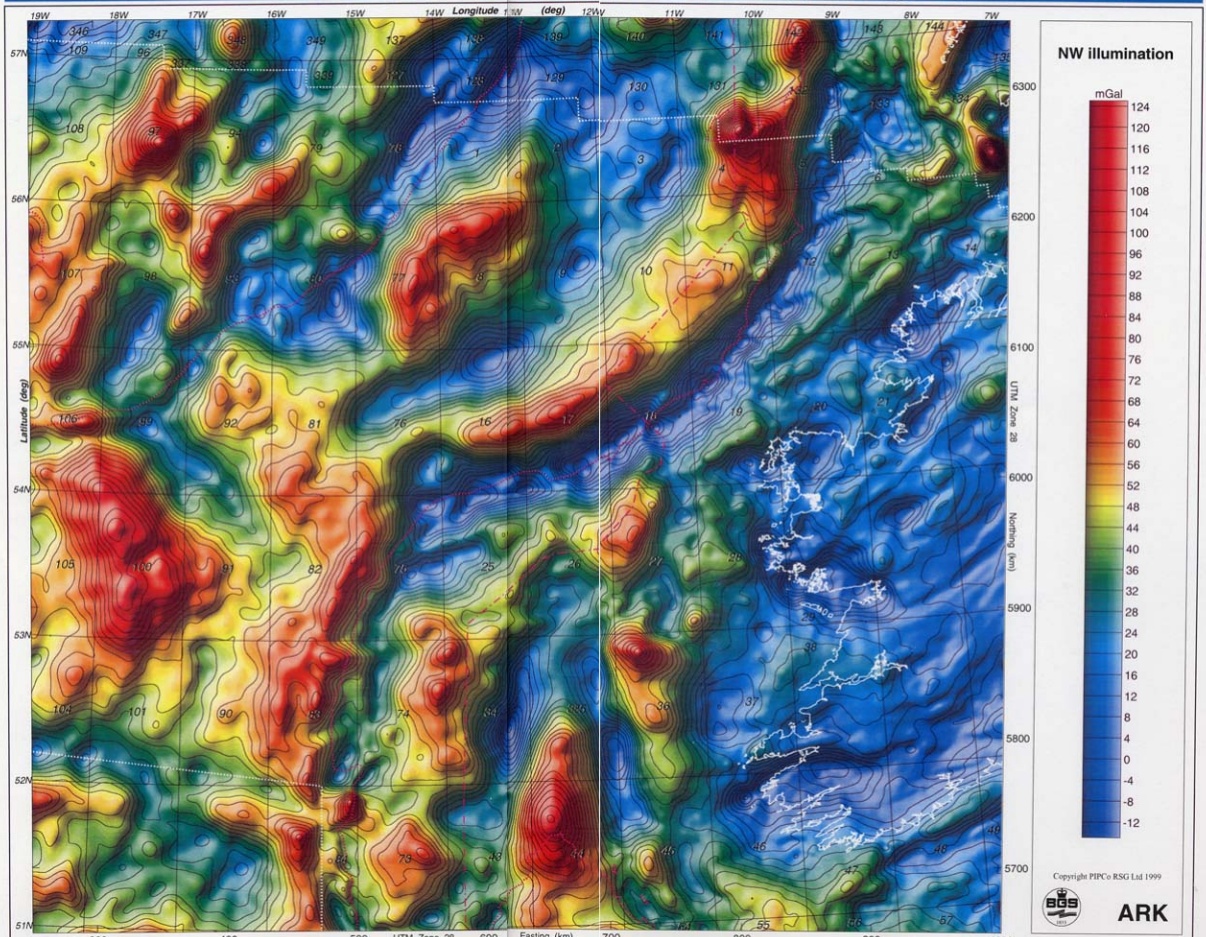

ARK

ROCKALL TROUGH - IRISH SECTOR PIP/RSG Project 98/1: Compilation/presentation/interpretation of gravity and magnetic data

MAP 9a: Horizontal gradient of isostatically-compensated Bouguer gravity anomaly

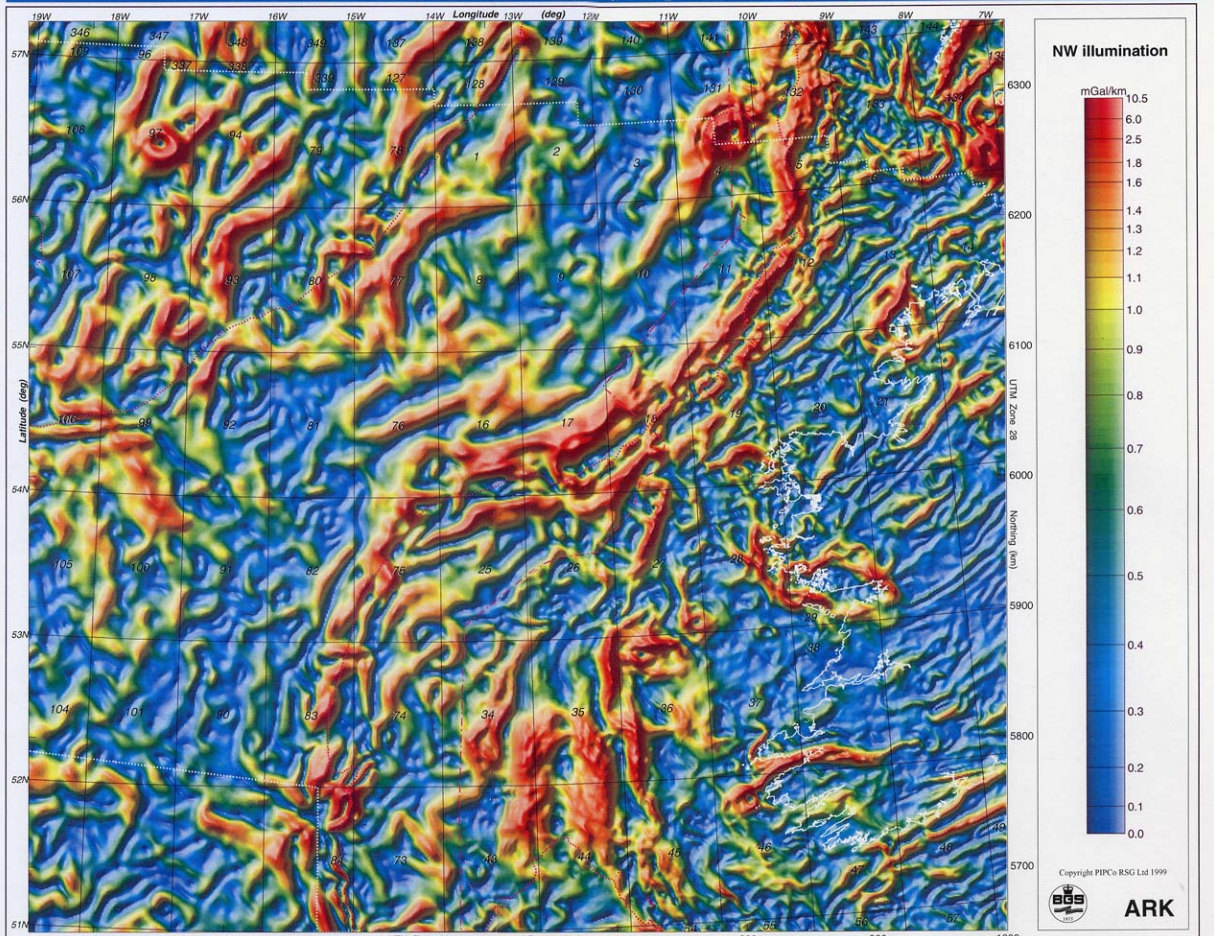

BGS

ARK

ROCKALL TROUGH - IRISH SECTOR PIP/RSG Project 98/1: Compilation/presentation/interpretation of gravity and magnetic data

MAP 9c: Horizontal gradient of isostatically-compensated gravity potential

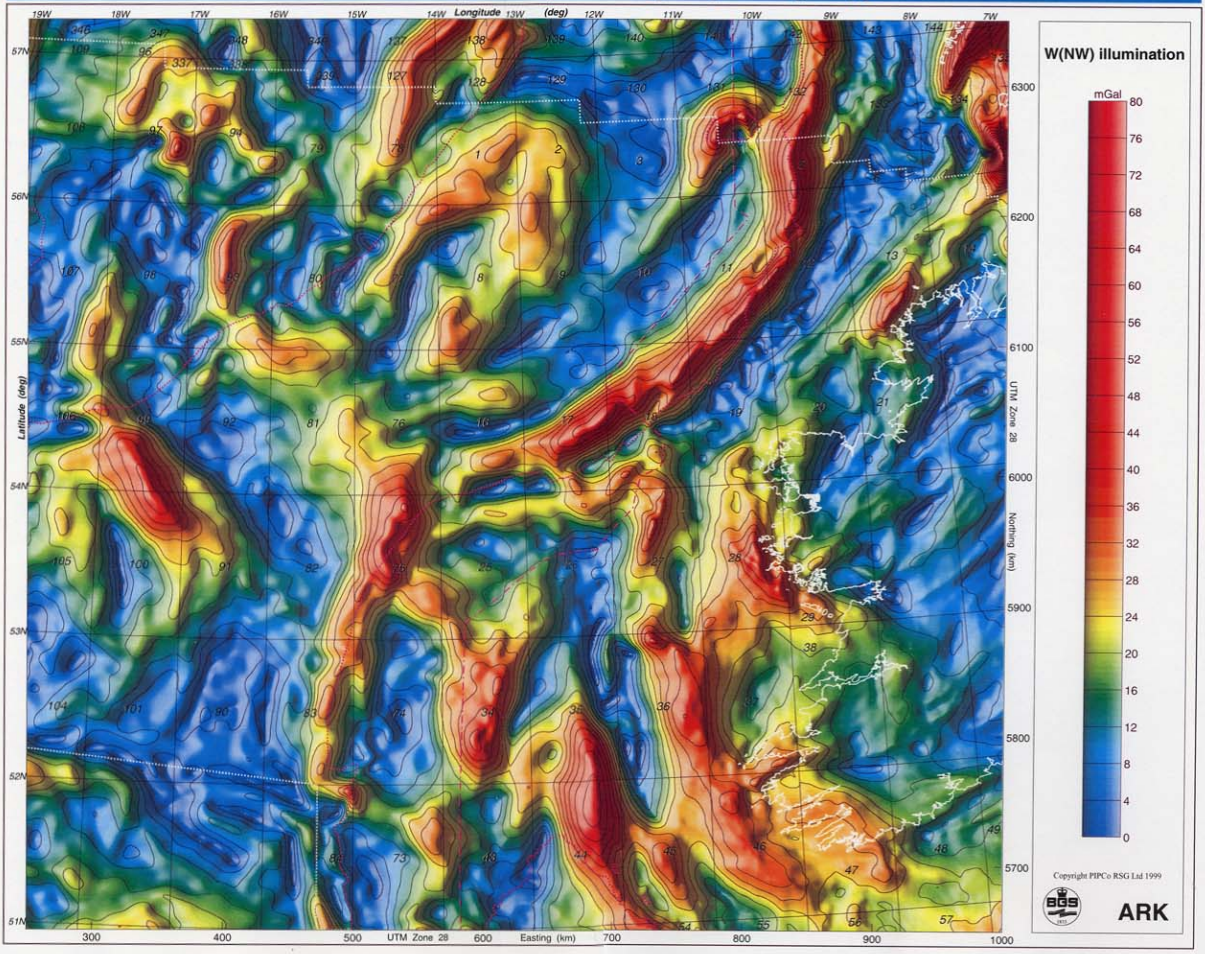

ARK

ROCKALL TROUGH - IRISH SECTOR PIP/RSG Project 98/1: Compilation/presentation/interpretation of gravity and magnetic data

MAP 10: 10 km continuation residual of Bouguer anomaly (isostatically-compensated)

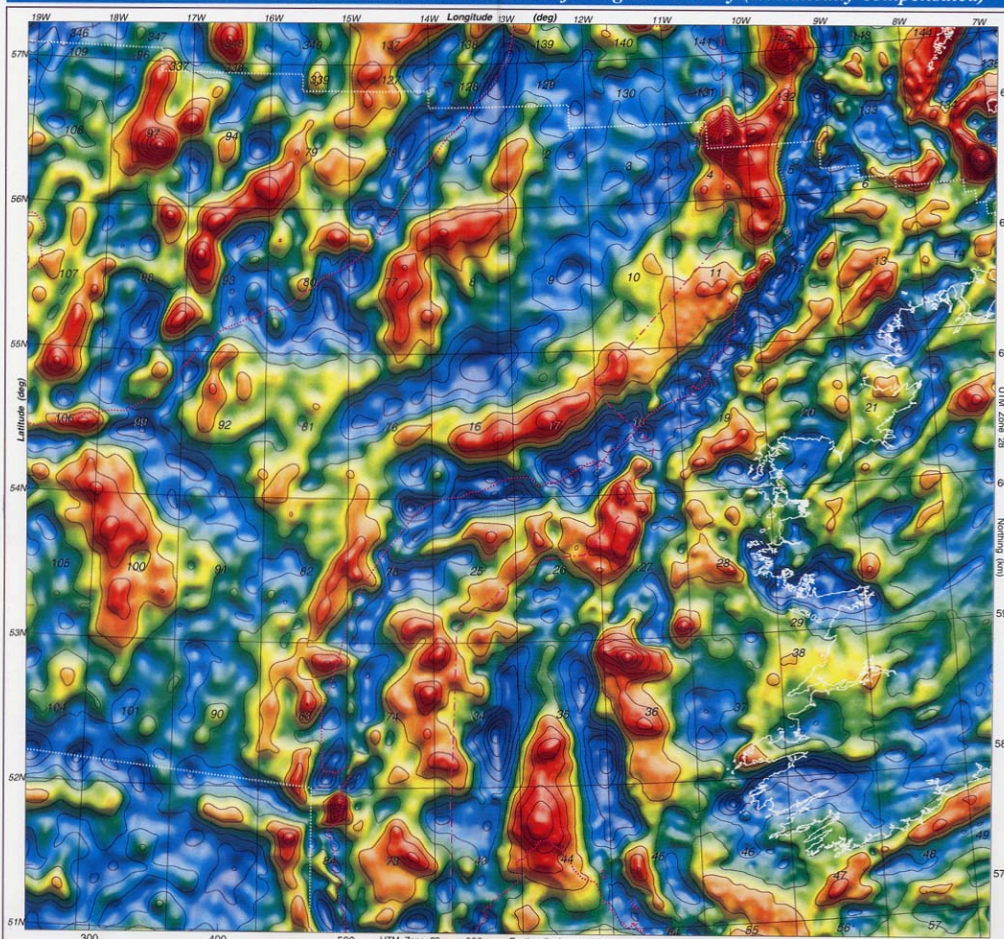

ARK

ROCKALL TROUGH - IRISH SECTOR PIP/RSG Project 98/1 Compilation/presentation/interpretation of gravity and magnetic data

MAP 12: Total magnetic field anomaly (as compiled at 450 m)

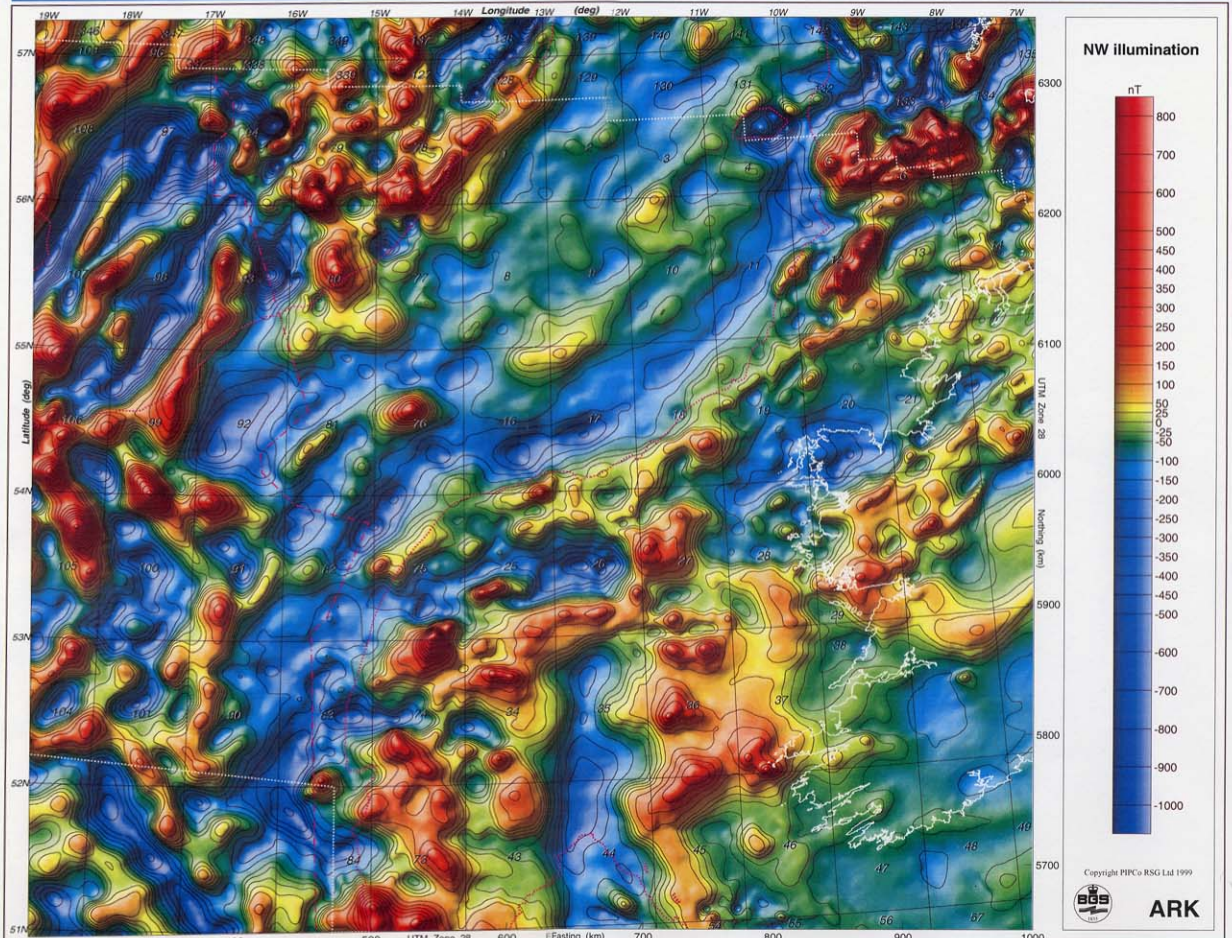

ARK

ROCKALL TROUGH - IRISH SECTOR PIP/RSG Project 98/1: Compilation/presentation/interpretation of gravity and magnetic data

MAP 14b: Horizontal gradient derived from reduced-to-pole magnetic anomaly

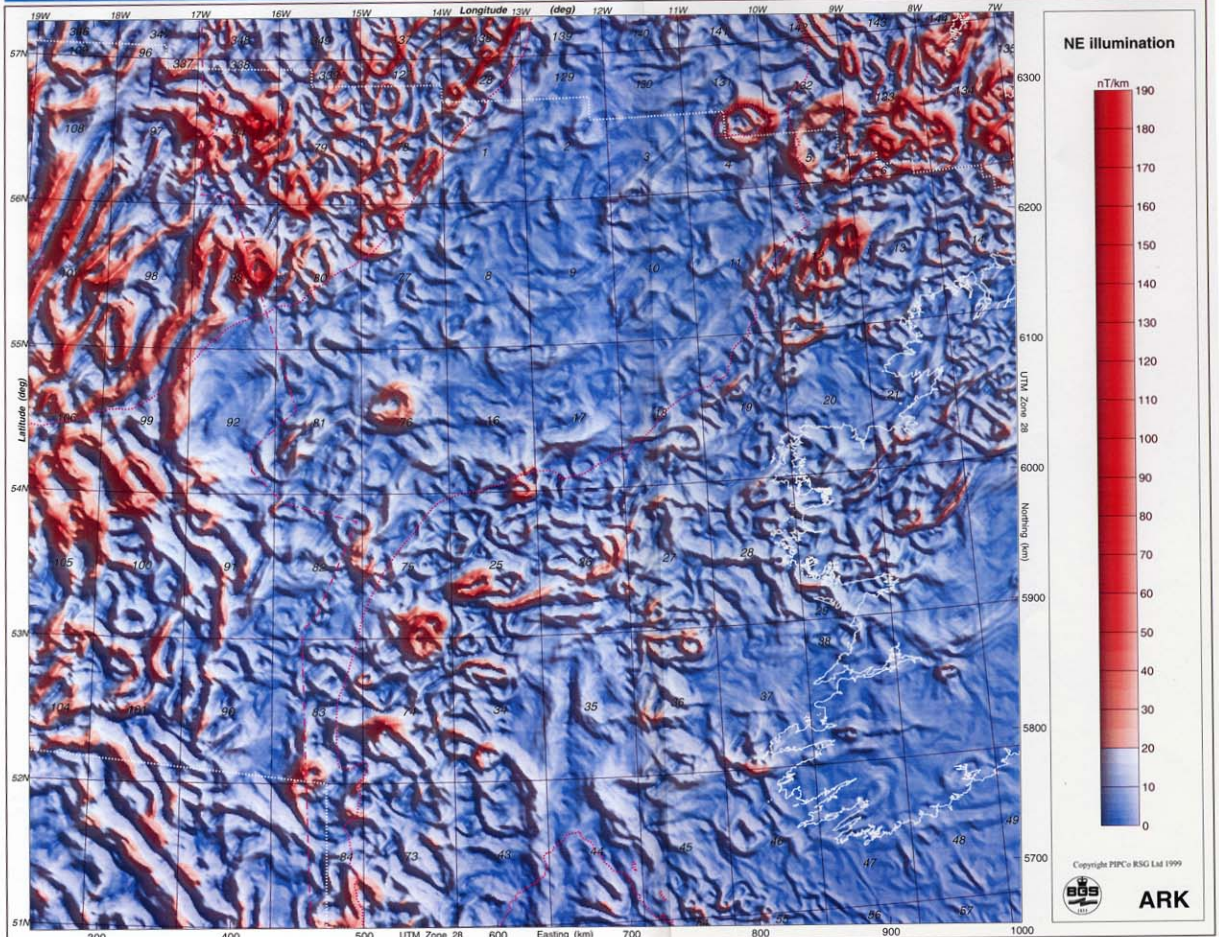

ROCKALL TROUGH - IRISH SECTOR PIP/RSG Project 98/1: Compilation/presentation/interpretation of gravity and magnetic data

MAP 16a: Residual RTP magnetic anomaly from 2.5 km upwardly-continued field

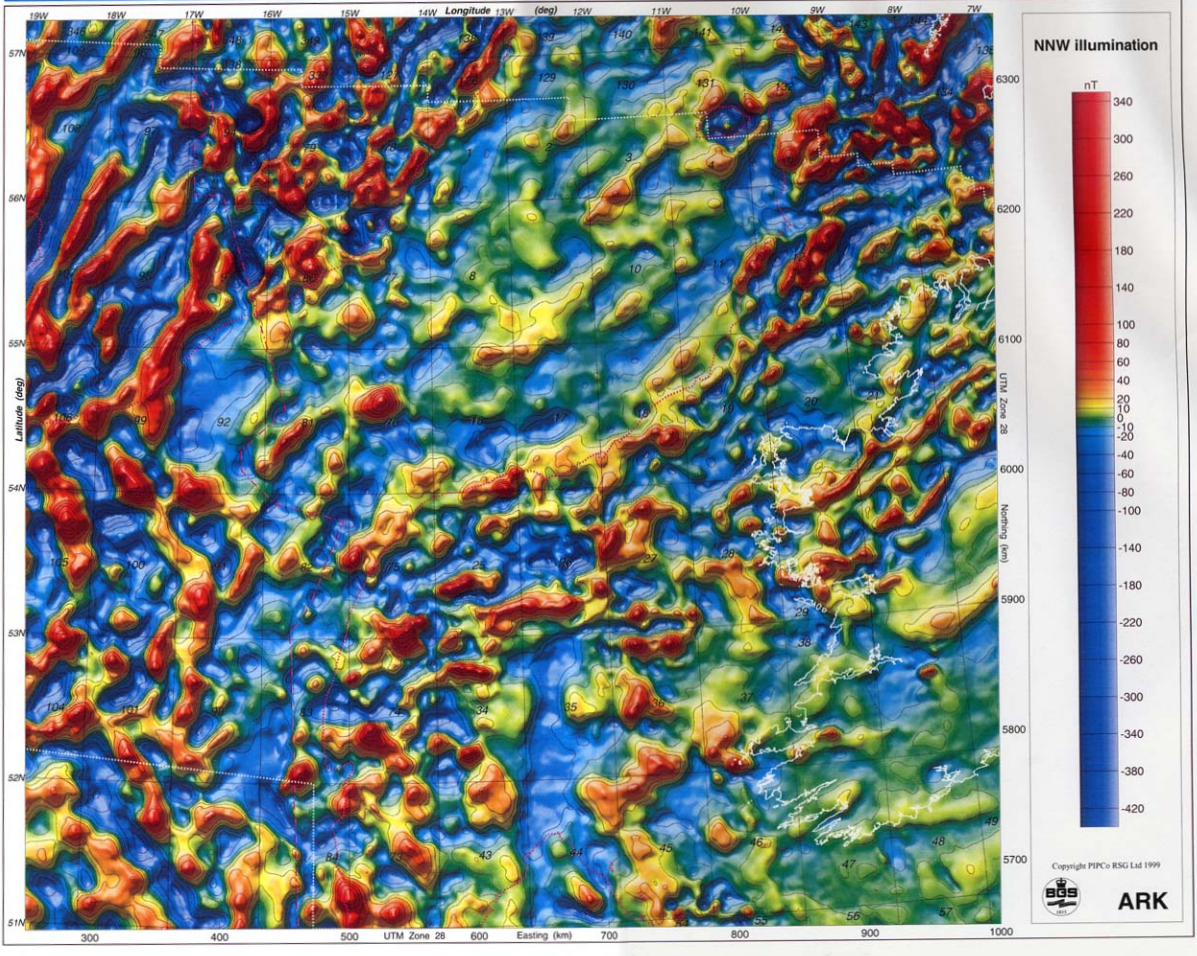

ROCKALL TROUGH - IRISH SECTOR PIP/RSG Project 98/1: Compilation/presentation/interpretation of gravity and magnetic data

MAP 18: Horizontal gradient of magnetic pseudo -gravity transformation

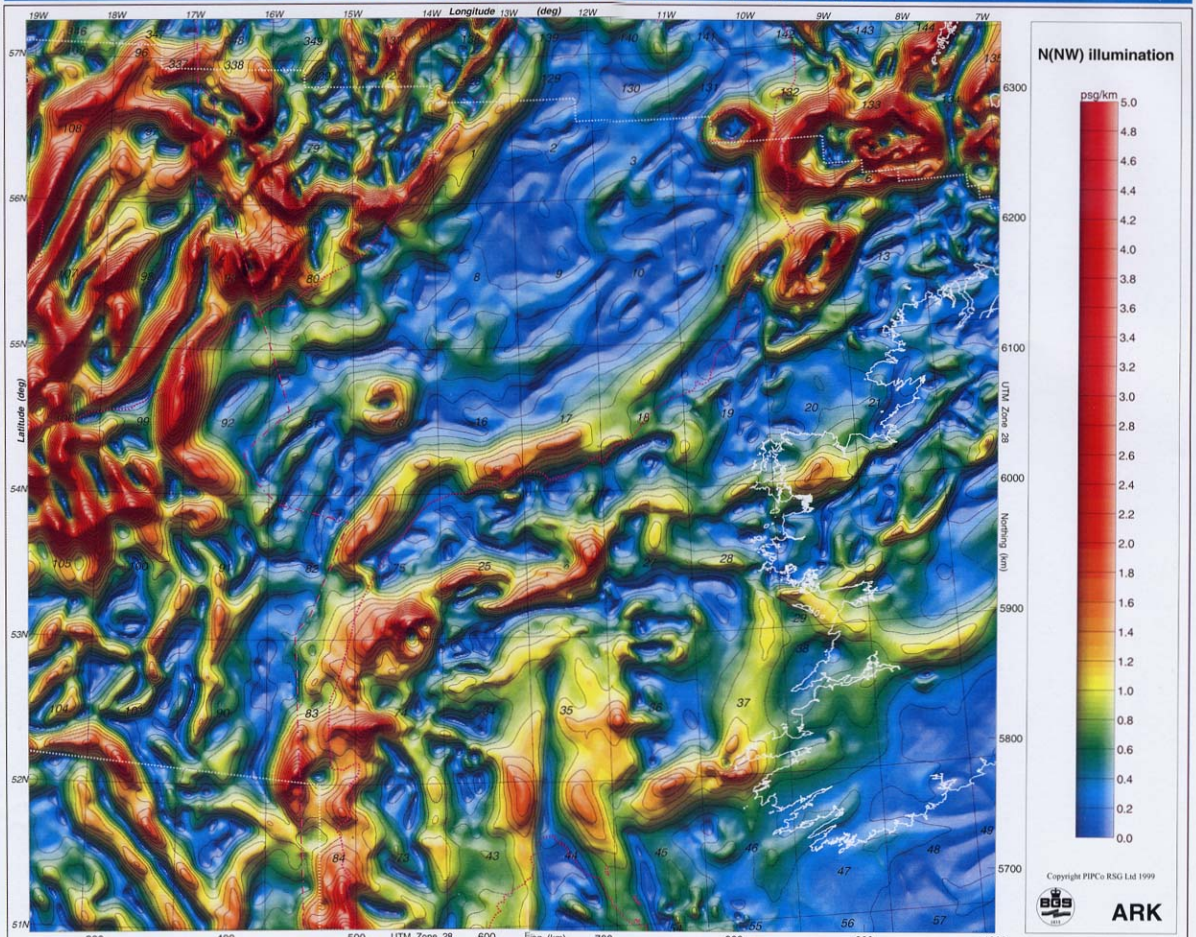

ARK

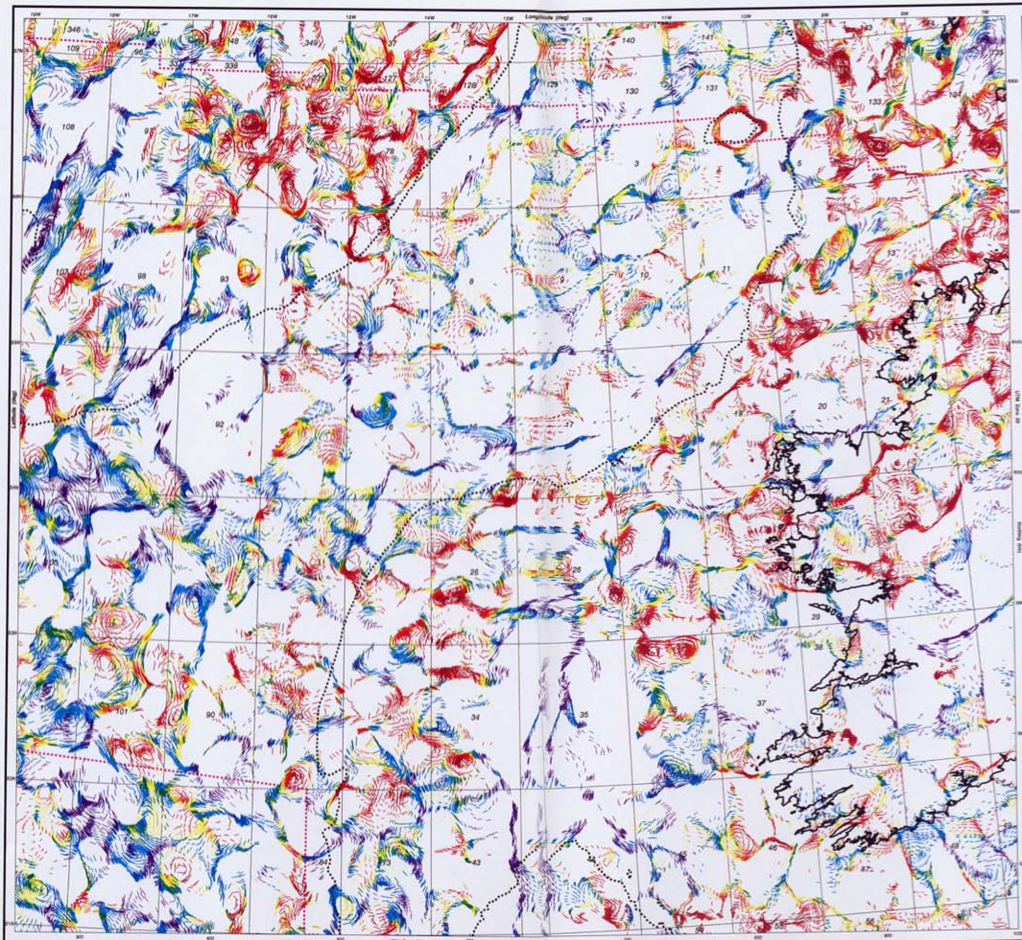

PIP/RSG Project 98/1 **ARK**

ROCKALL TROUGH – IRISH SECTOR

Compilation/presentation/interpretation of gravity and magnetic data

MAP 19

Euler deconvolution solutions from magnetic RTP anomaly data

Total gradient (AS) length scaling nT/km	Solution depth colour scaling km
~0	0
8	3
14	4
27	5
~200	6.5
	8
	10
	13
	~20

ANNOTATED BASE MAP

Euler solutions have been generated from 1 km grids of the reduced-to-pole aeromagnetic data using the calculation parameters:

structural index = 1.0
x,y solution tolerance = 7 km
z solution tolerance = 50 %
maximum solution offset = 9 km
x,y window size = 20 km
data point interval = 2 km
window shift = 2 km

Solutions are represented by lines coloured according to depth as measured nominally from mean sea level. The lines are orthogonal to the local gradient, with a length set by the analytic signal (ie. magnitude of the field gradient). Line colours/lengths have been set to give approximately equal numbers of solutions within each band.

Solution depths are reliable only as a guide to relative values. They have been revised upwards by 1–2 km to offset the limited high frequency content in the basic grids and the dependency on structural index.

The dotted magenta line represents the boundary of Irish designated continental shelf. The 1500 m bathymetric contour is drawn as a dotted line in black.

UTM grid on Hayford's spheroid (central meridian at 15°W)

0 10 20 30 40 50 60 70 80 90 100 km
1:1,000,000 image scale

IMAGE LOCATION MAP (bathymetric contours @ 500m intervals)

DATA SOURCES – ACKNOWLEDGEMENTS:

Data available directly to RSG included those from surveys undertaken in Irish waters before 1994 and some more recent data released by members of the consortium.

Of the other sources:

We thank The Dublin Institute for Advanced Studies who provided the onshore gravity data and The Geological Survey of Ireland who provided the onshore aeromagnetic data.

Satellite free-air gravity anomaly values were those released by the Scripps Institute of Oceanography.

Additional magnetic anomaly data were taken from the Arctic and North Atlantic Oceans Magnetic Compilation of the Geological Survey of Canada.

Additional bathymetric data were taken from the IOC/IHO General Bathymetric Chart of the Oceans (GEBCO) of 1997.

Details of the data and the processing techniques applied can be found in the accompanying report. Data compilation and compression of working grids were undertaken by Ark Geophysics Limited. Further processing and image production were carried out by the British Geological Survey.

Gravmag 97			
Mon Jul 19 11:19:07 1999			
UBDS	[illegible]	JOB	119

This Project, including data and survey results acquired for the purpose, has been undertaken on behalf of the Rockall Studies Group (RSG) of the Irish Petroleum Infrastructure Programme Group 2 which was established by the Petroleum Affairs Division of the Department of the Marine and Natural Resources on 4 June 1997 in conjunction with the award of exploration licences under the Rockall Trough Frontier Licensing Round. The RSG comprises:

Agip (UK) Ltd
Anadarko Ireland Company
ARCO Ireland Offshore Inc
BG Exploration & Production Ltd
BP Exploration Operating Company Ltd
British - Borneo International Ltd
Elf Petroleum Ireland BV
Enterprise Oil plc
Mobil Oil North Sea Ltd
Murphy Ireland Offshore Ltd
Petroleum Affairs Division
Phillips Petroleum Exploration Ireland
Saga Petroleum Ireland Ltd
Shell EP Ireland BV
Statoil Exploration (Ireland) Ltd
Total Oil Marine plc
Union Texas Petroleum Ltd

Petroleum Infrastructure Programme
Rockall Studies Group

ROCKALL TROUGH - IRISH SECTOR PIP/RSG Project 98/1: Compilation/presentation/interpretation of gravity and magnetic data

MAP 20: Reduced -to -pole magnetic image with gravity anomaly line contours

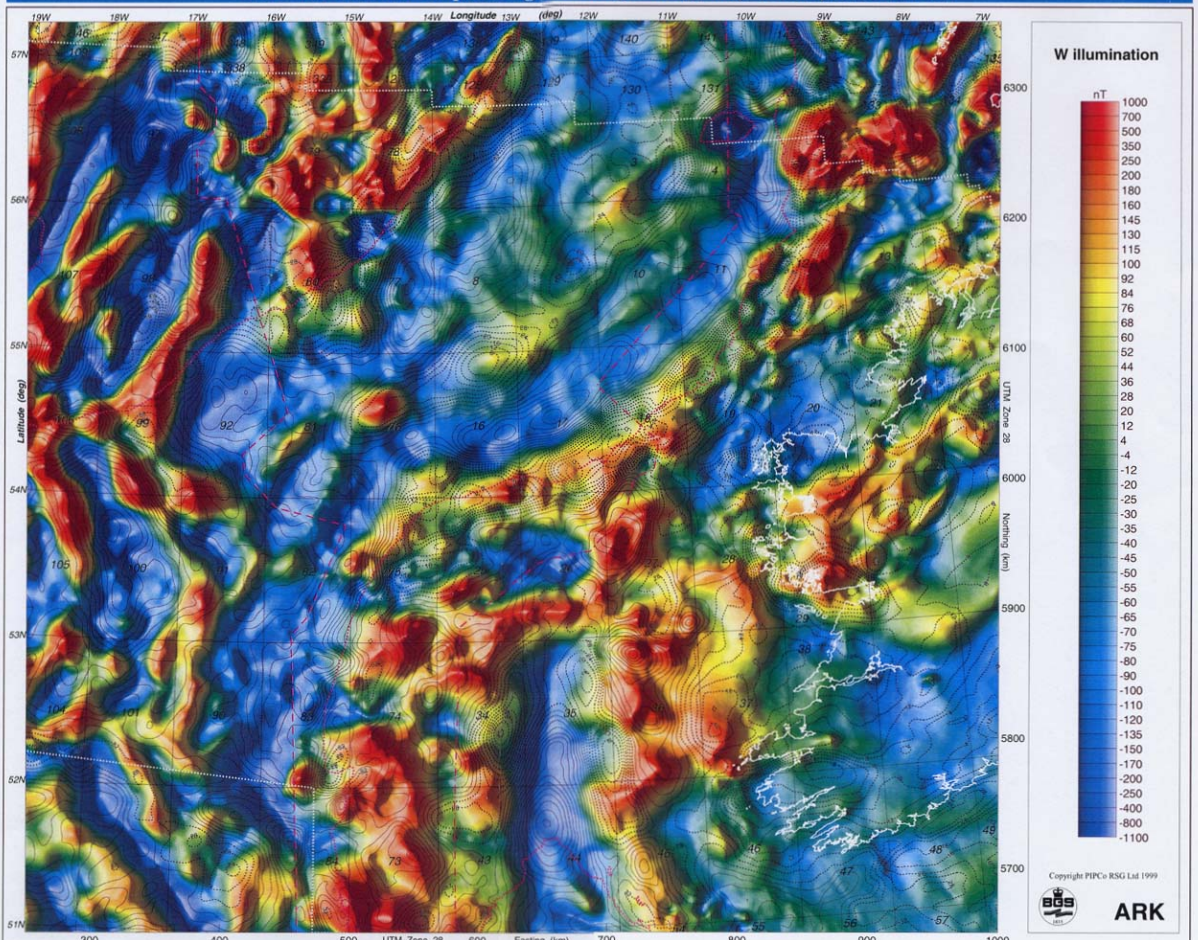

ROCKALL TROUGH - IRISH SECTOR PIP/RSG Project 98/1: Compilation/presentation/interpretation of gravity and magnetic data

MAP 22a: Apparent basin thicknesses as derived from a regional 3D full-crustal model

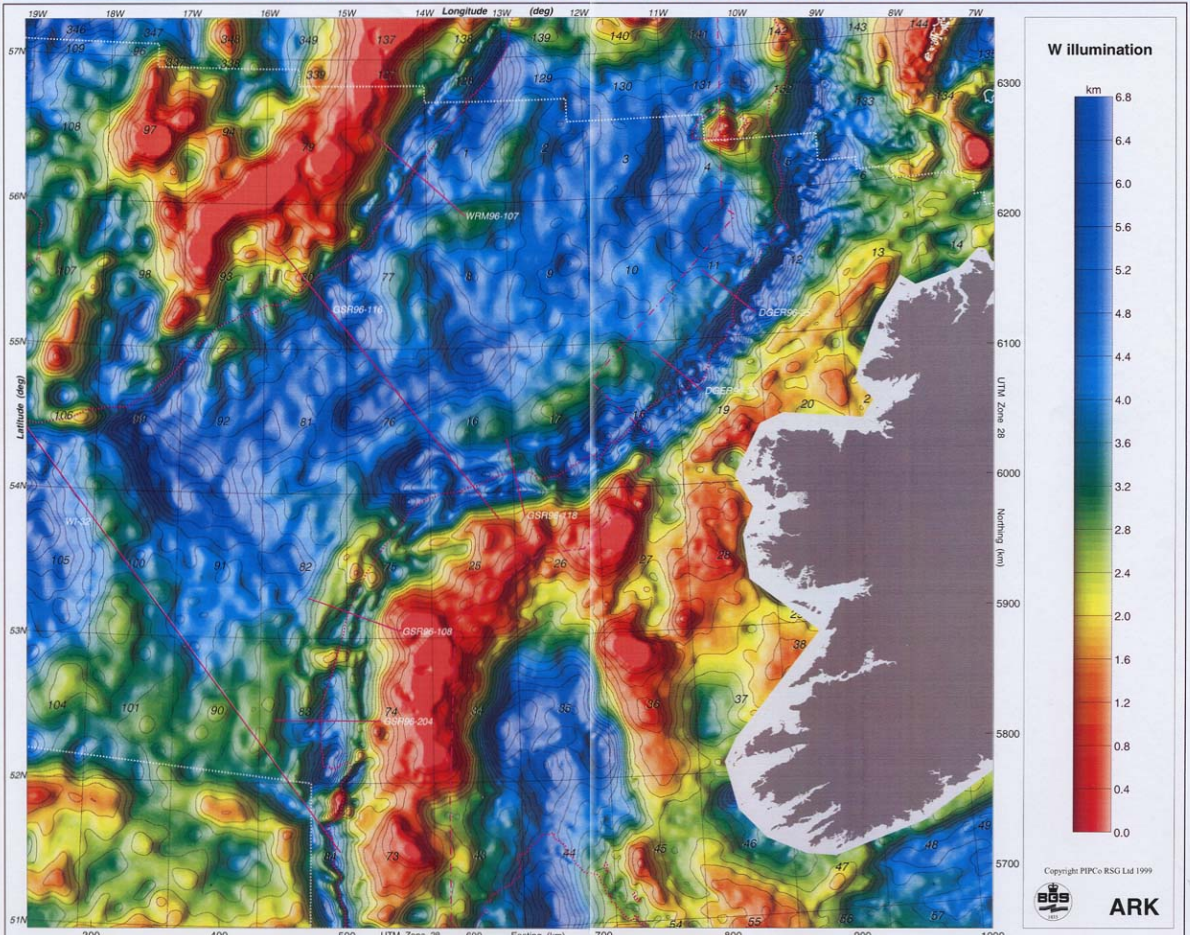

ROCKALL TROUGH - IRISH SECTOR PIP/RSG Project 98/1: Compilation/presentation/interpretation of gravity and magnetic data

MAP 22b: Apparent basement surface relief from a regional 3D full-crustal model

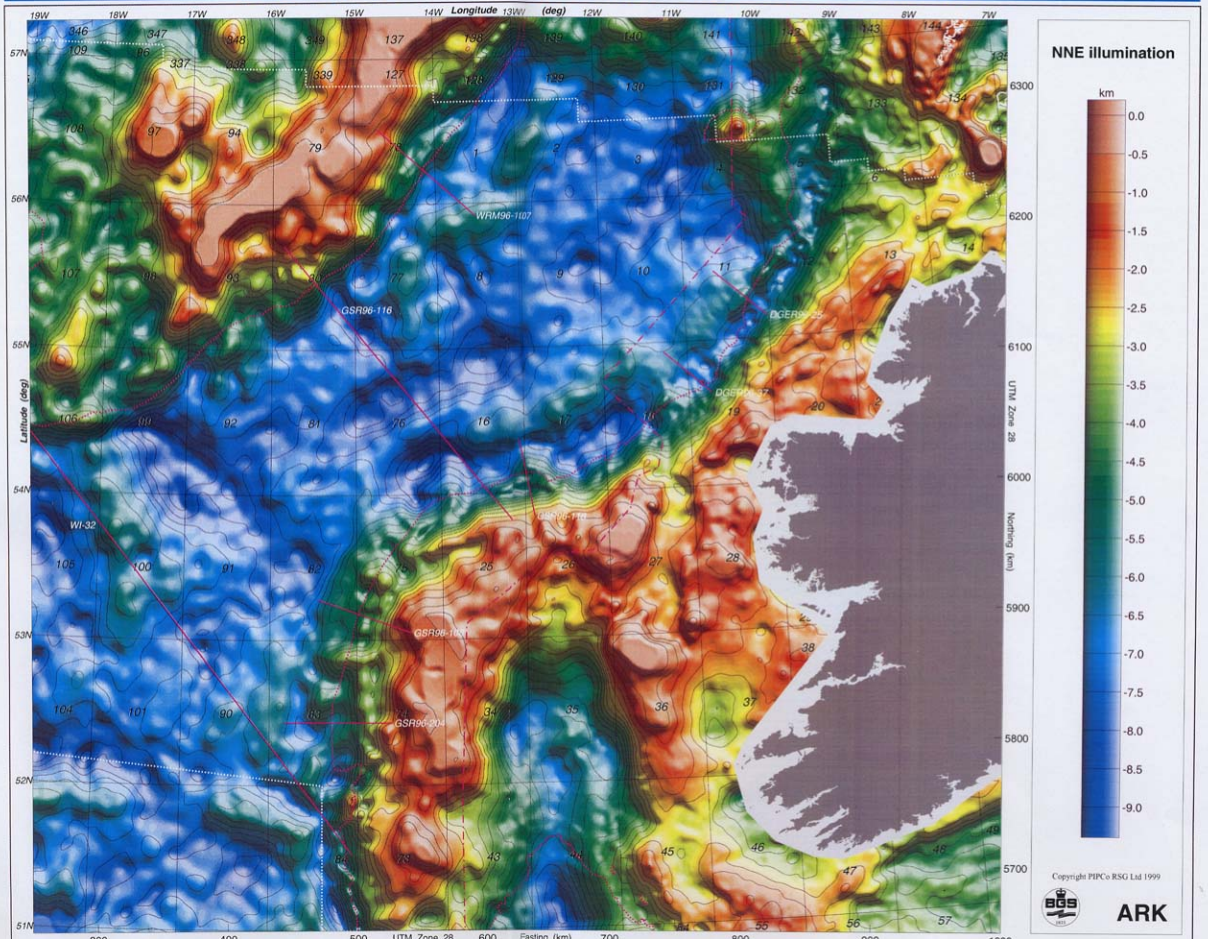

ROCKALL TROUGH - IRISH SECTOR PIP/RSG Project 98/1: Compilation/presentation/interpretation of gravity and magnetic data

MAP 23: Apparent magnetization in the upper crust from a regional 3D model

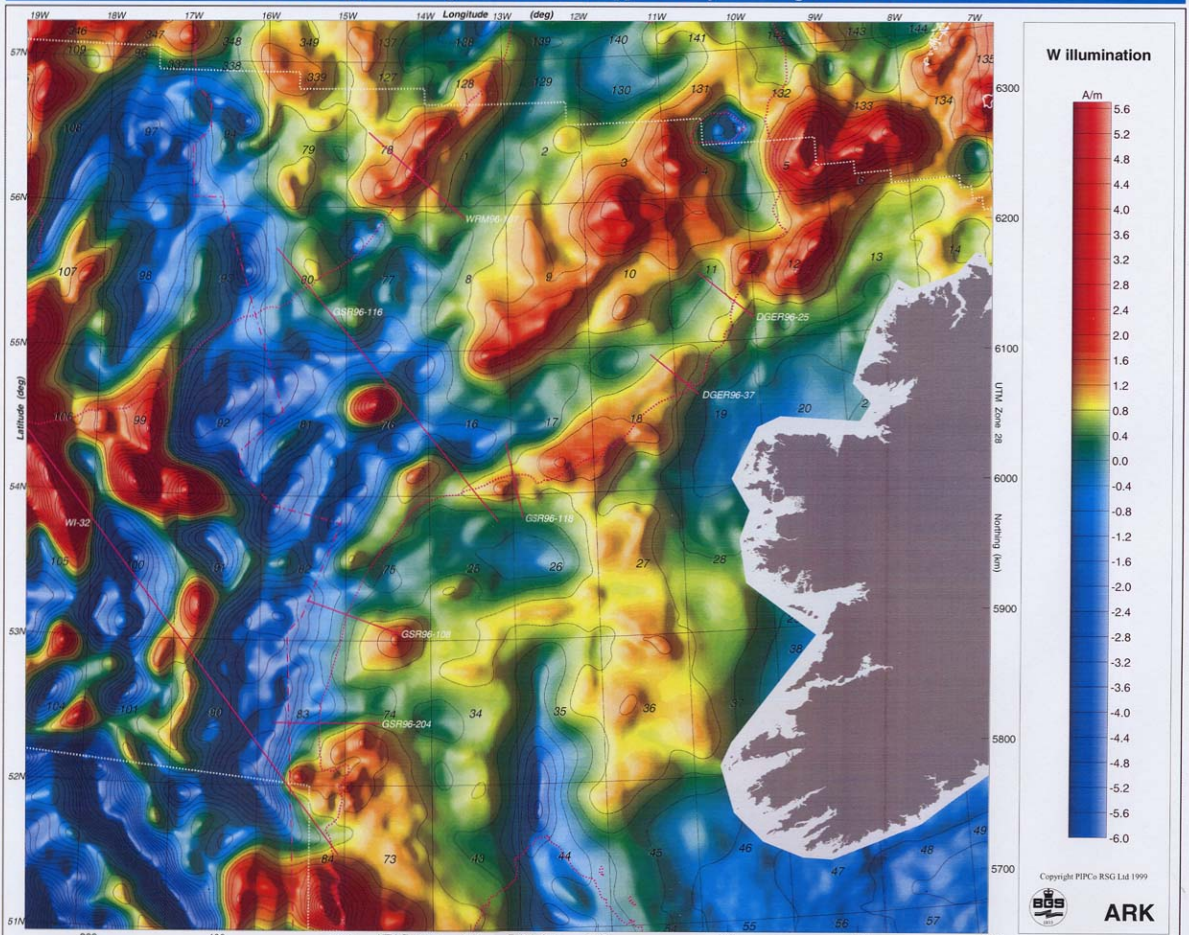

ANNEX A5: *FIGURES ILLUSTRATING RESULTS OF 2D MODELLING TOGETHER WITH PROFILES DERIVED FROM OPTIMIZED 3D GRAVITY MODEL*

Each profile, taken along a seismic line, is represented by two figures, the first being the results obtained from 2D modelling, based on the seismic interpretation, and the second being abstracted from the 3D gravity model after optimization of the cover sequence thickness (as described in Section 6 above) along the same line.

Line locations are shown in Figure 1 and on several of the maps included in Annex A4 (eg. Map 4).

Regional lines crossing the Rockall Trough:

Line GSR96-116
Line WI-32

The properties of the layers within the model are displayed as: density [susceptibility / magnetization] in units of Mg/m^3, $SIx10^{-3}$ units and A/m respectively. Magnetizations are aligned along the contemporary magnetic field direction or its reverse if negative.

Lines restricted to the margin of the Rockall Trough:

Line WRM96-107
Line DGER96-25
Line DGER96-37
Line GSR96-118
Line GSR96-108
Line GSR96-204

Only layer densities (Mg/m^3) are shown in these models. Magnetic susceptibilities (SI units) are indicated in the larger plots of the magnetic components of the models supplied as digital files.

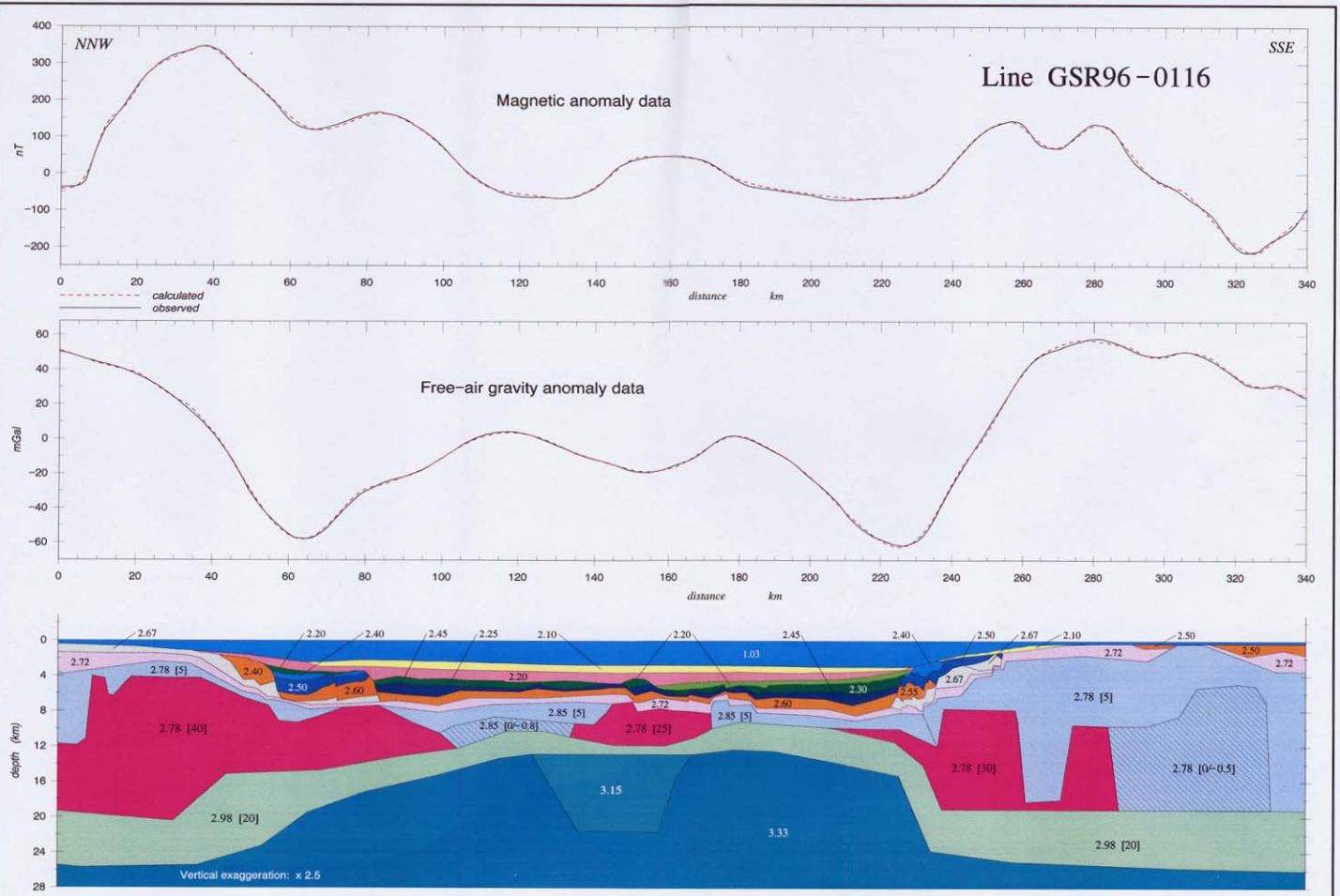

2D potential field modelling results along regional seismic line GSR96-0116

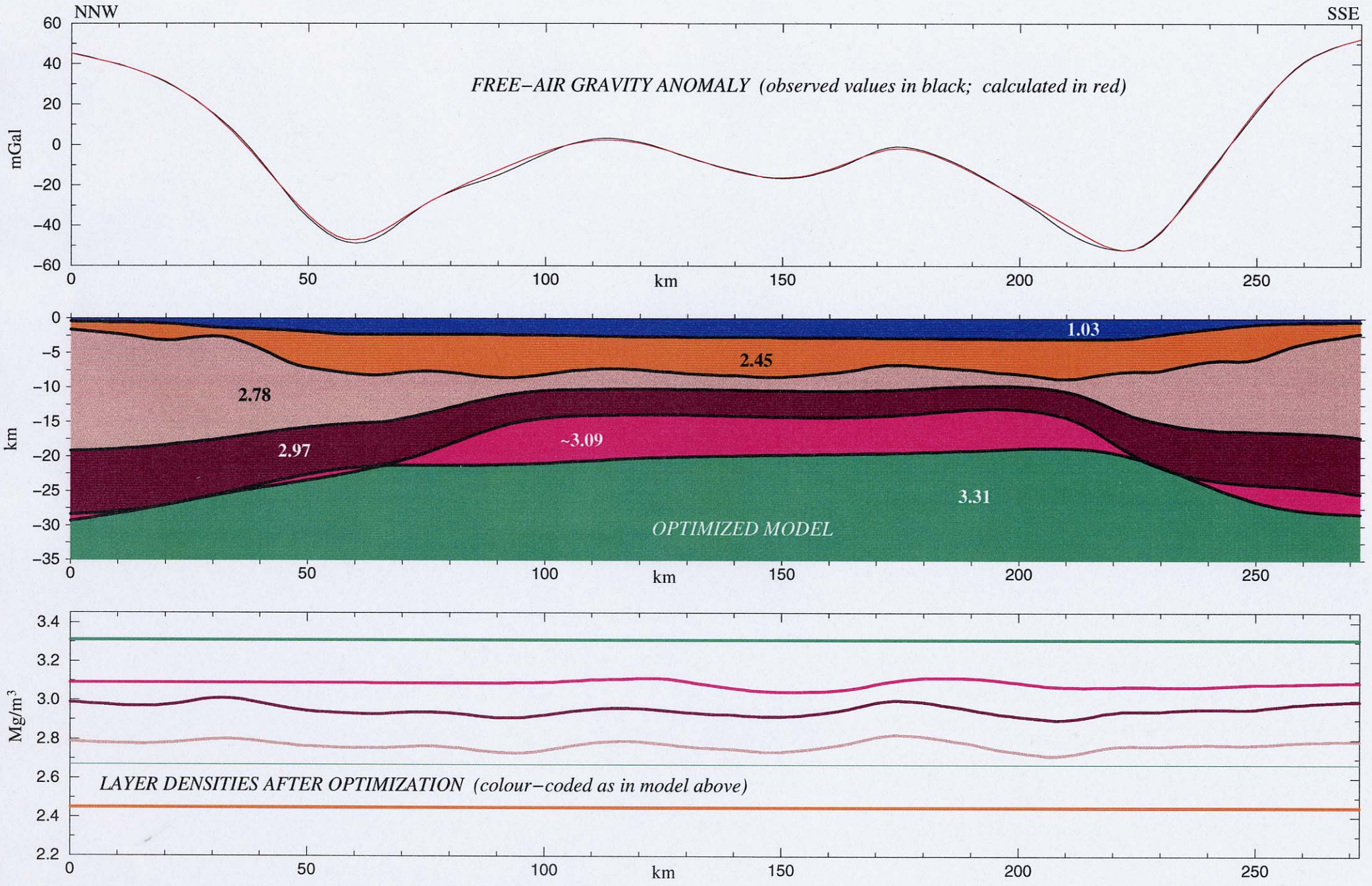

DATA EXTRACTED FROM 3D GRAVITY MODEL ALONG LINE OF PROFILE GSR96–116

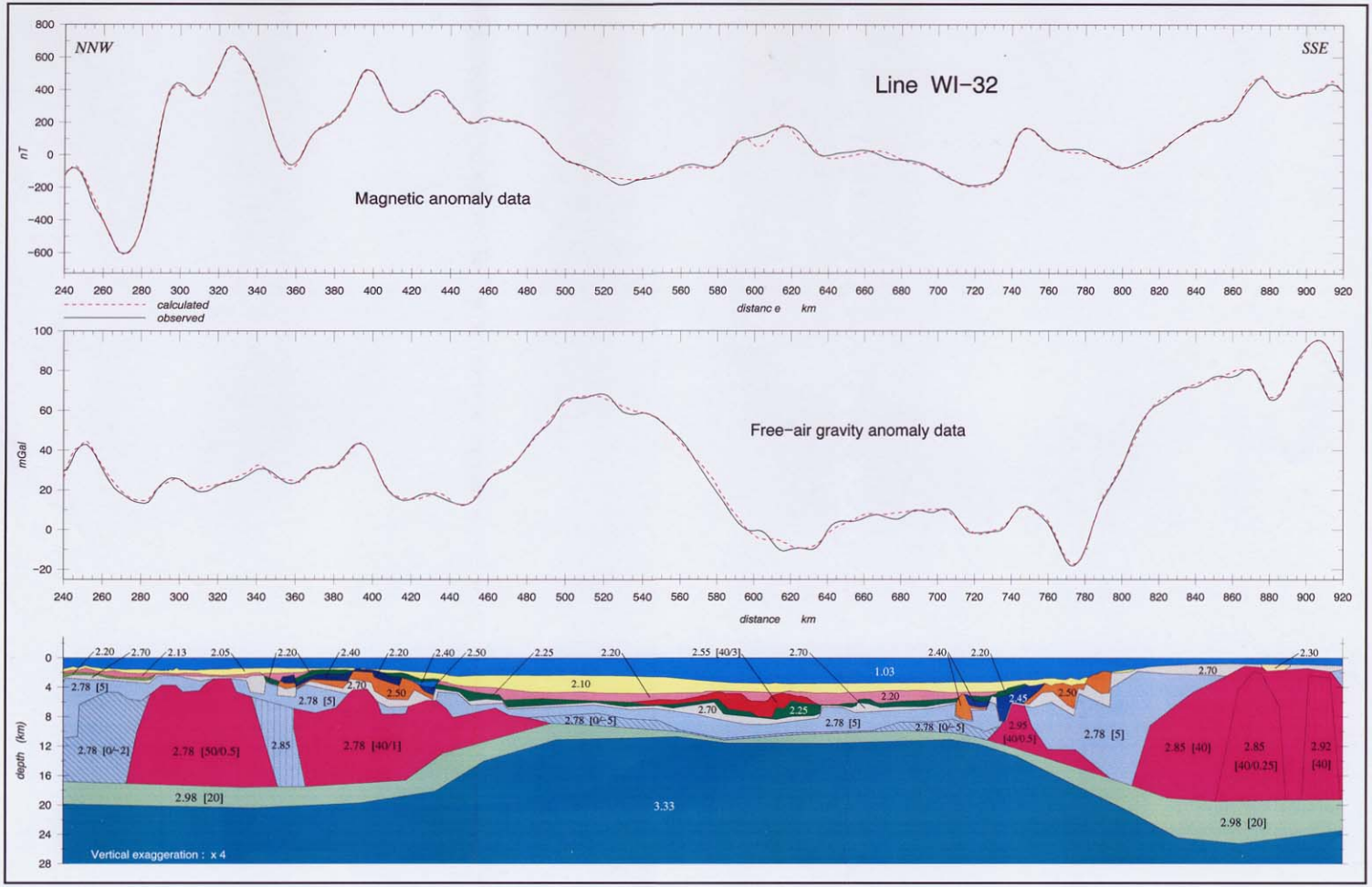

2D potential field modelling results along regional seismic line WI-32

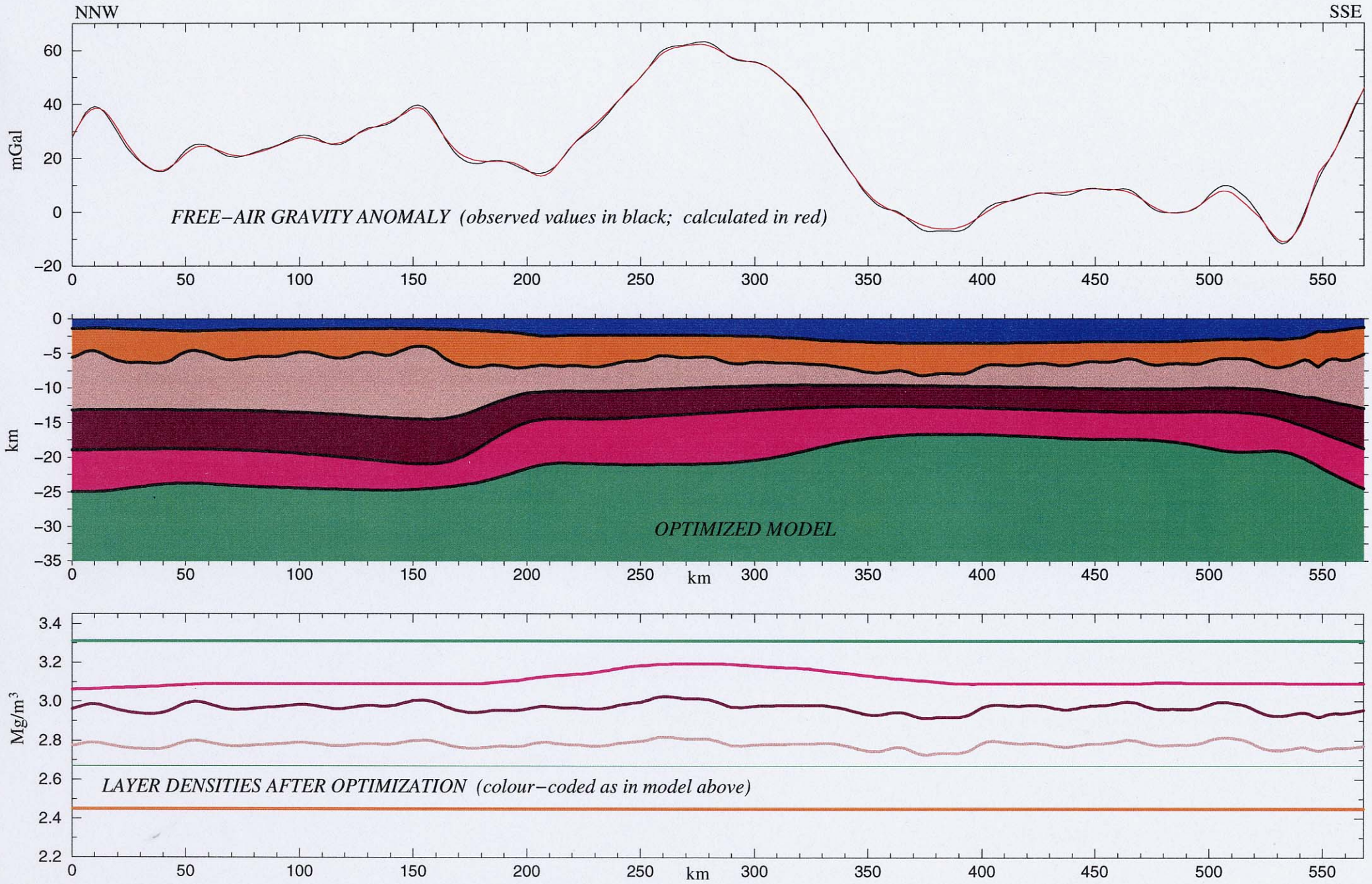

DATA EXTRACTED FROM 3D GRAVITY MODEL ALONG LINE OF PROFILE WI−32

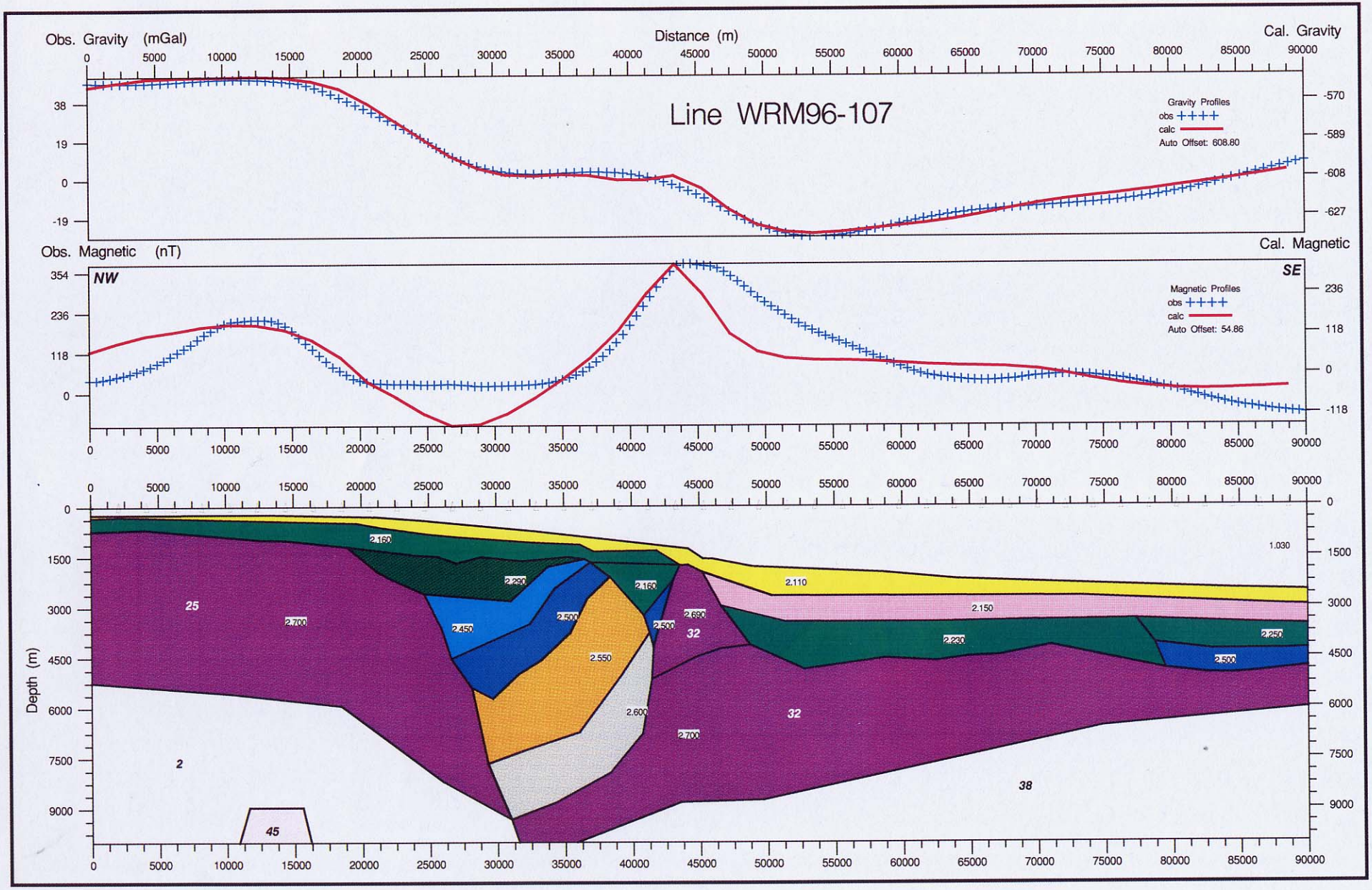

2D potential field modelling results along seismic line WRM96 – 107

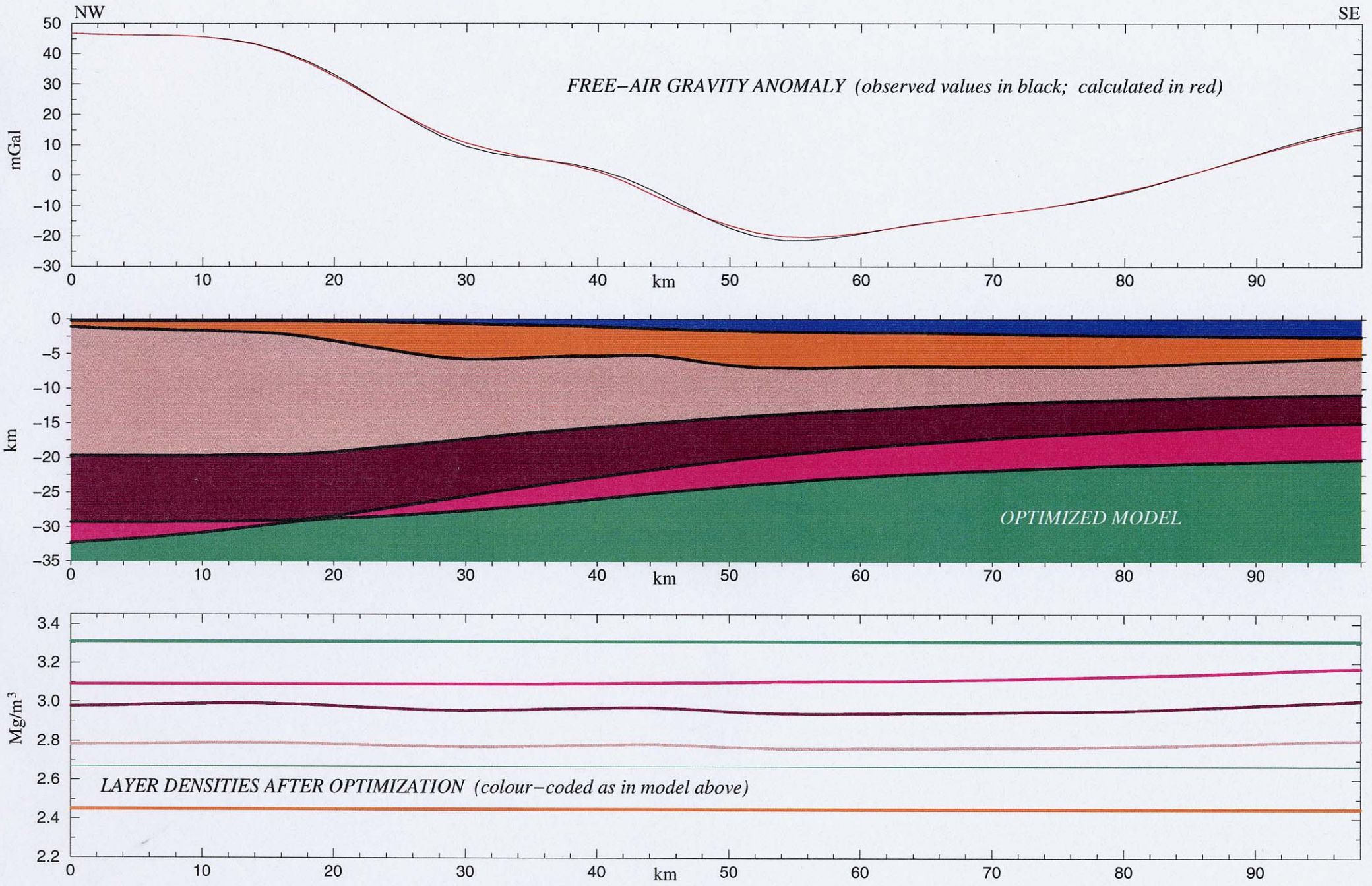

DATA EXTRACTED FROM 3D GRAVITY MODEL ALONG LINE OF PROFILE WRM96–107

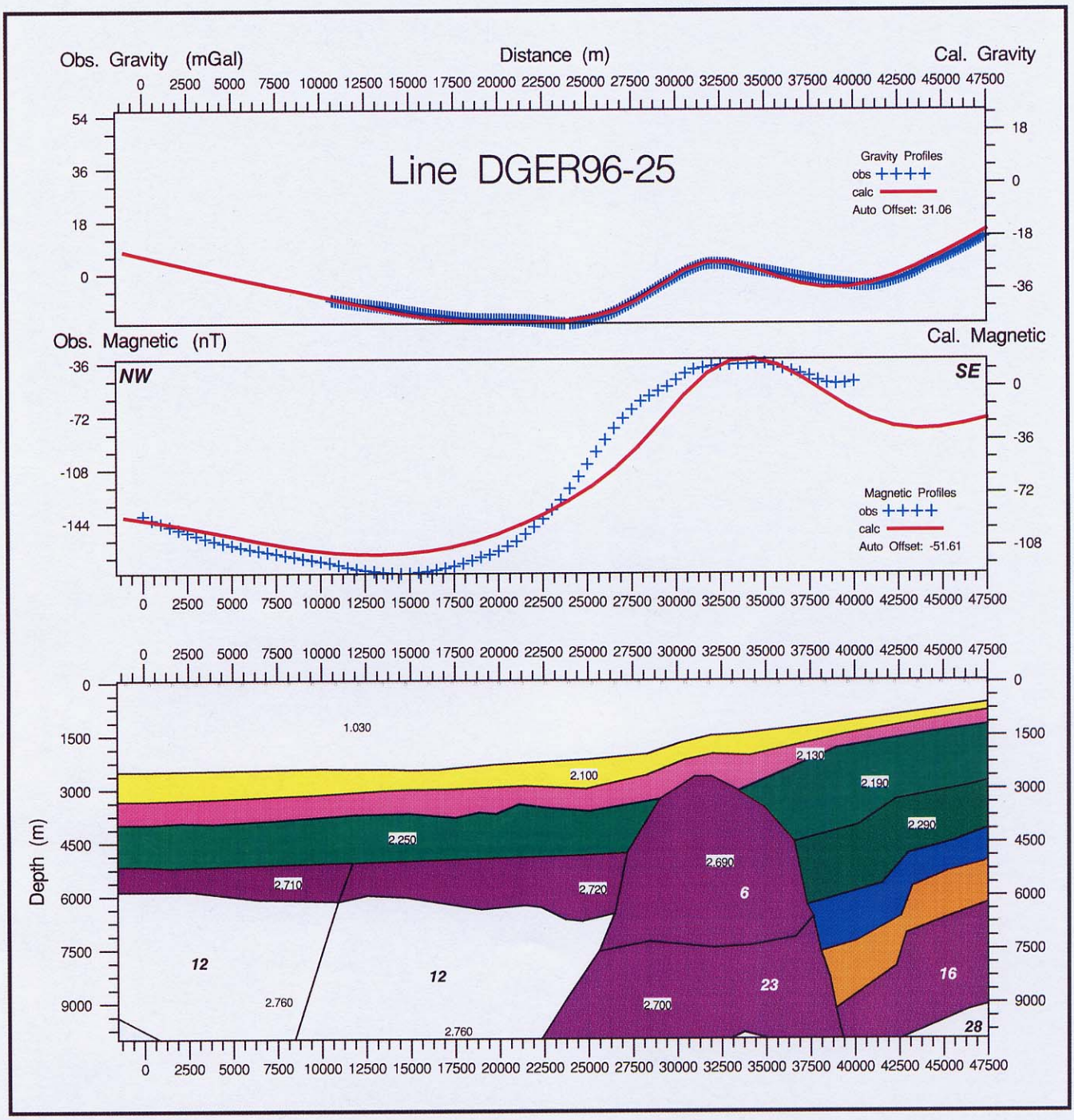

2D potential field modelling results along seismic line DGER96 – 25

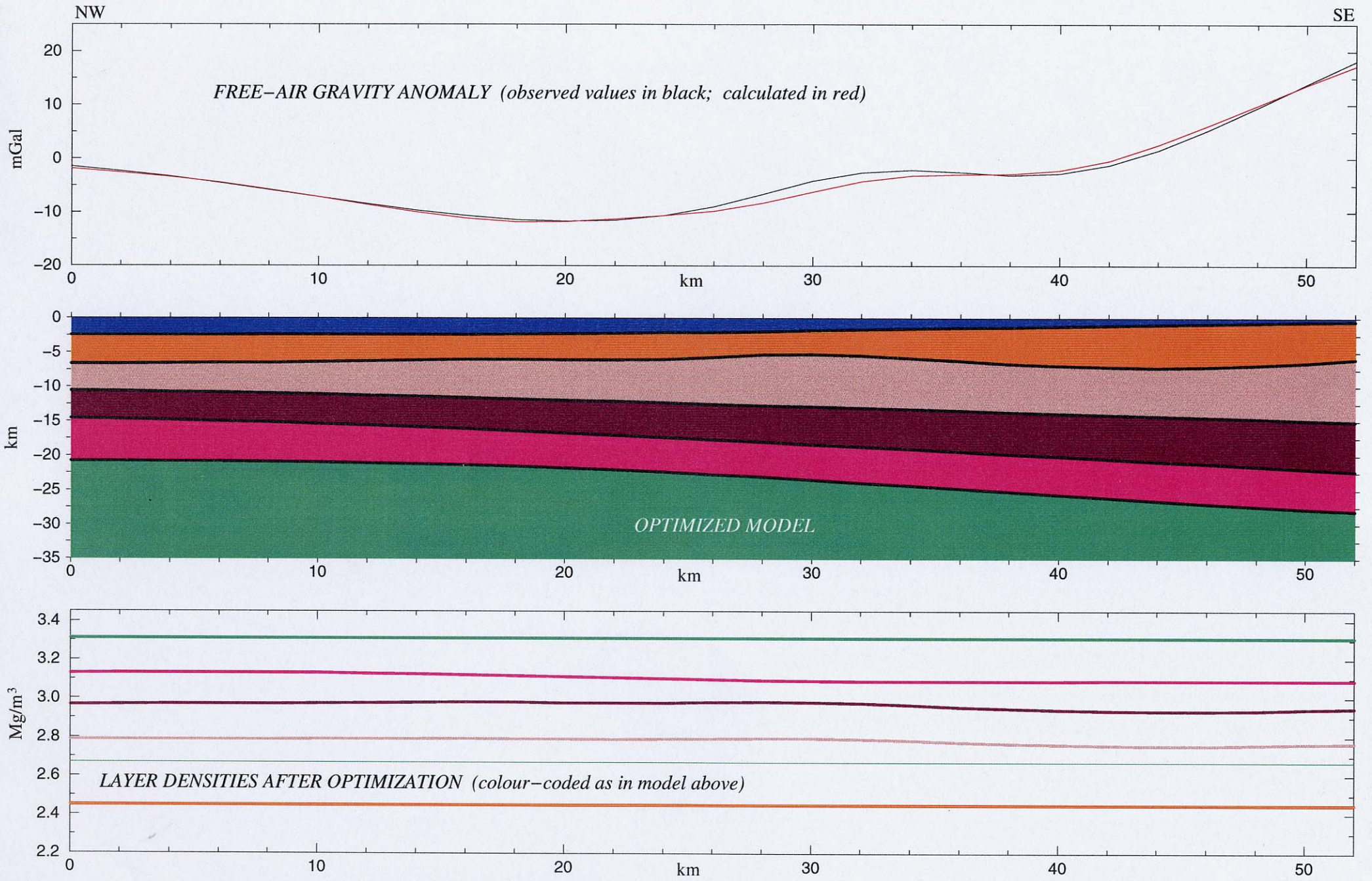

DATA EXTRACTED FROM 3D GRAVITY MODEL ALONG LINE OF PROFILE DGER96–25

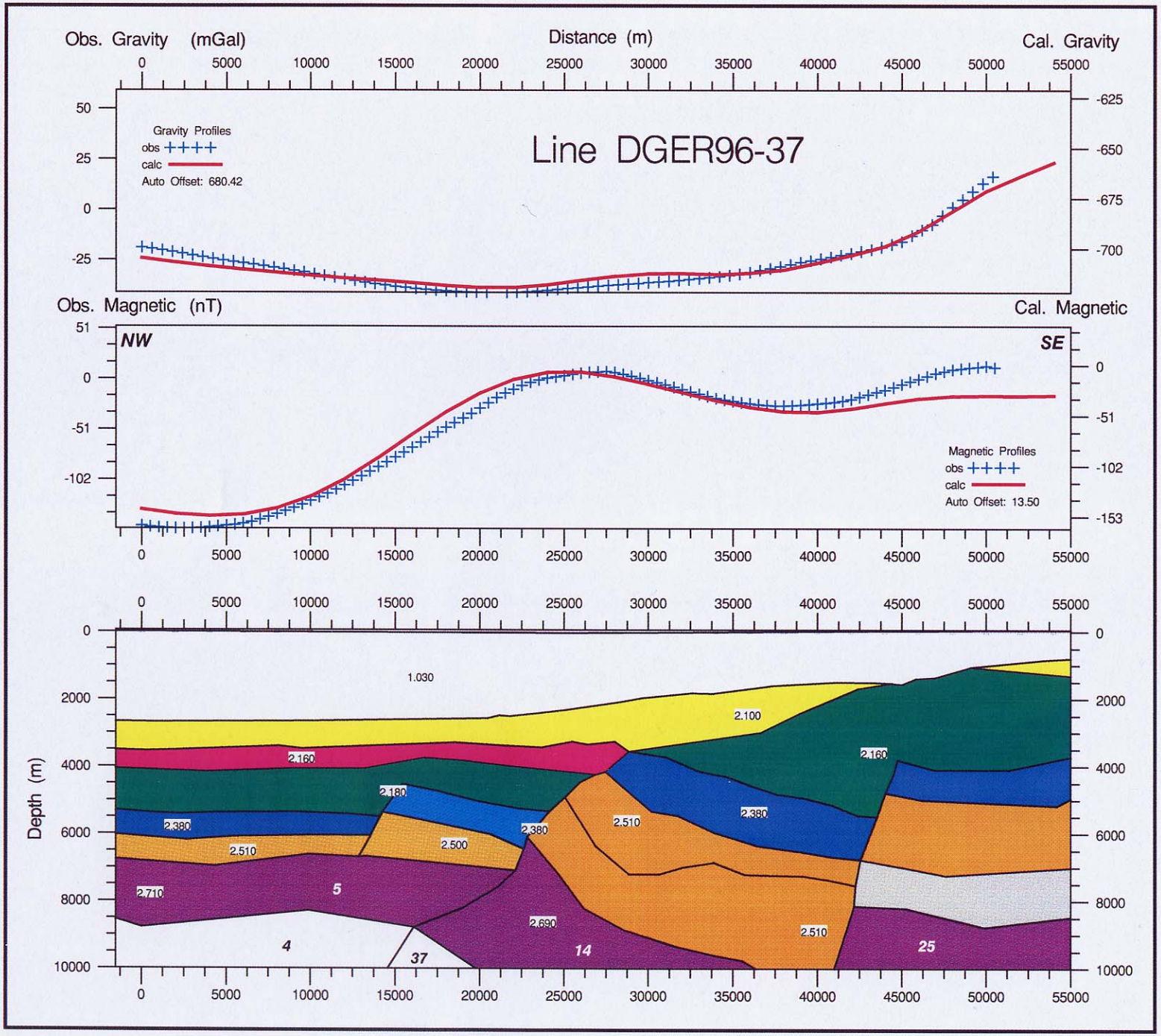
Obs. Gravity (mGal)
Distance (m)
Cal. Gravity
Line DGER96-37
Gravity Profiles
obs
calc
Auto Offset: 680.42
Obs. Magnetic (nT)
Cal. Magnetic
NW
SE
Magnetic Profiles
obs
calc
Auto Offset: 13.50
Depth (m)
1.030
2.100
2.160
2.180
2.380
2.510
2.500
2.710
2.690
5
4
37
14
25

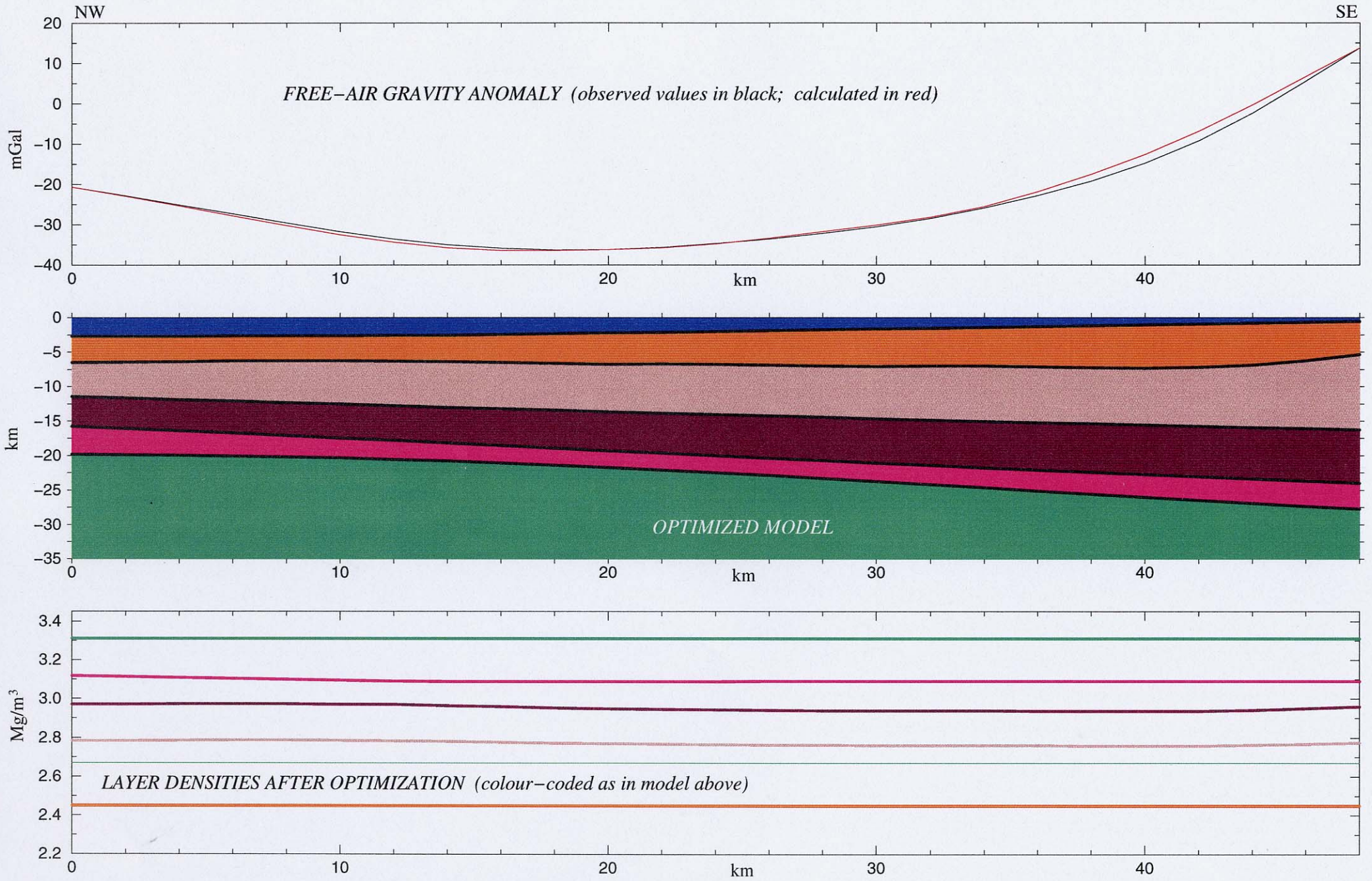

DATA EXTRACTED FROM 3D GRAVITY MODEL ALONG LINE OF PROFILE DGER96–37

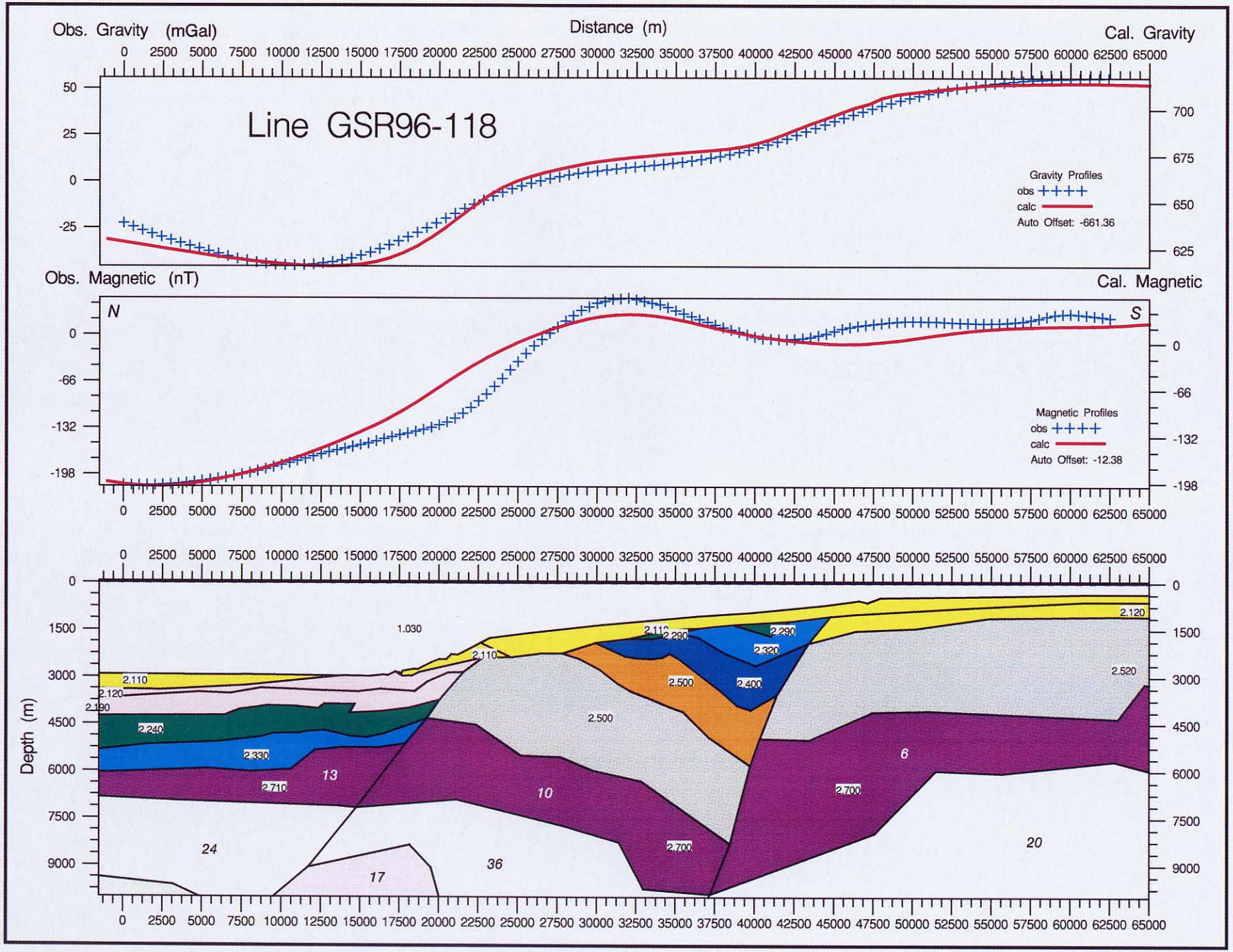
Obs. Gravity (mGal)
Distance (m)
Cal. Gravity
Line GSR96-118
Gravity Profiles
obs
calc
Auto Offset: -661.36
Obs. Magnetic (nT)
Cal. Magnetic
N
S
Magnetic Profiles
obs
calc
Auto Offset: -12.38
Depth (m)
1.030
2.110
2.120
2.190
2.240
2.330
2.710
2.290
2.320
2.500
2.400
2.520
13
10
6
24
17
36
20

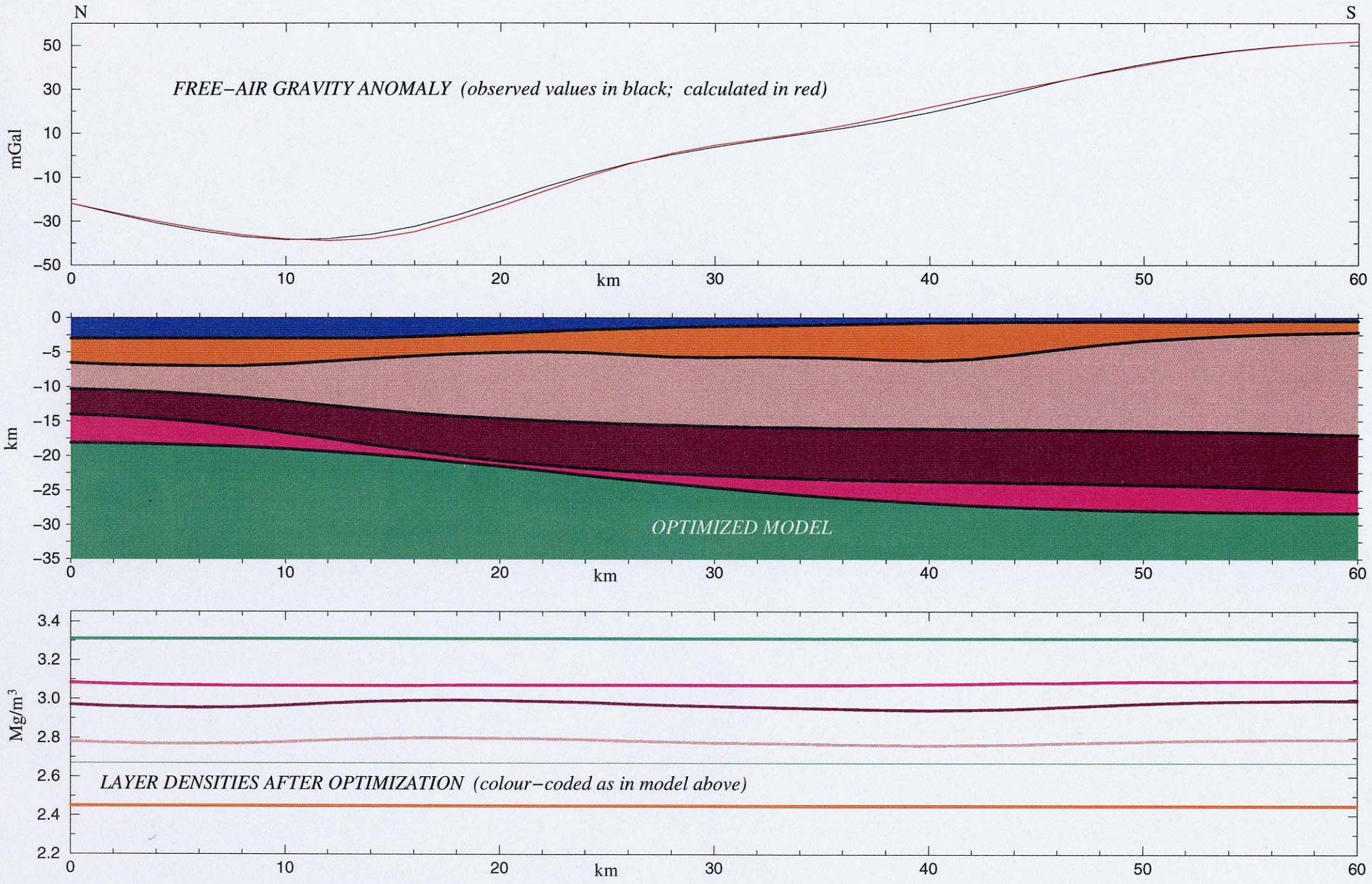

DATA EXTRACTED FROM 3D GRAVITY MODEL ALONG LINE OF PROFILE GSR96–118

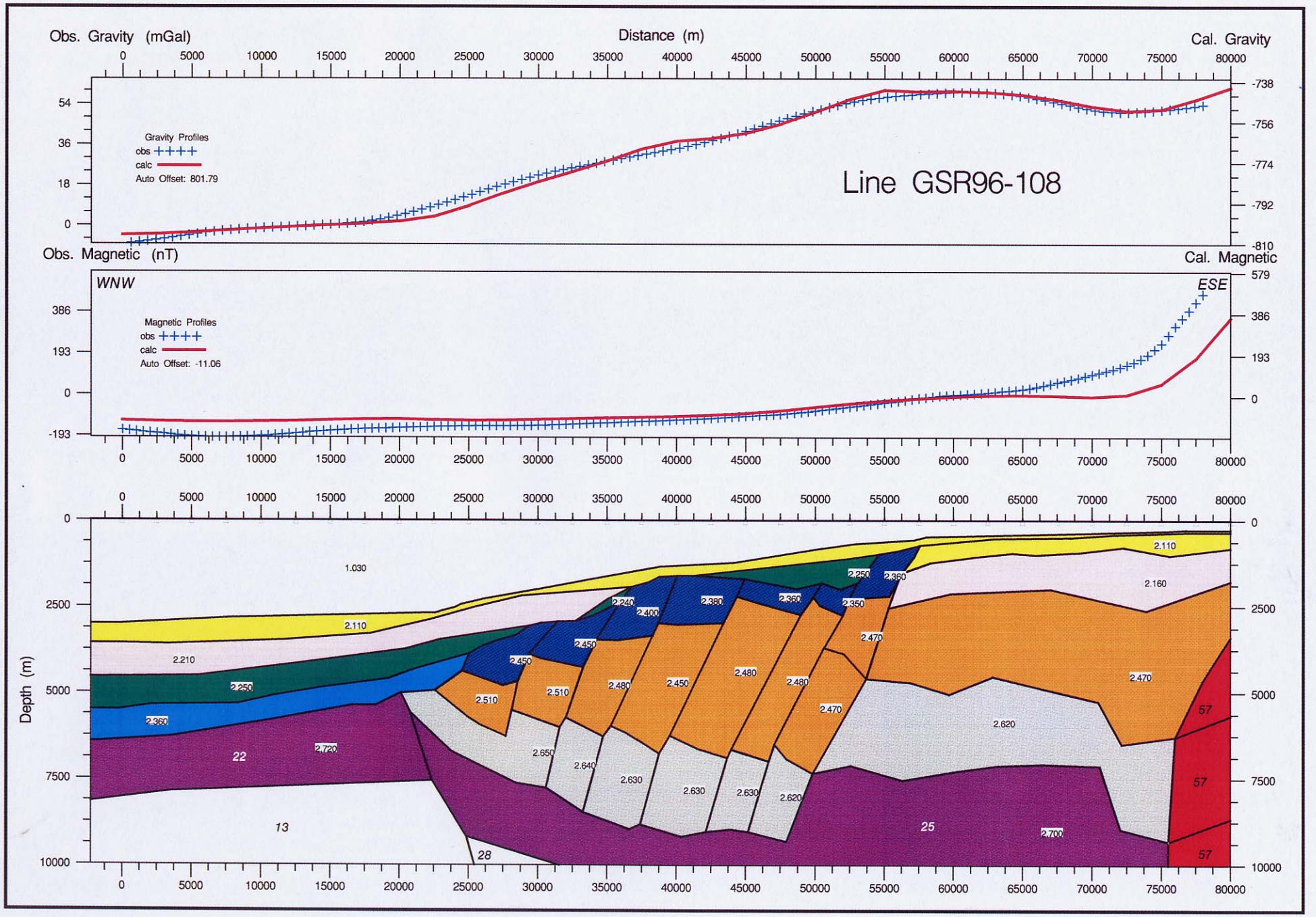
Obs. Gravity (mGal)
Distance (m)
Cal. Gravity
Gravity Profiles
obs
calc
Auto Offset: 801.79
Line GSR96-108
Obs. Magnetic (nT)
Cal. Magnetic
WNW
ESE
Magnetic Profiles
obs
calc
Auto Offset: -11.06
Depth (m)
1.030
2.110
2.210
2.250
2.360
22
2.720
13
28
2.510
2.450
2.240
2.400
2.380
2.360
2.250
2.350
2.470
2.480
2.160
2.620
2.650
2.640
2.630
2.620
25
2.700
57

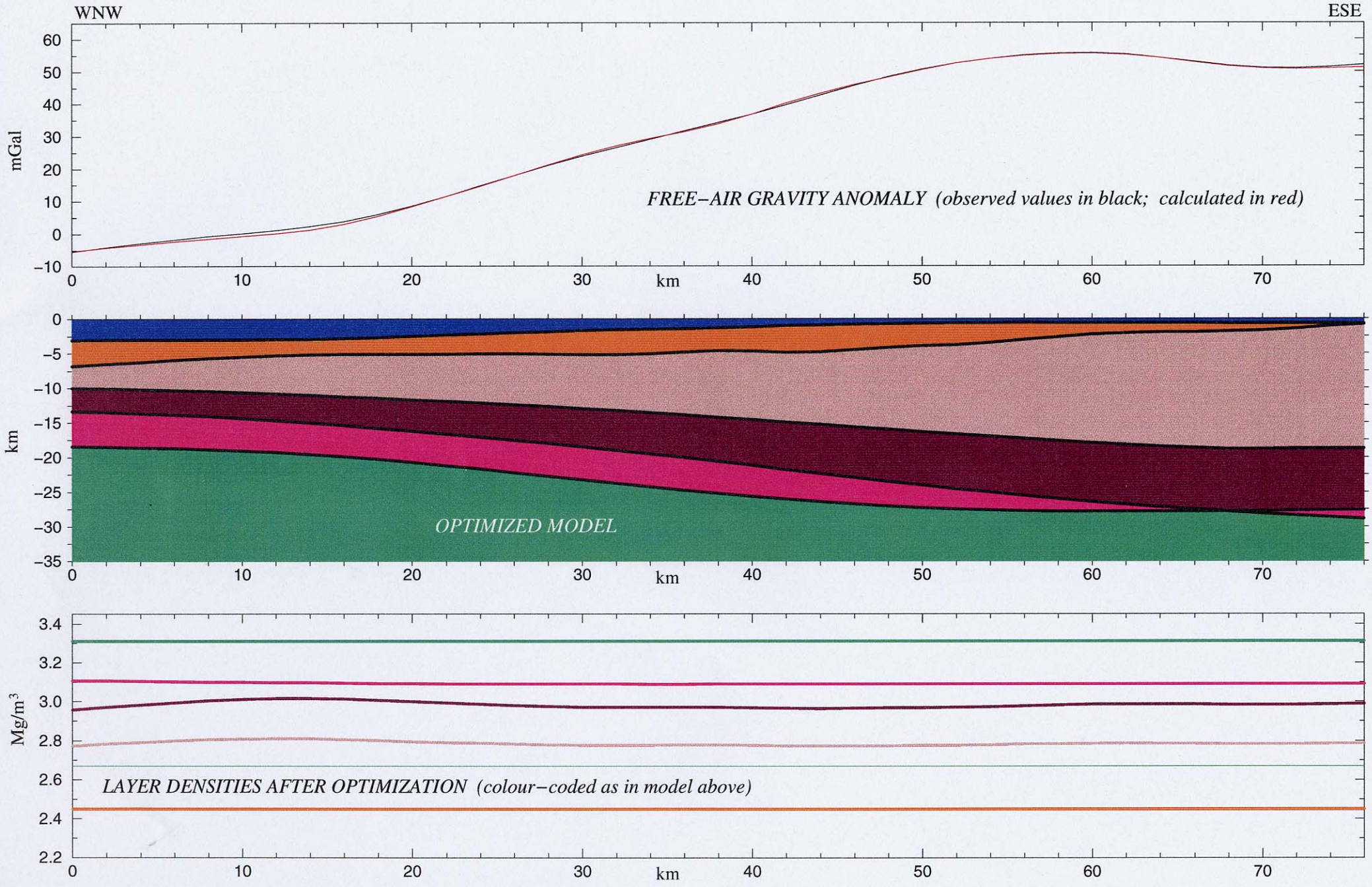

DATA EXTRACTED FROM 3D GRAVITY MODEL ALONG LINE OF PROFILE GSR96–108

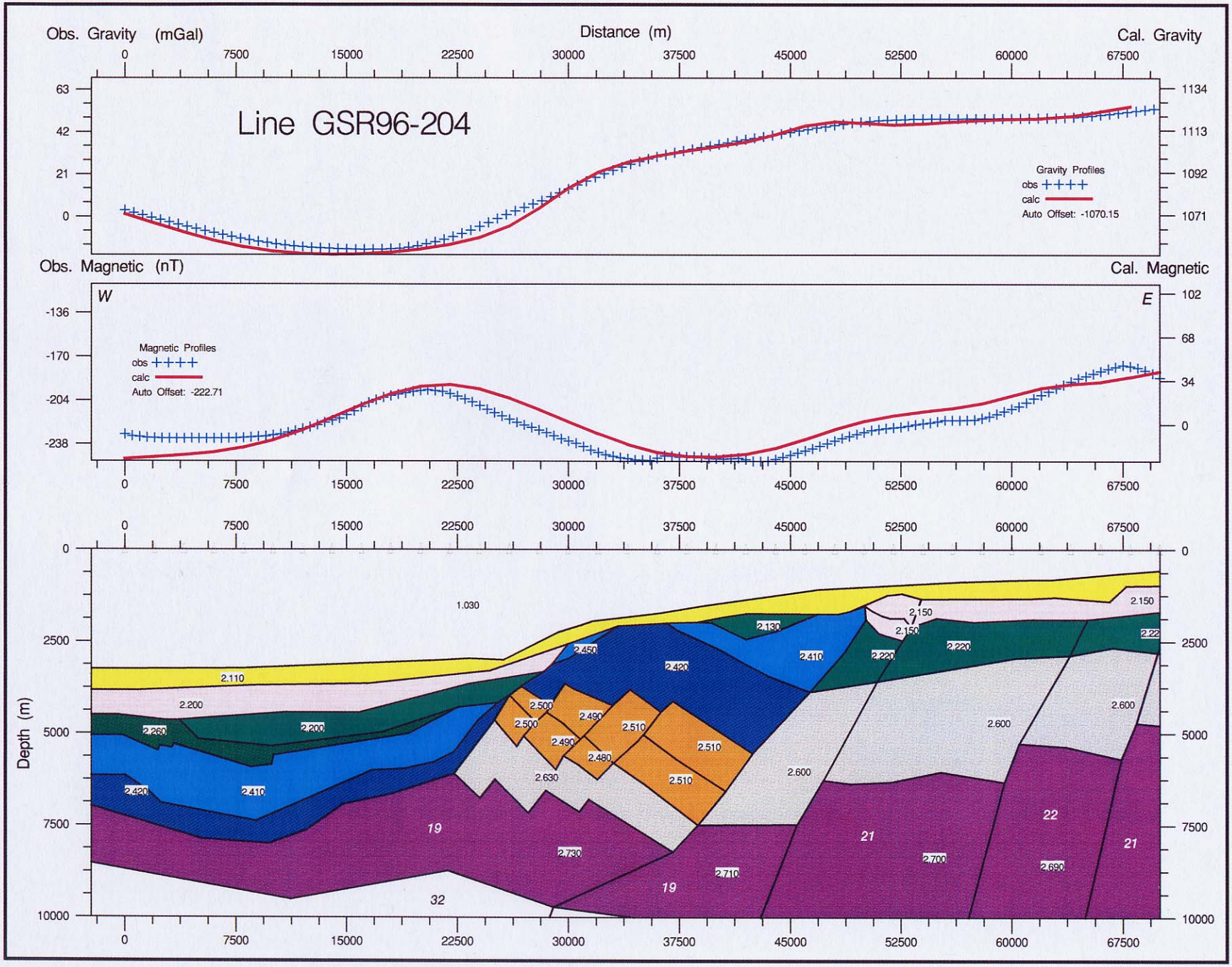

2D potential field modelling results along seismic line GSR96–204

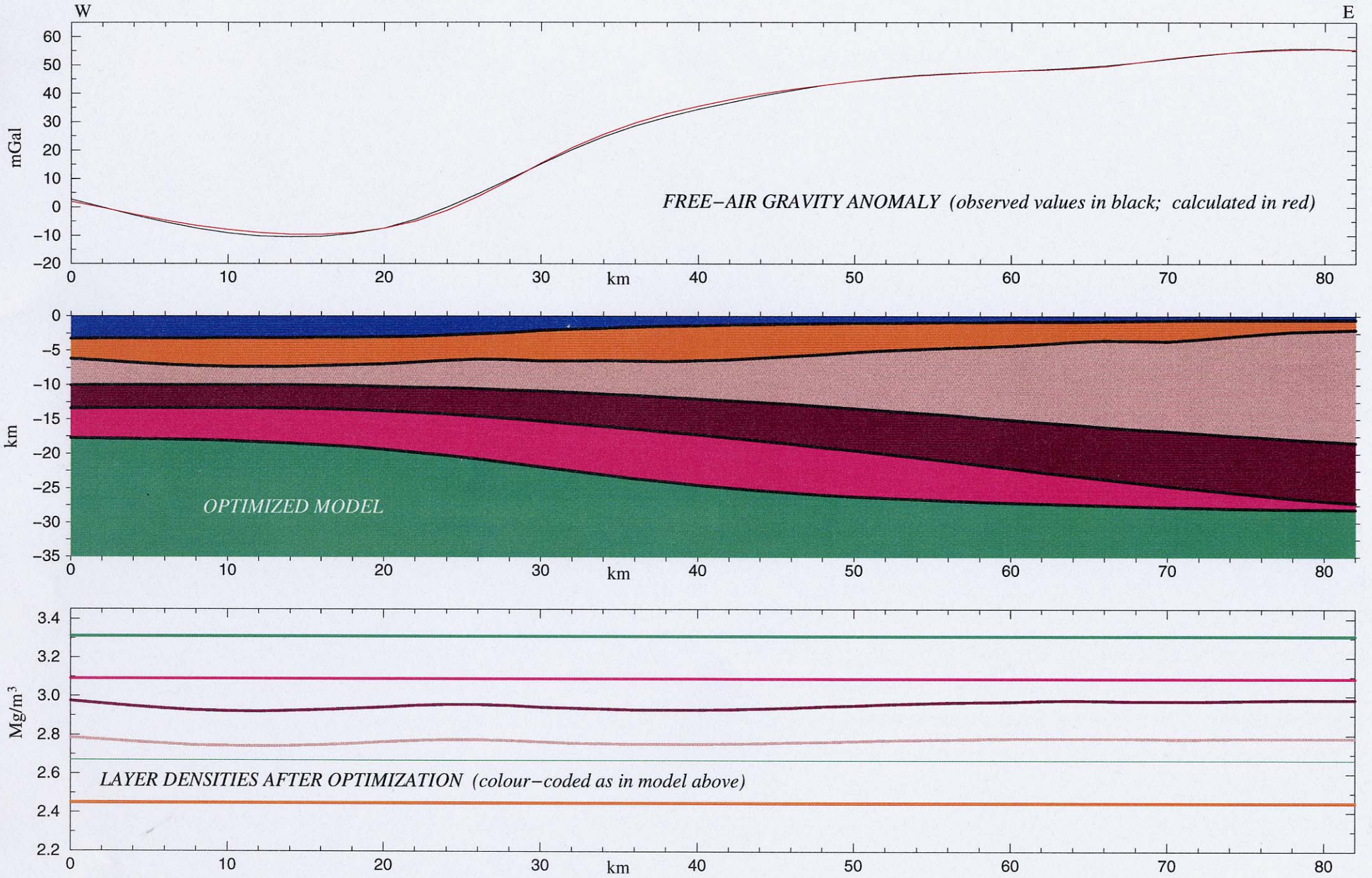

DATA EXTRACTED FROM 3D GRAVITY MODEL ALONG LINE OF PROFILE GSR96–204

ANNEX A6: *EXTENDED BIBLIOGRAPHY AND REFERENCES*

ABRAHAM, D A. and RITCHIE, J D. 1991. The Darwin complex, a Tertiary igneous centre in the northern Rockall Trough. *Scottish Journal of Geology*, **27**, 113-125.

ANDERSEN, M S and BOLDREEL, LARS O. 1995. Tertiary compression structures in the Faeroes-Rockall area. 215-216 in: *The Tectonics, Sedimentation and Palaeoceanography of the North Atlantic Region.* SCRUTTON, R A, STOKER, M S, SHIMMIELD, G B and TUDHOPE, A W (editors). (Geological Society, London, Special Publication, **90**.)

ANDREWS I J, LONG, D RICHARDS, P C, THOMSON, A R, BROWN, S, CHESHER J A and MCCORMAC, M. 1990. *United Kingdom offshore regional report: the geology of the Moray Firth* (London: HMSO for the British Geological Survey.)

BARTON, P J. 1992. LISPB revisited: a new look under the Caledonides of northern Britain. *Geophysical Journal International*, **110**, 371-391.

BARTON, A J and WHITE, R S. 1997. Volcanism on the Rockall continental margin. *Journal of the Geological Society,* **154**, 531-536.

BENTLEY, P A D and SCRUTTON, R A. 1987. Seismic investigations into the basement structure of southern Rockall Trough 667-675. in *Petroleum Geology of North West Europe: Proceedings of the 3rd conference.* BROOKS, J and GLENNIE, K W. (editors). (London:Graham and Trotman.)

BLACKBOURN, G A. 1987. Sedimentary environments and stratigraphy of the late Devonian-early Carboniferous Clair Basin, west of Shetland. 75-91 *in*: *European Dinantian Environments*. MILLER, J, ADAMS, A E and WRIGHT, V P (editors). (John Wiley and Sons, Chichester.)

BLAKELY, R J. 1996. *Potential theory in gravity and magnetic applications.* (Cambridge: Cambridge University Press)

BOILLOT, G, BESLIER, M O, KRAWCZYK C M, RAPPIN, D and RESTON, T J, 1995. The formation of passive margins: constraints from the crustal structure and segmentation of the deep Galacia margin, Spain. 71-91 in: *The Tectonics, Sedimentation and Palaeoceanography of the North Atlantic Region.* SCRUTTON, R A, STOKER, M S, SHIMMIELD, G B and TUDHOPE, A W (editors). (Geological Society, London, Special Publication, **90**.)

BOLDREEL, L O. and ANDERSEN, M S. 1993. Late Paleocene to Miocene compression in the Faeroe-Rockall area. 1025-1029 in *Petroleum Geology of Europe: Proceedings of the 4th conference.* PARKER, J.D. (editor). (London: Geological Society.)

BOLDREEL, L O. and ANDERSEN, M.S. 1994. Tertiary development of the Faeroe-Rockall Plateau based on reflection seismic data. *Bulletin of the Geological Society of Denmark*, **41**, 162-180.

BOOTH, J, SWIECICKI, T and WILCOCKSON, P. 1993. The tectono-stratigraphy of the Solan Basin, west of Shetland. 987-998. in *Petroleum Geology of North West Europe: Proceedings of the 4th conference.* PARKER, J.D. (editor). (London: Geological Society.)

BOTT, M H P, HOLLAND, J G, STORRY, P G and WATTS, A B. 1972. Geophysical evidence concerning the structure of the Lewisian of Sutherland, NW Scotland. *Journal of the Geological Society*, **128**, 599-612.

BOTT, M H P, SUNDERLAND, J, SMITH, P J, CASTEN, U and SAXOV, S. 1974. Evidence for continental crust beneath the Faeroe Islands, *Nature*, **248**, 202-204.

BOTT, M H P 1978. The origin and development of the continental margins between the British Isles and southeastern Greenland. 377-392 in: Crustal evolution in Northwest Britain and adjacent regions. BOWES, D.R. and LEAKE, N.E. (editors). (Geological Society, London, Special Publication, **10**.)

BOTT, M H P. and SMITH, P J. 1984. Crustal structure of the Faeroe-Shetland Channel. *Geophysical Journal of the Royal Astronomical Society*, **76**, 383-398.

BREWER, J A. and SMYTHE, D K. 1984. MOIST and the continuity of crustal reflector geometry along the Caledonian-Appalachian orogeny. *Journal of the Geological Society*, **141**, 105-120.

BRIGGS, I C, 1974. Machine contouring using minimum curvature. *Geophysics*, **39**, 39-48.

BRITISH GEOLOGICAL SURVEY. 1998. Colour shaded relief magnetic anomaly map of Britain, Ireland and adjacent areas. ROYLES, C P and SMITH I F. (compilers). 1:1500000 (Keyworth, Nottingham, United Kingdom: British Geological Society.)

BRITISH GEOLOGICAL SURVEY. 1997. Colour shaded relief gravity anomaly map of Britain, Ireland and adjacent areas. SMITH, I F and EDWARDS, J W F. (compilers). 1:1500000 (Nottingham: British Geological Society.)

BRITISH GEOLOGICAL SURVEY. 1996. Tectonic Map of Britain, Ireland and adjacent areas. PHAROAH, T C, MORRIS J H, LONG C B and RYAN P D. (compilers). 1:1500000 (Keyworth, Nottingham, United Kingdom: British Geological Society.)

BRODIE, J and WHITE, N. 1995. The link between sedimentary basin inversion and igneous underplating. 21-36 in: *Basin inversion.* BUCHANAN, J G and BUCHANAN, P G (editors). Geological Society, London, Special Publication, **88**.

BUCKLEY, J S and BAILEY, R J. 1975. Geophysical evidence on the nature of the Hebrides Terrace Seamount. *Scottish Journal of Geology*, **11**, 37-45.

CANDE, S C and KENT, D V. 1995. Revised calibration of the geomagnetic polarity timescale for the Late Cretaceous and Cenozoic. *Journal of Geophysical Research*, **100**, 6093-6095.

CARLOWICZ, M. 1995. New map of seafloor mirrors surface. *EOS, Transactions of the American Geophysical Union,* **76,** 441-442.

CHALMERS, J A and WESTERN, P G. 1979. A Tertiary igneous centre north of the Shetland Islands. *Scottish Journal of Geology*, **15**, 333-341.

CORNWELL, J C, RAINES, M R, WALKER, A S D, BUSBY, J P, GIBBERD, A J, and MORAGN, D J R. 1996. Sources of low amplitude aeromagnetic anomalies in UK sedimentary basins and establishment of a magnetic properties database. *British Geological Survey Technical Report* WK/96/4C.

CUNNINGHAM, G A and SHANNON, P M. 1997. The Erris Ridge: a major geological feature in the NW Irish offshore basins. *Journal of the Geological Society*, **154**, 503-508.

DAGLEY, P, MUSSETT, A E and SKELHORNE, R R. 1990. Magnetic polarity stratigraphy of the Tertiary igneous rocks of Skye, Scotland. *Geophysical Journal International,* **101**, 395-409.

DANMARKS GEOLOGISKE UNDERSØGELSE. 1995. *Arsberetning for 1994.* Miljo-og Energiministeriet.

DEWEY, J F AND SHACKLETON, R M. 1984. A model for the evolution of the Grampian tract in the early Caledonides and Appalachians. *Nature*, **312**, 115-121.

DICKIN, A.P. 1992. Evidence for an Early Proterozoic crustal province in the North Atlantic region. *Journal of the Geological Society*, **149**, 483-486.

DOBINSON, A. 1970. 1. The development of a marine seismic recording system, 2. A magnetic survey of the Faeroe Bank. Unpublished PhD thesis, University of Durham.

DOBSON, M R and WHITTINGTON, R J. 1992. Aspects of the geology of the Malin Sea area. 291-311 in: *Basins on the Atlantic Seaboard: Petroleum Geology, Sedimentology and Basin Evolution.* PARNELL, J (editor). (Geological Society, London, Special Publication, **62**.)

DUINDUM, P. and VAN HOORN, B. 1987. Structural evolution of the West Shetland continental margin. 765-773 in *Petroleum Geology of North West Europe*. BROOKS, K. and GLENNIE, K W. (editors). (London: Graham and Trotman.)

DYNAMIC GRAPHICS, 1990. *Integrated Surface Modelling User's Guide (Release 7.0).* (California: Dynamic Graphics.)

DYNAMIC GRAPHICS, 1994. *EarthVision User's Guide (Release 2.0).* (California: Dynamic Graphics, Alameda.)

EARLE, M M, JANKOWSKI, E J and VANN, I R. 1989. Structural and stratigraphic evolution of the Faeroe-Shetland Channel and northern Rockall Trough. 461-469 *in* Extension tectonics and stratigraphy of the North Atlantic margins, Tankard, A J and Balkwill, H R. (editors). *Memoir of the American Association of Petroleum Geologists*, **46**.

ENFIELD, M A and COWARD, M P. 1987. The structure of the West Orkney Basin, northern Scotland. *Journal of the Geological Society,* **144**, 871-884.

ENGLAND, R W. 1995. Westline: a deep near-normal incidence reflection profile across the Rockall Trough. 423-427 in: *The Petroleum Geology of Ireland's Offshore Basins*. CROKER, P F and SHANNON, P M. (editors). (Geological Society, London, Special Publication, **93**.)

ENGLAND, R W and HOBBS, R W. 1997. The structure of the Rockall Trough imaged by deep seismic reflection profiling. *Journal of the Geological Society,* **154**, 497-502.

EVANS, D., ABRAHAM, D A. and HITCHEN, K. 1989. The Geikie igneous centre, west of Lewis: its structure and influence on Tertiary geology. *Scottish Journal of Geology*, **25**, 339-352.

FOWLER, S R, WHITE, R S, WESTBROOK, G K and SPENCE, G D. 1989. The Hatton Bank continental margin - II, deep structure from two-ship expanding spread seismic profiles. *Geophysical Journal of the Royal Astronomical Society*, **96**, 295-309.

FYFE, J. A, LONG, D and EVANS, D. 1993. *United Kingdom offshore regional report: the geology of the Malin-Hebrides sea area.* (London: HMSO for the British Geological Survey.)

GATLIFF, R W, HITCHEN, K, RITCHIE, J D and SMYTHE, D K. 1984. Internal structure of the Erlend Tertiary volcanic complex, north of Shetland, revealed by seismic reflection data. *Journal of the Geological Society*, **141**, 555-562.

HALL, J, BREWER, J A, MATTHEWS, D H and WARNER, M R. 1984. Crustal structure across the Caledonides from the WINCH seismic reflection profile: influences on the evolution of the Midland Valley of Scotland. *Transactions of the Royal Society of Edinburgh: Earth Sciences*, **75**, 97-109.

HAMAR, G P. and HJELLE, K. 1984. Tectonic framework of the Møre Basin and the northern North Sea. 349-358 in *Petroleum Geology of the North European Margin*, Spencer, A M. (editor). (Oslo: Norwegian Petroleum Society.)

HANISCH, J. 1984. The Cretaceous opening of the north-east Atlantic. *Tectonophysics*, **101**, 1-23.

HARLAND, W B, ARMSTRONG, R L, COX, A V, CRAIG, L E, SMITH, A G and SMITH, D G. 1990. *A geologic time scale 1989*. Cambridge University Press, Cambridge.

HASZELDINE, R S. 1984. Carboniferous North Atlantic palaeogeography: stratigraphic evidence for rifting, not megashear or subduction. *Geological Magazine*, **121**, 443-463.

HILLIS, R. 1995. Regional Tertiary exhumation in and around the United Kingdom. 167-190 in: *Basin Inversion*. BUCHANAN, J G and BUCHANAN, P G (editors). (Geological Society, London, Special Publication, **88**).

HITCHEN, K. and RITCHIE, J D. 1987. Geological review of the West Shetland area. 737-749 in *Petroleum Geology of North West Europe*. BROOKS, K. and GLENNIE, K W. (editors). (London: Graham and Trotman.)

HITCHEN, K and RITCHIE, J D. 1993. New K-Ar ages, and a provisional chronology, for the offshore part of the British Tertiary Igneous Province. *Scottish Journal of Geology*, **29**, 73-85.

HITCHEN, K and STOKER, M S. 1993. Mesozoic rocks on the Hebrides Shelf and implications for hydrocarbon prospectivity in the northern Rockall Trough. *Marine and Petroleum Geology*, **10**, 246-254.

HITCHEN, K, STOKER, M S, EVANS, D and BEDDOE-STEPHENS, B. 1995. Permo-Triassic sedimentary and volcanic rocks in basins to the north and west of Scotland. 87-102 in: *Permian and Triassic Rifting in Northwest Europe.* BOLDY, S A R. (editor). (Geological Society, London, Special Publication, **91**.)

HODGSON, B D, DAGLEY, P and MUSSETT, A E. 1990. Magnetostratigraphy of the Tertiary igneous rocks of Arran. *Scottish Journal of Geology*, **26**, 99-118.

IOC, IHO and BODC, 1994. *Supporting volume to the GEBCO Digital Atlas.* Published on behalf of the Inter-governmental Oceanographic Commission (of UNESCO) and the International Hydrographic Organisation as part of the General Bathymetric Chart of the Oceans (GEBCO) in combination with a CD-ROM. (Birkenhead, British Oceanographic Data Centre.)

JONES, T M, TABOR, R and WEATHERALL, P. 1997. *Supporting volume to the GEBCO digital atlas (1997 supplement).* (Birkenhead: British Oceanographic Data Centre)

JOPPEN, M and WHITE, R S. 1990. The structure and subsidenec of the Rockall Trough from two-ship experiments. *Journal of Geophysical Research*, **95**, 19821-19837.

KARNER, G D. and WATTS, A B. 1982. On isostasy at Atlantic-type continental margins. *Journal of Geophysical Research,* **87**, 2923-2948.

KESER NEISH, J. 1993. Seismic structure of the Hatton-Rockall area: an integrated seismic/modelling study from composite data-sets. 1047-1056 in: *Petroleum Geology of Northwest Europe: Proceedings of the 4th conference*. PARKER, J.R. (editor). (Geological Society, London.)

KLEMPERER, S L and HURICH, C A. 1990 Lithospheric structure of the North Sea from deep seismic reflection profiling. In: *Evolution of the North Sea Rifts*. BLUNDELL, D J. and GIBBS, A D. (editors) (Oxford University Press.)

LAILEY, M, STEIN, A M. and RESTON, T J. 1989. The Outer Hebrides fault: a major Proterozoic structure in NW Britain. *Journal of the Geological Society*, **146**, 253-259.

LARSEN, H C, SAUNDERS, A D, CLIFT, P D *et al.* 1994. *Proceedings of the Ocean Drilling Program, Initial Reports,* **152** (College Station, Texas: Ocean Drilling Program.)

LAUGHTON, A S, BERGGREN, W A. *et al.* 1972. Initial reports of the Deep Sea Drilling Project, Vol.12. (Washington: U.S. Government Printing Office)

MAKRIS, J, GINZBURG, A, SHANNON, P M, JACOB, A W B, BEAN, C J and VOGT, U. 1991. A new look at the Rockall region, offshore Ireland. *Marine and Petroleum Geology*, **8**, 410-416.

McDONALD, A J W, FLETCHER, C J N, CARRUTHERS, R M, WILSON, D and EVANS, R B. 1992. Interpretation of the regional gravity and magnetic surveys of Wales, using shaded relief and Euler deconvolution techniques. *Geological Magazine*, **129**, 523-531.

McGEARY, S. 1989. Reflection seismic evidence for a Moho offset beneath the Walls Boundary strike-slip fault. *Journal of the Geological Society*, **146**, 261-269.

McGEARY, S and WARNER, M R. 1985. Seismic profiling of the continental lithosphere. *Nature*, **317**, 795-797.

MEGSON, J B. 1987. The evolution of the Rockall Trough and implications for the Faeroe-Shetland Trough 653-665. in *Petroleum Geology of North West Europe: Proceedings of the 3rd conference.* BROOKS, J and GLENNIE, K W. (editors). (London:Graham and Trotman.)

MILES, P R and ROBERTS, D G. 1981. The magnetisation of Rosemary Bank Seamount, Rockall Trough, northeast Atlantic. *Earth and Planetary Science Letters*, **54**, 442-448.

MORGAN, J V, BARTON, J P and WHITE, R S. 1989. The Hatton Bank continental margin - III. Structure from wide-angle OBS and multi-channel seismic refraction profiles. *Geophysical Journal International*, **98**, 367-384.

MORTON, A C, DIXON, J E, FITTON, J G, MACINTYRE, R M, SMYTHE, D K and TAYLOR, P N. 1988. Early Tertiary volcanic rocks in Well 163/6-1A, Rockall Trough. 293-308 in: *Early Tertiary Volcanism and the Opening of the NE Atlantic.* MORTON, A C and PARSON, L M. (editors.) (Geological Society, London, Special Publication, **39**.)

MORTON, A C and TAYLOR, P N. 1991. Geochemical and isotopic constraints on the nature and age of basement rocks from Rockall Bank, NE Atlantic. *Journal of the Geological Society*, **148**, 631-634.

MUDGE, D C. and RASHID, B. 1987. The geology of the Faeroe Basin. 751-763 in *Petroleum Geology of North West Europe*. BROOKS, K. and GLENNIE, K W. (editors). (London: Graham and Trotman.)

MUSGROVE, F W AND MITCHENER, B, 1996. Analysis of the pre-Tertiary rifting history of the Rockall Trough. *Petroleum Geoscience*, 2, 353-360.

MUSSETT, A E , DAGLEY, P and SKELHORN, R R. 1988. Time and duration of activity in the British Tertiary Igneous Province. 337-348 in: *Early Tertiary Volcanism and the Opening of the NE Atlantic.* MORTON, A C and PARSON, L M. (editors.) (Geological Society, London, Special Publication, **39**.)

NAYLOR, D AND SHANNON, P M, 1999. Structural Nomenclature Project - Final Report, April 1999. *Rockall Studies Group Project 97/3 - internal report.*

OFOEGBU, C O and BOTT, M H P. 1985. Interpretation of the Minch linear magnetic anomaly and of a similar feature on the shelf north of Lewis by non-linear optimization. *Journal of the Geological Society*, **142**, 1077-1087.

O'NEILL P S and ENGLAND, R W. 1994. The structure of the Sea of the Hebrides Basin: an integrated gravity and seismic model. *Scottish Journal of Geology,* **30**, 1-9.

O'REILLY, B M, HAUSER, F, JACOB, A W B and SHANNON, P M. 1996. The lithosphere below the Rockall Trough: wide-angle seismic evidence for extensive serpentinisation. *Tectonophysics,* **255**, 1-23.

PARKER, R L and HUESTIS, S P. 1974. The inversion of magnetic anomalies in the presence of topography. *Journal of Geophysical Research*, **79**, 1587-1593.

PHARAOH, T C, MORRIS, J H, LONG, C B and RYAN, P D. 1996. *Tectonic Map of Britain, Ireland, and adjacent areas*, (Nottingham: British Geological Survey.)

POWELL, D W. 1970. Magnetised rocks within the Lewisian of Western Scotland and under the Southern Uplands. *Scottish Journal of Geology*, **6**.

PRICE, I and RATTEY, R P. 1984. Cretaceous tectonics off mid-Norway: implications for the Rockall and Faeroe-Shetland Troughs. *Journal of the Geological Society*, **141**, 985-992.

RESTON, T J, KRAWCZYK C M and HOFFMAN H-J. 1995. Detachment tectonics during Atlantic rifting: analysis and interpretation of the S reflection, the West Galacia margin. 93-109 in: *The Tectonics, Sedimentation and Palaeoceanography of the North Atlantic Region.* SCRUTTON, R A, STOKER, M S, SHIMMIELD, G B and TUDHOPE, A W. (editors). (Geological Society, London, Special Publication, **90**.)

RITCHIE, J D and HITCHEN, K. 1996. Early Palaeogene offshore igneous activity to the northwest of the UK and its relationship to the North Atlantic Igneous Province. 63-76 in: *Correlation of the Early Palaeogene in Northwest Europe.* KNOX, R W O'B., CORFIELD, R. and DUNAY, R E. (editors.). (Geological Society, London, Special Publication, **101**.)

ROBERTS, D G, HUNTER, A S and LAUGHTON, A S. 1977. *Bathymetry of the Northeast Atlantic, sheet 2, Continental Margin around the British Isles*. Chart C6567, published by the Hydrographic Office on behalf of the Institute of Oceanographic Sciences, Natural Environment Research Council.

ROBERTS, D G and JONES, M T. 1978. A bathymetric, magnetic and gravity survey of the Rockall Bank. HMS Hecla 1969. *Admiralty Marine Science Publication*, No. 19. Hydrographic Department, Ministry of Defence, Taunton.

ROBERTS, D G, BOTT, M H P and URUSKI, C. 1983. Structure and origin of the Wyville-Thomson Ridge. 133-158 in *Structure and development of the Greenland-Scotland Ridge: new methods and concepts*. BOTT, M H P, SAXOV, S, TALWANI, M and THEIDE, J. (editors). (Plenum, New York.)

ROBERTS, D G, GINZBERG, A, NUNN, K and MCQUILLIN, R. 1988. The structure of the Rockall Trough from seismic refraction and wide-angle reflection measurements. *Nature*, **332**, 632-635.

ROLLIN, K E. 1997. North Britain. *Geophysics CD Series of the British Geological Survey*

RUMPH, B, REAVES, C M, ORANGE, V G. and ROBINSON, D L. 1993. Structuring and transfer zones in the Faeroe Basin. In: *Petroleum Geology of Europe: Proceedings of the 4th conference*, PARKER, J D. (editor). (London: Geological Society.)

SANDWELL, D T. 1992. Antarctic marine gravity field from high density satellite altimetry, *Geophysical Journal International*, **109**, 437-448.

SHANNON, P M, JACOB, A W B., MAKRIS, J, O'REILLY, B, HAUSER, F and VOGT, U. 1994. Basin evolution in the Rockall region, North Atlantic. *First Break*, **12**, 515-522.

SIMPSON, R W, JACHENS, R C and BLAKELEY, R J. 1983. *AIRYROOT: a FORTRAN program for calculating the gravitational attraction of an Airy isostatic root out to 166.7 km.* United States Geological Survey Open File Report 83-0883.

SMITH, P J and BOTT, M H P. 1975. Structure of the crust beneath the Caledonian foreland and Caledonian belt of the North Scottish shelf region. *Geophysical Journal of the Royal Astronomical Society*, **40**, 187-205.

SMYTHE, D K. 1983. Faeroe-Shetland Escarpment and continental margin north of the Faeroes. 109-119 in *Structure and development of the Greenland-Scotland Ridge: new methods and concepts.* BOTT, M H P, SAXOV, S, TALWANI, M and THEIDE, J. (editors). (Plenum, New York.)

SMYTHE, D K. 1989. Rockall Trough - Cretaceous or Late Palaeozoic? *Scottish Journal of Geology*, **25**, 5-43.

SNYDER, D B. 1990. The Moine thrust in the BIRPS data-set. *Journal of the Geological Society*, **147**, 81-86.

SOPER, N J. 1994. Neoproterozoic sedimentation on the northeast margin of Laurentia and the opening of Iapetus. *Geological Magazine*, **131**, 291-299.

STEIN, A M. and BLUNDELL, D J. 1990. Geological inheritance and crustal dynamics of the northwest Scottish continental shelf. *Tectonophysics*, **173**, 455-467.

STOKER, M S. 1997. Mid- to late Cenozoic sedimentation on the continental margin off NW Britain. *Journal of the Geological Society*, **154**, 509-516.

STOKER, M S, HITCHEN, K and GRAHAM, C C 1993. United Kingdom offshore regional report: the geology of the Hebrides and West Shetland shelves, and adjacent deep-water areas. (London: HMSO for the British Geological Survey.)

TATE, M P and DOBSON, M R. 1988. Syn- and post-rift igneous activity in the Porcupine Seabight Basin and adjacent continental margin west of Ireland. 309-334 in: *Early Tertiary Volcanism and the Opening of the NE Atlantic*. MORTON, A.C. & PARSON, L.M. (editors). (Geological Society, London, Special Publication **39**.)

WAAGSTEIN, R. 1988. Structure, composition and age of the Faeroe basalt plateau. 225-238 in: *Early Tertiary Volcanism and the Opening of the NE Atlantic*. MORTON, A.C. & PARSON, L.M. (editors). (Geological Society, London, Special Publication **39**.)

WATTS, A B and FAIRHEAD, J D. 1997. Gravity anomalies and magmatism along the western continental margin of the British Isles. *Journal of the Geological Society*, **154**, 523-529.

WATTS, A B and MARR. 1995. Gravity anomalies and the thermal and mechanical structure of rifted continental margins. 65-94 in Rifted ocean-continent boundaries. BANDA, E, TALWANI, M and TORNE, M. (editors). *NATO ASI Series C, Volume 463* (Kluwer Academic Publishers)

WESSEL, P and SMITH, W H F. 1991. Free software helps map and display data. *EOS Transactions of the American Geophysical Union*, **72**, 441.

WHITE, R S, WESTBROOK, G K, FOWLER, S R, SPENCE, G D, BARTON, P J, JOPPEN, M, MORGAN, J, BOWEN, A N, PRESTCOTT, C and BOTT, M H P. 1987. Hatton Bank (north-west UK) continental margin structure. *Geophysical Journal of the Royal Astronomical Society*, **89**, 265-272.

WINCHESTER, J A. 1973. Pattern of regional metamorphism suggests a sinistral displacement of 160km along the Great Glen Fault. *Nature*, **246**, 81-84.

ZIEGLER, P A. 1982. *Geological Atlas of Western and Central Europe.* (The Hague: Shell Internationale Petroleum Maatshappij B.V.)

ANNEX A7: *NOTES ON EULER DECONVOLUTION*

Euler's homogeneity relationship links source location to the observed potential field. This leads to a set of equations, solvable using matrix inversion techniques, within a window which is moved systematically across a grid of gravity/magnetic anomaly data. Although the procedure is automated, the user has to specify both a number of parameters which affect the values calculated and the criteria for discriminating between spurious solutions and those retained for display. One of these parameters is the so-called structural index (SI) which relates to the rate of change in the field with distance and, hence, to the geometry of the source itself: a higher SI implies a more localized body (eg. a small intrusion as against an extended step or a contact between units with differing properties). In principle, the appropriate SI value can be derived as part of the solution but it is usually more effective to compare source locations as calculated for several pre-set values.

The Euler deconvolution method will produce a solution (in x,y,z) for every position of the calculation window. However, if anomaly gradients are slack the solution will be poorly constrained and be attributed to a source well outside the calculation window. One approach to selecting only the more reliable solutions uses the standard errors in x,y,z given by the least-squares procedure. Further constraints can be applied by limiting solutions to points where the local anomaly gradients are at a maximum ie. implying there is a nearby source. Similarly, the SI values can be restricted by model studies based on the expected geology. It should be noted that modelling indicates a marked deterioration in the reliability of solutions as the quality of the field data deteriorates; this follows from their sensitivity to noise in both vertical and horizontal gradients. Further discussion on the method and its geological application is provided in McDonald *et al.* (1992).

The examples of Euler deconvolution selected for this volume provide some indication of source depths but, in view of a number of caveats associated with the methodology, are best regarded as only a qualitative guide. The maps can be approached in two different ways. First, to gain a general impression of the trends and patterns; second, to look at specific areas in more detail.

Each solution is depicted as a line, coloured according to the depth range in which it lies. Separated colour scales, blue-green and yellow-red, are used to identify the type of solution where two are combined on the same map (eg. gravity/magnetic, different structural index and window size settings etc.). Each line is oriented according to the local direction of the horizontal gradient: the alignment is orthogonal to the gradient, so as to indicate the contour trend and structural grain. The length of line is determined by the analytic signal ie. by the magnitude of the full gradient vector (vertical plus horizontal components), such that the longer lines should be associated with shallower solutions.

Influences on the reliability of calculated source locations:

(i) depths calculated from Euler deconvolution are not simply related to a specific level, such as the uppermost surface of the inferred source, even where its geometry is simple. Thus, for a faulted step the best solutions will lie somewhere between the top and mid-point.

(ii) the 'structural index' (SI) parameter affects the degree to which a solution is focussed correctly for any particular source geometry: higher SI values are more appropriate as the curvature increases eg. from near zero for a vertical contact to three for a sphere in the magnetic case; from zero to two for gravity solutions. Use of too high an SI value results in exaggerated depths passing

the solution acceptance criteria but the geographic location of these solutions can still be valid for bringing out structural trends. In some cases, characteristic curved strings of false solutions result from the use of an inappropriate SI. Solutions calculated with lower SI values generally show larger standard deviations and are more likely to be degraded where data quality is poorer.

(iii) the size of the calculation window should be related to the wavelength of each anomaly so that it is sampled effectively: large windows act as a low pass filter, resulting in over-estimates of source depths and in sampling adjacent anomalies; small windows are more susceptible to seeing noise within the data-set.

(iv) the criteria adopted for accepting/rejecting solutions can be relaxed or constrained. Relevant parameters include:

- standard errors of the x,y and/or z values of each solution;
- distance by which the solution is offset from the centre of the window;
- proximity of window to a local maximum in the horizontal gradient;
- magnitude of the horizontal gradient (for limiting/selecting SI value).